

**Meson Spectra from a Dynamical Three-Field Model of  
AdS/QCD**

**A THESIS  
SUBMITTED TO THE FACULTY OF THE GRADUATE SCHOOL  
OF THE UNIVERSITY OF MINNESOTA  
BY**

**Sean Peter Bartz**

**IN PARTIAL FULFILLMENT OF THE REQUIREMENTS  
FOR THE DEGREE OF  
DOCTOR OF PHILOSOPHY**

**Joseph I. Kapusta**

**August, 2014**

© Sean Peter Bartz 2014  
ALL RIGHTS RESERVED

# Acknowledgements

There are many people that have earned my gratitude for their contribution to my time in graduate school. First, I would like to thank my adviser, Joe Kapusta, for taking a chance on a young graduate student, and for guiding my research during my time at Minnesota.

I would also like to thank Tom Kelley, who helped guide me through the beginnings of my research and helped me understand the basics of the AdS/CFT correspondence.

My graduate school experience was shaped by my participation in the Department of Energy Office of Science Graduate Fellowship for three years. The research support for travel made my graduate career a great experience, and the camaraderie with the other fellows was also fulfilling. I would like to thank Dr. Ping Ge, Cayla Stephenson, Igrid Gregory, and everyone else who made the DOE SCGF program a fulfilling, eye-opening experience.

This research is supported by the Department of Energy Office of Science Graduate Fellowship Program (DOE SCGF), made possible in part by the American Recovery and Reinvestment Act of 2009, administered by ORISE-ORAU under contract no. DE-AC05-06OR23100, by the US Department of Energy (DOE) under Grant No. DE-FG02-87ER40328, and by a Doctoral Dissertation Fellowship from the University of Minnesota.

# Dedication

To my parents, Larry and Colleen, my first teachers. To my sister, Haley, my first student. To my wife, Alicia, my greatest support.

## Abstract

Gauge/gravity dualities are a tool that allow the analytic analysis of strongly-coupled gauge theories. The Anti-de Sitter Space/Conformal Field Theory conjecture posits a duality between ten-dimensional string theory and a super Yang-Mills theory. A phenomenologically-motivated modification of this correspondence is known as AdS/QCD, a duality between strongly-coupled QCD-like theories and weakly-coupled gravitational theories in an additional dimension. QCD is not scale-invariant, so the dual theory must be modified in the conformal dimension to reflect this.

This thesis examines “soft-wall” models of AdS/QCD, wherein the conformal symmetry is broken by a field known as a dilaton. The dynamics of the dilaton and other background fields are examined, and a potential for these fields is determined. The background fields are numerically derived from this potential and used in the calculation of meson spectra, which match well to experiment.

The work presented here is based upon previously-published work by the author:

# Contents

<b>Acknowledgements</b>	<b>i</b>
<b>Dedication</b>	<b>ii</b>
<b>Abstract</b>	<b>iii</b>
<b>List of Tables</b>	<b>vii</b>
<b>List of Figures</b>	<b>viii</b>
<b>1 Introduction</b>	<b>1</b>
<b>2 Background</b>	<b>4</b>
2.1 What is AdS/CFT? . . . . .	4
2.2 Applying AdS/CFT to Quantum Chromodynamics . . . . .	8
2.3 Top-Down Approach . . . . .	8
2.4 Bottom-Up Approach . . . . .	9
2.5 Dynamical AdS/QCD . . . . .	11
2.6 Summary . . . . .	11
<b>3 Soft-Wall Model of AdS/QCD</b>	<b>12</b>
3.1 Minimal Soft-Wall Model . . . . .	13
3.1.1 Metric and Field Content . . . . .	13
3.1.2 Equations of Motion . . . . .	18
3.2 Modified Soft-Wall Model . . . . .	24
3.2.1 Chiral Symmetry Breaking . . . . .	25

3.2.2	Meson Spectra . . . . .	27
3.2.3	Pions in Modified Soft-Wall Model of AdS/QCD . . . . .	29
3.2.4	Gell-Mann–Oakes–Renner Relation . . . . .	36
3.3	Summary . . . . .	39
<b>4</b>	<b>Dynamical AdS/QCD</b>	<b>41</b>
4.1	Gravity-Dilaton Action . . . . .	42
4.2	Gravity-Dilaton-Tachyon Action . . . . .	44
4.2.1	Alternative Approach to Chiral Symmetry Breaking in Dynamical AdS/QCD . . . . .	47
4.3	Summary . . . . .	49
<b>5</b>	<b>Dynamical Three-Field Model</b>	<b>51</b>
5.1	Review and Motivation . . . . .	52
5.2	Construction of Potential . . . . .	54
5.2.1	Infrared Limit . . . . .	55
5.2.2	Ultraviolet Limit . . . . .	56
5.3	Numerical Solution . . . . .	59
5.4	Summary . . . . .	67
<b>6</b>	<b>Meson Spectra</b>	<b>69</b>
6.1	Vector Sector . . . . .	70
6.2	Axial-Vector Sector . . . . .	70
6.3	Pseudoscalar Sector . . . . .	71
6.4	Summary . . . . .	75
<b>7</b>	<b>Scalar and Glueball Sectors</b>	<b>77</b>
<b>8</b>	<b>Conclusion and Discussion</b>	<b>79</b>
	<b>References</b>	<b>84</b>
	<b>Appendix A. Numerical Methods for solving Ordinary Differential Equations</b>	<b>91</b>
A.1	Shooting Method . . . . .	92

A.2	Matrix Method . . . . .	93
<b>Appendix B. General Relativity Reference</b>		<b>95</b>
B.1	Covariant Derivative and Christoffel Symbols . . . . .	95
B.2	Ricci Tensor and Ricci Scalar . . . . .	96
B.3	Equations of Motion . . . . .	97



# List of Tables

3.1	Operators and fields of the model. The matrices $t^a$ are the generators of the $SU(N_f)$ symmetry. . . . .	16
3.2	The observed masses [1] and calculated masses using the linear representations. The large- $n$ limit solutions are valid from $n \approx 4$ . From that point onward, the numerical method used is increasingly inaccurate and fails to find the linear Regge trajectories expected. *=Appears only in the further states of [1]. . . . .	34
5.1	Best fit parameters for the phenomenological model. The parameters $\lambda, \theta$ , and $\beta_2$ are chosen for the best visual fit to the $\rho$ and $a_1$ data, with the rest set by minimizing the error in the equations of motion (5.12), (5.15-5.16). . . . .	61
5.2	The dimensionless parameters for the fitting to $\Delta U$ . . . . .	67
6.1	The experimental [1] and predicted values for the masses of the vector mesons. . . . .	70
6.2	The experimental [1] and predicted values for the masses of the axial-vector mesons. . . . .	73
6.3	The experimental [1] and predicted values for the masses of the pseudoscalar mesons. The states marked with an * appear only in the further states of the PDG. The state marked with a $\dagger$ is an unconfirmed resonance X(2210) with unknown quantum numbers. Whether it really represents the $n = 5$ state is pure speculation. . . . .	74

# List of Figures

3.1	The pion mass spectrum calculated in the modified AdS/QCD model is plotted along with the experimental data [1]. The eigenvalues display two important characteristics of the experimental pion spectrum: (1) light ground state and (2) a large gap between the ground state and the first excited state. The large- $n$ mass trajectory clearly follows our calculated eigenvalues from $n \approx 4$ when our numerical routine inadequately follows the oscillations of the higher eigenfunctions. . . . .	35
3.2	Plot of $m_\pi^2$ vs $m_q$ yields a straight line from which the pion decay constant $f_\pi$ is calculated using (3.152). . . . .	39
5.1	A plot of the dilaton field $\Phi$ generated by the parameterization (5.63). The UV and IR asymptotic behavior is apparent. The coordinate $x$ is a dimensionless re-scaling of the conformal coordinate, $x = \sqrt{\lambda}z$ . . . . .	63
5.2	A plot of the chiral field $\chi$ generated by the parameterization (5.64). The UV and IR asymptotic behavior is apparent, with a rapid transition between them. The coordinate $x$ is a dimensionless re-scaling of the conformal coordinate, $x = \sqrt{\lambda}z$ . . . . .	64
5.3	A plot of the glueball field $G$ generated by the parameterization (5.64). The UV and IR asymptotic behavior is apparent, with a rapid transition between them. The coordinate $x$ is a dimensionless re-scaling of the conformal coordinate, $x = \sqrt{\lambda}z$ . . . . .	65
5.4	Plot of the “extra” term in the potential, $\Delta U(\phi)$ . The solid line represents the numerical result, while the dashed line is the fitting of (5.66) using the parameters of Table 5.2. . . . .	66

6.1	Comparison of the predicted mass eigenvalues for the vector sector with the experimental $\rho$ meson spectrum [1]. . . . .	71
6.2	Comparison of the predicted mass eigenvalues for the axial-vector sector with the experimental $a_1$ meson spectrum [1]. . . . .	72
6.3	Comparison of the predicted mass eigenvalues for the pseudoscalar sector with the experimental $\pi$ meson spectrum [1]. The states plotted here with $n = 4$ and $n = 6$ are identified as radial excitations of the pion only in the further states of the PDG. The unconfirmed state X(2210), with unknown quantum numbers, is plotted here as the $n = 5$ state of the pion. . . . .	75
A.1	An illustration of the shooting method. . . . .	93

# Chapter 1

## Introduction

It's turtles  
all the way down.  
–Unknown

Each of the four fundamental forces of the universe is described by a particular theory. Gravity is understood through the techniques of general relativity, while electromagnetism and the weak nuclear force are united in the electroweak theory of the standard model. Quantum chromodynamics (QCD) describes the behavior of the strong nuclear force, which is the subject of this thesis.

The strong nuclear force binds together the constituents of nuclear matter. The fundamental constituents of the theory are quarks and the force-carrying particles known as gluons. The strength of an interaction is characterized by a parameter known as the coupling constant. Traditional perturbation techniques involve a series expansion in this constant, which works well when the coupling constant is small. When the coupling constant is large, each successive term in this expansion is larger than the preceding one, so the perturbation expansion is not useful. The value of the coupling constant of QCD varies with energy scale. At high energies, the coupling constant is small, but the strength of the interaction grows at lower energies. At these energies, quarks and gluons are confined within particles known as hadrons, and investigating their dynamics requires new techniques.

Beginning in the late 1990's, new techniques were proposed to tackle these non-perturbative problems. In the framework of string theory it was conjectured that a duality exists between strongly-coupled gauge theories and weakly-coupled gravitational theories. Calculations that are analytically intractable in the field theory can be related to more easily calculated results from the gravity theory. These models are known as gauge/gravity dualities. There has been recent excitement about results testing the duality by calculating the equivalent quantity on both sides of the duality, with positive results [2, 3]. While not a proof of the correspondence, this result impressively supports the validity of ongoing efforts into developing such theories.

One proposed gauge/gravity model is the AdS/CFT (Anti-de Sitter space/Conformal Field Theory) correspondence, which relates certain strongly-coupled field theories to weakly-coupled gravitational theories with an extra dimension. The potential application of the AdS/CFT correspondence to non-perturbative aspects of QCD was quickly recognized, although there are some assumptions in the correspondence that do not apply to QCD. While a gravitational dual to QCD has not been discovered, there has been much success over the past fifteen years in developing five-dimensional models that capture key features of hadron phenomenology. These effective models are known as AdS/QCD.

This thesis is organized as follows

- In Chapter 2, we introduce the AdS/CFT duality by reviewing the existing literature and presenting an argument for the correspondence.
- In Chapter 3, we describe previous work done on soft-wall AdS/QCD models. We cover the application of the model to the calculation of meson spectra and the modeling of chiral symmetry breaking. We discuss one particular modification to the simplest soft-wall model that accurately describes the explicit and spontaneous breaking of chiral symmetry. The application of this model to the pseudoscalar sector of mesons was contributed to by the author [4].
- In Chapter 4, we review the literature on dynamical models of AdS/QCD. This includes gravity-dilaton and gravity-dilaton-tachyon models.
- In Chapter 5, we detail the construction of a three-field dynamical AdS/QCD model. The need for a third background field is motivated by the analysis of chiral

symmetry breaking. We derive the equations of motion for the background fields, and construct a potential with the correct behavior. We describe the numerical techniques needed to derive the form of the background fields from this potential. This model was originally described in a paper by the author [5].

- In Chapter 6, we present the mass spectra for the vector, axial-vector, and pseudoscalar mesons that result from the three-field dynamical AdS/QCD model. We describe the method for calculating the meson spectra and compare the model to experimental results, showing good agreement. These results were also presented in [5].
- In Chapter 7, we discuss the mixing of the scalar meson field with the scalar glueball field. The mass eigenvalues will also be found in a forthcoming publication.
- Finally, in Chapter 8, we discuss the major conclusions of this analysis, along with open questions and the future prospects of this research program.

## Chapter 2

# Background

listen: there's a hell  
of a good universe next door; let's go  
—e.e. cummings

In this chapter, we cover the background of gauge/gravity dualities and the AdS/CFT correspondence. Our focus is on the phenomenological applications of these models, so many of the technical details of the correspondence will not be presented here. A variety of review articles cover the topic in more mathematical detail [6, 7, 8, 9, 10, 11, 12]. Once we have motivated the AdS/CFT correspondence, we will review the applications of the duality to hadronic physics. We discuss the two major approaches to alter the conformal field theory to more closely resemble quantum chromodynamics. We also introduce a scheme to put these models on a more consistent theoretical basis.

### 2.1 What is AdS/CFT?

The general principle of dualities is to describe the same physical systems with two different but equivalent theories. The goal of this approach is to find that one of the theories is more analytically tractable than the other, and therefore more useful in describing physical phenomena. The original work on the AdS/CFT correspondence began with a duality between ten-dimensional string theory on  $AdS_5 \times S^5$  and  $\mathcal{N} = 4$  Super Yang-Mills Theory. The details of the string theory are not crucial to the

understanding of the derivation of the correspondence. The constituents of the theory are extended objects known as  $p$ -branes, where  $p$  refers to the spatial dimension of the object. One-dimensional  $p$ -branes are more commonly known as strings, which can be either closed or open. Closed strings propagate freely through space, while open strings have their endpoints on  $p$ -dimensional Dirichlet-branes (D-branes). These strings are characterized by their length  $l_s$  and the coupling constant  $g_s$  that describes the strength of their interactions. These parameters are related to the  $D$ -dimensional Newton's constant

$$G_D \sim g_s^2 l_s^{D-2}. \quad (2.1)$$

The string length can also be related to the Regge slope parameter

$$\alpha' = l_s^2. \quad (2.2)$$

We motivate the AdS/CFT correspondence by examining a stack of  $N$  D3 branes as a background for a type IIB string theory. We consider the dynamics of this system by taking the limits of low energy and strong coupling. The order in which these limits are taken determines the appearance of the result, yielding the two sides of the duality.

Taking the low-energy limit first gives an  $SU(N)$  gauge theory,  $\mathcal{N} = 4$  Super Yang-Mills (SYM) Theory.<sup>1</sup> The gauge coupling in this theory is related to the string coupling by

$$g_{YM}^2 = 4\pi g_s. \quad (2.3)$$

Assuming the string length is small, any interactions involving the open strings in the bulk (the region away from the branes) can be ignored. We are now free to make the assumption of strong coupling in the SYM theory. There are now two decoupled components of the low-energy system: the string theory governing the open strings in the bulk, and the strongly-coupled SYM theory on the branes.

Now, let us take the strong coupling limit first. In this instance, we have a large number of coincident D-branes resulting in a large energy density, and we must use general relativity to take into account its effect on the curvature of spacetime. The

---

<sup>1</sup> N.B.  $N$  refers to the number of D3 branes and the number of colors in the gauge theory, while  $\mathcal{N}$  indicates the number of supercharges in the SYM theory.



classical metric that solves the supergravity equations is

$$ds^2 = \frac{1}{\sqrt{1 + \frac{L^4}{r^4}}} (-dt^2 + d\vec{x}^2) + \sqrt{1 + \frac{L^4}{r^4}} (dr^2 + r^2 d\Omega_5), \quad (2.4)$$

where the curvature radius  $L$  sets the scale and is given by [13, 14]

$$L^4 = 4\pi g_s N \alpha'^2. \quad (2.5)$$

The vector  $\vec{x}$  runs over three spatial dimensions, and  $d\Omega_5$  is the five-dimensional angular element.

The stack of  $N$  D3 branes is located at  $r = 0$ , and to an observer located at  $r = \infty$ , any excitations near the branes appears to be low energy due to gravitational red-shifting. As a consequence, taking the low-energy limit is equivalent to taking the limit  $r \ll L$ . The metric becomes

$$ds^2 = \frac{r^2}{L^2} (-dt^2 + d\vec{x}^2) + \frac{L^2}{r^2} dr^2 + L^2 d\Omega_5, \quad (2.6)$$

where  $r$  is strictly positive. This metric is a product of five dimensional anti-de Sitter space with a five-dimensional sphere ( $AdS_5 \times S_5$ ). We can re-write this metric using the coordinate transformation

$$z = \frac{L^2}{r}. \quad (2.7)$$

This transformation gives a metric with a single warp factor,

$$ds^2 = \frac{L^2}{z^2} (-dt^2 + d\vec{x}^2 + dz^2), \quad (2.8)$$

where  $z > 0$ , with a UV cut-off at an infinitesimal  $z$ -value,  $z = z_0$ . The closed string excitations in the bulk are decoupled from the excitations near the branes.

In each of these descriptions, we began with a stack of  $N$  D3 branes and ended with a low-energy, strongly-coupled system. Taking the low-energy limit first results in an  $\mathcal{N} = 4$  SYM gauge theory, while taking the strong coupling limit first yields a system of excitations on an  $AdS_5 \times S_5$  metric. Maldacena's conjecture is that these two systems should describe the same physics. Each system has closed strings in the bulk that are decoupled from the rest of the system, so the conjecture results in a proposed duality between the  $\mathcal{N} = 4$  SYM theory and type IIB string theory in anti-de Sitter space.

This duality is particularly useful if we can ignore all stringy effects and treat the type IIB string theory as a classical supergravity theory on the metric (2.6). This approximation is valid if the string length is much less than the radius of curvature,

$$l_s \ll L. \quad (2.9)$$

We can relate these quantities to the Yang-Mills coupling using (2.2), (2.3), and (2.5), yielding

$$\frac{L^4}{l_s^4} = g_{YM}^2 N. \quad (2.10)$$

The quantity  $g_{YM}N$  is known as the 't Hooft coupling,  $\lambda$ . Thus, the requirement that the string length be small is equivalent to requiring the 't Hooft coupling to be large,  $\lambda \gg 1$ . In other words, the classical approximation is valid when the dual gauge theory is strongly coupled. The 't Hooft coupling acts as the effective gauge coupling, which is often expressed as a scalar field called the dilaton,  $\Phi$ , where

$$\Phi = \log \lambda. \quad (2.11)$$

The behavior of the dilaton field will take a central role in this thesis.

In summary, Maldacena conjectured that a ten-dimensional string theory is dual to  $\mathcal{N} = 4$  super Yang-Mills theory. We showed that the regime in which stringy effects can be neglected is equivalent to the strong-coupling limit of the gauge theory. The usefulness of this duality is evident, because the strong-coupling regime of a gauge theory is the limit in which it is difficult to perform calculations. Conveniently, this regime is dual to the string theory regime where calculations are easy because they can be done classically.

For our purposes, we reduce the 10-dimensional metric (2.6) to a five-dimensional space by ignoring the  $S_5$  manifold and keeping only the  $AdS_5$  metric (2.8). It turns out that discarding  $S_5$  removes the supersymmetry from the SYM theory, resulting in a non-supersymmetric conformal field theory. In the end, we have a duality between a classical gravity theory in five dimensional anti-de Sitter space and a four-dimensional conformal field theory, our AdS/CFT correspondence. It is this relationship between a field theory in four dimensions and a gravitational theory in five dimensions that lends these models the evocative name *holography*.

## 2.2 Applying AdS/CFT to Quantum Chromodynamics

Phenomenologists would like to apply gauge/theory dualities to physical theories like quantum chromodynamics, rather than supersymmetric Yang-Mills theories that do not directly relate to real-world phenomena. These theories are closely-related enough to encourage a variety of attempts to bridge this gap. To do so, we must examine the differences between SYM theories and QCD.

We have shown how to remove the supersymmetry aspect of the gauge theory in the correspondence in the preceding section, which is necessary because QCD is not supersymmetric. However, we are still left with a conformal field theory, with no intrinsic energy scale. QCD has an energy scale called  $\Lambda_{QCD}$ , which is related to the phenomenon of confinement. Confinement is caused by the running of the QCD coupling with respect to energy scale. Conformal field theories have coupling constants which do not run, and therefore are not confining. Finally, the Yang-Mills theory has  $N \gg 1$ , while  $N_c$ , the number of colors in QCD is 3. Despite these differences, there are a variety of approaches to adapt the AdS/CFT correspondence to apply to QCD.

## 2.3 Top-Down Approach

One approach, known as the top-down approach, consists of modifying the string theory in some way in an attempt to produce a gauge theory that more accurately models QCD. Models that break conformal symmetry can study confinement [?]. The pure gauge theory with  $N$  D3 branes consists of only gluons, leading to the insertion of D7 “flavor branes” in the bulk to include quarks in the theory. [15] Strings that begin and end on the D7 branes represent quark/anti-quark pairs. These strings lack color indices and are therefore color singlets because they do not begin and end on the D3 branes. The excitations of this system corresponds to hadronic states. A prominent example that adds flavor and chiral symmetry breaking to the confining models is the Sakai-Sugimoto model [16, 17].

## 2.4 Bottom-Up Approach

Another approach, known as bottom-up or AdS/QCD models, begin from a phenomenological viewpoint, modifying the existing AdS background to capture some essential features of QCD. Because of this motivation, it is not known whether such models could eventually be derived from string theory. However, it is useful to investigate AdS/QCD as an effective phenomenological model, as well as a means to gain insights that may help in constructing an eventual string theory dual.

The modifications to the AdS background are constructions imposed by hand to introduce features such as confinement and chiral dynamics. Fields that are dual to the operators of the field theory are introduced by hand into the bulk of the AdS background. A Lagrangian is constructed from these fields, and the Euler-Lagrange equations that result are the equations of motion of the gauge field excitations. The normalizable solutions to these equations of motion are the hadronic states of the theory. The masses of the excited states of the mesons are calculated immediately from these eigenvalue problems, and other factors including decay constants and form factors can be calculated as well.

The backgrounds of these bottom-up models are imposed by hand, and not dynamically generated from any equations of motion. They are not derived from string theory, nor is it likely that they could be somehow embedded within any such theory. Despite the *ad hoc* nature of these models, the phenomenological results are often accurate to 10% or better. Importantly, they also give insight into how to capture the major features of QCD, such as confinement and chiral symmetry breaking. There are two major approaches to AdS/QCD, distinguished by the means used to break the conformal symmetry.

### The Hard Wall

The simplest way to break the conformal symmetry of the gauge theory is to impose a hard cutoff in the conformal ( $z$ ) dimension. The model was proposed by [18] and further explored by [19, 20] These so-called hard-wall AdS/QCD models insert both a UV brane located at  $z \rightarrow 0$  and an IR brane at

$$z_1 = \frac{1}{\Lambda_{QCD}}. \quad (2.12)$$

The fields can propagate only between these two branes. The confinement scale is introduced by the IR brane.

These hard-wall models capture a variety of features of QCD, including correlation functions and form factors. The major failing of the hard-wall model is in describing the spectrum of radially excited mesons. It is well established experimentally that these excited states scale as  $m_n^2 \sim n$  as  $n$  becomes sufficiently large, a phenomenon known as linear Regge trajectories or linear confinement. Hard-wall models produce a spectrum with a  $m_n \sim n$  scaling, in conflict with experiment.

### The Soft Wall

Instead of cutting off the metric, soft-wall models insert a  $z$ -dependent scalar dilaton field that breaks the conformal symmetry by acting as an effective cutoff. This model was proposed in [21] and further explored in [22, 23, 24, 25, 26, 27]. The dilaton multiplies the Lagrangian

$$\mathcal{S} = \int d^5x e^{-2\Phi} \sqrt{-g} \mathcal{L}, \quad (2.13)$$

modifying the equations of motion of the fields contained in  $\mathcal{L}$ . A common and simple choice for the dilaton's behavior is a power-law,

$$\Phi = (\mu z)^\nu, \quad (2.14)$$

where  $\mu$  introduces an energy scale into the model on the order of  $\Lambda_{QCD}$ . It was shown by Karch, *et al* [21] that a quadratic dilaton field

$$\Phi \sim z^2 \quad (2.15)$$

yields meson spectra with the desired  $m_n^2 \sim n$  behavior. Because these linear Regge trajectories apply only when  $n$  becomes large, the power-law behavior is necessary strictly when  $z$  becomes large. Improved predictions for the lower meson states can be obtained by modifying the UV behavior of the dilaton field. Such modifications to this model were explored in [28]. The details of past work on soft-wall models will be explored further in Chapter 3.

## 2.5 Dynamical AdS/QCD

The early AdS/QCD models rely on parameterizations for the background fields such as the dilaton. A power law is the simplest choice for the dilaton's behavior, and was suggested in [21]. Later models including [28] improved phenomenology by modifying the dilaton in the UV limit. However, the models rely on *ad hoc* choices for the parameterization of the background fields and do not examine the dynamics of these fields.

So-called dynamical AdS/QCD models attempt a more rigorous examination of the vacuum dynamics of the dual model, as an attempt to remedy some of the shortcomings of the bottom-up approach discussed above [29, 30, 31, 32, 33, 34, 35]. These models examine terms in the Lagrangian involving the dilaton field as well as a tachyonic field that may be related to the chiral symmetry breaking of the model. Previous work examines the construction of the potential terms in the Lagrangian that will give rise to the desired behavior of the background fields. There has also been some work on examining meson spectra in dynamical AdS/QCD models, with some success.

## 2.6 Summary

In this chapter, we have presented the basics of AdS/CFT, including a conceptual motivation for the correspondence. We have also discussed the application of the correspondence to QCD, including the main research programs attempting to make this connection: the top-down and bottom-up approaches. Finally, we have introduced two areas of research in bottom-up AdS/QCD: the soft-wall model and dynamical AdS/QCD. These topics will be elaborated upon in the following chapters.

## Chapter 3

# Soft-Wall Model of AdS/QCD

*Ad astra per alas porci.*

To the stars on the wings of a pig.

–Motto on John Steinbeck’s personal stamp

In this chapter, we will provide detail on previous work done on the soft-wall AdS/QCD model. We will present the set-up of the background metric and the fields that must be included in simplest version of the soft-wall model. The method for modeling the chiral symmetry breaking of QCD is discussed. The Euler-Lagrange equations for the gauge fields are derived, and the eigenvalue equations for the masses of the meson excited states are presented.

We will also describe work done to modify this soft-wall model to capture the correct form of chiral symmetry breaking by adding additional terms to the action. The changes to the meson equations of motion due to these additional terms are presented.

Finally, we present work on the pseudoscalar sector of the modified soft-wall model, contributed to by the author. Two alternative representations for the pseudoscalar field are presented and shown to be equivalent. We then calculate the meson spectrum for the pions and show that this model satisfies the Gell-Mann–Oakes–Renner relation.

### 3.1 Minimal Soft-Wall Model

The soft-wall model of AdS/QCD was introduced by Karch, *et al* [21] and studied further by [36, 22, 23, 24, 25, 26, 27]. This work showed that the behavior of highly-excited mesons is controlled by the infrared behavior of the AdS/CFT dual theory. They argued to replace the simple cut-off of the hard-wall model with a field known as the *dilaton* whose IR behavior would act as a smooth cut-off to the AdS space. In this section, we will describe the set-up and field content of such a simple model and compare the resulting behavior to that of a hard-wall model.

#### 3.1.1 Metric and Field Content

The gravitational dual theory exists in five-dimensional anti-de Sitter space, with a metric given by

$$ds^2 g_{MN} dx^M dx^N = a^2(z)(\eta_{\mu\nu} dx^\mu dx^\nu + dz^2), \quad (3.1)$$

where  $a(z) = L/z$  is the warp factor and  $L$  is the curvature radius of the anti-de Sitter space. We will often work in units where the curvature radius is unity. The Minkowski metric is given by

$$\eta_{\mu\nu} = \begin{pmatrix} -1 & 0 & 0 & 0 \\ 0 & 1 & 0 & 0 \\ 0 & 0 & 1 & 0 \\ 0 & 0 & 0 & 1 \end{pmatrix}. \quad (3.2)$$

The coordinate  $z$  has a range  $0 \leq z < \infty$ .

The bulk coordinate  $z$  is associated with inverse energy scales, with the ultraviolet limit of QCD represented by fields at  $z \rightarrow 0$  [24]. The AdS/CFT dictionary [37, 38] states that each operator  $\mathcal{O}(x)$  in the 4D conformal field theory is associated with a bulk field  $\psi(x, z)$ . The values of the bulk fields at the UV boundary act as sources for the corresponding 4D currents. Global symmetries of the 4D field theory become gauged symmetries for the bulk fields.

The generating functional of gauge-invariant operators of the gauge theory is dual to the minimum of the supergravity action. On the boundary, the supergravity fields must coincide with the sources of the gauge theory [39, 9]. That is,

$$\langle e^{\int_{\partial AdS} d^4x \phi^0(\vec{x}) \mathcal{O}(\vec{x})} \rangle_{\text{CFT}} = e^{iS_{\text{SUGRA}}(\phi)}|_{\phi=\phi_0}, \quad (3.3)$$



where  $\phi^0$  is a source term on the boundary of the five-dimensional supergravity (SUGRA) model. The gauge theory exists on the boundary,  $\partial AdS$ , of the dual gravitational theory. For each operator of conformal dimension  $\Delta$  in the gauge theory, there is a coupling,  $\phi^0 \mathcal{O}$ . For each of these terms, a scalar field with mass  $m$  is inserted into the  $AdS_5$  gravity dual.

We can write down the Lagrangian of such a free massive scalar field,

$$\mathcal{L} = g^{MN} \partial_M \phi \partial_N \phi - m^2 \phi^2. \quad (3.4)$$

The Euler-Lagrange equation is found by varying the action with respect to  $\phi$ ,

$$\begin{aligned} \delta \mathcal{S} &= \delta (\sqrt{-g} g^{MN} \partial_M \phi \partial_N \phi - \sqrt{-g} m^2 \phi^2) \\ &= \sqrt{-g} g^{\mu\nu} \partial_\mu \delta \partial_\nu \phi + \sqrt{-g} g^{zz} \partial_z \phi \delta \partial_z \phi - \sqrt{-g} m^2 \phi \delta \phi \\ &= -a(z)^3 \eta^{\mu\nu} \partial_\mu \partial_\nu \phi \delta \phi - \eta^{zz} \partial_z (a(z)^3 \partial_z \phi \delta \phi) - a(z)^5 m^2 \phi \delta \phi \\ &= (z^5 \partial_z (z^{-3} \partial_z \phi) + z^2 \partial_i^2 \phi - m^2 \phi) \delta \phi, \end{aligned} \quad (3.5)$$

resulting in the equation of motion

$$z^5 \partial_z (z^{-3} \partial_z \phi) + (m^2 + z^2 \partial_i^2) \phi = 0. \quad (3.6)$$

Using the substitution  $\partial_i^2 \phi = -k^2 \phi$ , we can write this equation in momentum space

$$z^5 \partial_z (z^{-3} \partial_z \phi) + (m^2 - k^2 z^2) \phi = 0. \quad (3.7)$$

Near the  $z = 0$  boundary, the  $k^2$  term is neglected, and the asymptotic field behavior becomes [37, 40]

$$\phi \approx \phi^0 z^{\Delta_-} + \langle \mathcal{O} \rangle z^{\Delta_+}, \quad (3.8)$$

where the two solutions are

$$\Delta_{\pm} = \frac{d}{2} \pm \sqrt{\frac{d^2}{4} + m^2 R^2}. \quad (3.9)$$

The mass is determined by the spatial dimension  $d$  and the operator dimension  $\Delta$

$$m^2 = \Delta(\Delta - d), \quad (3.10)$$

giving the two possible solutions of (3.9),

$$\Delta_+ = d, \quad (3.11)$$

$$\Delta_- = d - \Delta. \quad (3.12)$$

An operator  $\mathcal{O}$  on the boundary may also be coupled to a  $p$ -form  $\mathcal{C}$  in AdS space, via the coupling

$$\int_{M_d} \mathcal{C} \wedge \mathcal{O}. \quad (3.13)$$

In this case, the mass of the scalar field in the gravity dual is [40]

$$m^2 = (\Delta - p)(\Delta - p - d). \quad (3.14)$$

It seems that we should require  $\Delta > p + d$ , to avoid instabilities from tachyons with  $m^2 < 0$ . However, it has been shown [41] that tachyons with mass above the bound

$$m^2 > -\frac{d^2}{4} \quad (3.15)$$

are allowed.

The symmetries of the gauge field are also included in the gravitational dual through a prescription provided by the correspondence dictionary. A global symmetry of the gauge theory is represented by invariance under a transformation

$$U = e^{i\eta}, \quad (3.16)$$

with  $\eta$  constant. This means that  $\eta$  should remain constant on the boundary of the gravity dual, but in the bulk, nothing prevents  $\eta$  from becoming a function of spacetime coordinates,  $x$  and  $z$ . The symmetry in the gravity dual is then represented by the transformation

$$U = e^{i\eta(x,z)}. \quad (3.17)$$

In this way, the global symmetry of the gauge theory is represented by a local symmetry of the gravitational theory. A gauge field is inserted into the gravity dual for each relevant global symmetry.

For our AdS/QCD model, the field content of the five-dimensional gravitational dual theory is dictated by the operators relevant to the chiral dynamics of QCD. The gauge fields  $L_\mu$ ,  $R_\mu$  correspond to the left- and right-handed currents of the  $SU(N_f)_L \times SU(N_f)_R$  chiral symmetry, where  $N_f$  is the number of quark flavors in the model. The scalar field  $X$  is associated with the chiral operator  $\bar{q}q$  [18]. The masses of the bulk fields are set by the AdS/CFT relation [26]

$$m_5^2 L^2 = (\Delta - p)(\Delta + p - 4), \quad (3.18)$$

where  $\Delta$  is the dimension of the  $p$ -form QCD operator. Table 3.1 illustrates the fields and operators of our model, showing that the scalar field is the only field in this model that is not massless.

4D Operator	5D Field	$p$	$\Delta$	$m_5^2 L^2$
$\bar{q}_L \gamma^\mu t^a q_L$	$L_\mu^a$	1	3	0
$\bar{q}_R \gamma^\mu t^a q_R$	$R_\mu^a$	1	3	0
$\bar{q}_R^a q_L^b$	$\frac{2}{z} X^{ab}$	0	3	-3

Table 3.1: Operators and fields of the model. The matrices  $t^a$  are the generators of the  $SU(N_f)$  symmetry.

The simplest soft-wall action involving the fields from Table 3.1 is given in [21] as

$$S_5 = \int d^5x \sqrt{-g} e^{-\Phi(z)} \text{Tr} \left[ |DX|^2 + m_X^2 |X|^2 + \frac{1}{4g_5^2} (F_L^2 + F_R^2) \right]. \quad (3.19)$$

The 5D gauge coupling constant  $g_5$  is fixed by calculating the vector current two-point function using this model and then comparing this to the leading order result from QCD, leading to the identification  $g_5^2 = 12\pi^2/N_c$ . This calculation will be performed in Section 3.1.2.

The field  $X$  includes both the scalar and pseudoscalar fields, as well as a non-trivial vacuum expectation value (VEV)

$$X_e^{ab} = \left( \frac{\chi(z)}{2} + S^a(x, z) t^b \right) I e^{2i\pi_e(x, z)^a t^b} \quad (3.20)$$

$$X_l^{ab} = \left( \frac{\chi(z)}{2} + S^a(x, z) t^b \right) I + i\pi_l(x, z)^a t^b, \quad (3.21)$$

with  $I$  the  $N_f \times N_f$  identity matrix and  $t^a$  the  $SU(N_f)$  generators, which are normalized as

$$\text{Tr}[t^a t^b] = \delta^{ab}/2. \quad (3.22)$$

The indices  $a, b$  of the field  $X$  will be suppressed unless needed. The details of the representation choice will be discussed in Section 3.2.3. The field strength tensors are defined as

$$F_L^{MN} = \partial^M L^N - \partial^N L^M - i[L^M, L^N] \quad (3.23)$$

$$F_R^{MN} = \partial^M R^N - \partial^N R^M - i[R^M, R^N], \quad (3.24)$$

where we have used the shorthand notation  $L^M = L^{Ma}t^a$ . The covariant derivative becomes

$$D^M X = \partial^M X - iL^M X + iXR^M. \quad (3.25)$$

The physical vector ( $V$ ) and axial-vector ( $A$ ) fields are defined in terms of the  $L$  and  $R$  gauge fields

$$L^M = V^M + A^M, \quad (3.26)$$

$$R^M = V^M - A^M. \quad (3.27)$$

Substituting equations (3.26) and (3.27) into the last field strength tensors,

$$\begin{aligned} F_L^2 + F_R^2 &= 2 \left( \partial^M L^N \partial_M L_N - \partial^M L^N \partial_N L_M + \frac{1}{2} [L^M, L^N] [L_M, L_N] \right) \\ &+ 2 \left( \partial^M R^N \partial_M R_N - \partial^M R^N \partial_N R_M + \frac{1}{2} [R^M, R^N] [R_M, R_N] \right), \\ &= 4 \left( \partial^M V^N \partial_M V_N - \partial^M V^N \partial_N V_M + \frac{1}{2} [V^M, V^N] [V_M, V_N] \right) \\ &+ 4 \left( \partial^M A^N \partial_M V_N - \partial^M A^N \partial_N A_M + \frac{1}{2} [A^M, A^N] [A_M, A_N] \right), \\ &= 2 (F_V^2 + F_A^2), \end{aligned} \quad (3.28)$$

where the vector and axial field-strength tensors have the form

$$F_V^{MN} = \partial^M V^N - \partial^N V^M - \frac{i}{\sqrt{2}} [V^M, V^N], \quad (3.29)$$

$$F_A^{MN} = \partial^M A^N - \partial^N A^M - \frac{i}{\sqrt{2}} [A^M, A^N]. \quad (3.30)$$

The covariant derivative can also be written in terms of the vector and axial fields

$$D_M X = \partial_M X - i\{A_M^a, X\} + i[V_M^a, X]. \quad (3.31)$$

This relation allows us to re-write the action (3.19),

$$S_5 = \int d^5x \sqrt{-g} e^{-\Phi(z)} \text{Tr} \left[ |DX|^2 + m_X^2 |X|^2 + \frac{1}{2g_5^2} (F_A^2 + F_V^2) \right]. \quad (3.32)$$

The scalar field  $X$  takes on a  $z$ -dependent vacuum expectation value (VEV), breaking the chiral symmetry. In a flavor-symmetric model, the VEV has the form

$$\langle X \rangle = \frac{\chi(z)}{2} I, \quad (3.33)$$

where  $I$  is the  $N_f \times N_f$  identity matrix.

### 3.1.2 Equations of Motion

By varying the action (3.19), one obtains the equations of motion for the scalar, pseudoscalar, vector, and axial-vector mesons, as well as for the scalar vacuum expectation value.

Substituting the chiral field into the Lagrangian using (3.20), we vary the Lagrangian with respect to  $\chi(z)$ ,

$$\begin{aligned}
\delta\mathcal{L}_{VEV} &= -\delta \left( e^{-\Phi} \sqrt{-g} \text{Tr} \left[ \frac{g^{zz}}{4} \partial_z \chi \partial_z \chi + m_X^2 \frac{\chi^2}{4} \right] \right) \\
&= -\delta \left( \frac{1}{2} e^{-\Phi} a(z)^5 \left( a(z)^{-2} \partial_z \chi \partial_z \chi + m_X^2 \chi^2 \right) \right) \\
&= -e^{-\Phi} a(z)^3 \partial_z \chi \delta \partial_z \chi - e^{-\Phi} a(z)^5 m_X^2 \chi \delta \chi \\
&= \left( \partial_z (e^{-\Phi} a^3 \partial_z \chi) - e^{-\Phi} a^5 m_X^2 \chi \right) \delta \chi,
\end{aligned} \tag{3.34}$$

The equation of motion becomes

$$\partial_z^2 \chi - \partial_z \Phi \partial_z \chi + \frac{\partial_z a(z)}{a(z)} \partial_z \chi - a(z)^2 m_X^2 \chi = 0. \tag{3.35}$$

In this model, the warp factor  $a(z) = 1/z$  and the mass of the scalar field  $m_X^2 L^2 = -3$ . With these substitutions, the equation of motion becomes

$$\chi'' - \Phi' \chi' - \frac{3}{z} \chi' + \frac{3}{z^2} \chi = 0. \tag{3.36}$$

In the hard wall model, there is no dilaton, so we can set  $\Phi' = 0$ , finding the exact solution to (3.36) to be

$$\chi_{\text{hw}}(z) = c_1 z + c_2 z^3, \tag{3.37}$$

where  $c_1$  and  $c_2$  are integration constants. Comparing this solution to the UV behavior of the bulk fields in the AdS/CFT dictionary (3.8),  $c_1$  and  $c_2$  correspond to the source term and the operator expectation value, respectively,

$$c_1 \sim m_q, \tag{3.38}$$

$$c_2 \sim \langle q\bar{q} \rangle \equiv \sigma. \tag{3.39}$$

Here  $m_q$  is the quark mass and  $\sigma = \langle \bar{q}q \rangle$  is the chiral condensate, the variation of the vacuum energy with respect to  $m_q$ .

In the simplest soft-wall model, it has been shown [21, 26] that the solution to (3.36) is given by

$$\chi_{sw}(z) = \frac{m_q}{L} z \Gamma\left(\frac{3}{2}\right) U\left(\frac{1}{2}, 0, \lambda z^2\right), \quad (3.40)$$

where  $U(a, b, y)$  is the Tricomi confluent hypergeometric function. (There is also another solution that is disregarded because it leads to an action that is not finite in the IR.) In the small- $z$  limit, (3.40) expands to [26]

$$\chi_{sw}(z) \rightarrow \frac{m_q}{L} z - \frac{\lambda m_q}{2L} z^3 \left(1 - 2\gamma_E - 2\log(\sqrt{\lambda}z) - \psi\left(\frac{3}{2}\right)\right), \quad (3.41)$$

where  $\psi$  is the Euler function. However, comparing this solution to the UV behavior of the chiral condensate in the AdS/CFT dictionary (3.8), we see that  $\sigma \sim m_q$ . This is undesirable in a theory with spontaneous chiral symmetry breaking. In addition, when  $z$  becomes large, we see that the chiral condensate becomes a constant,  $\chi \sim m_q$ , linking the IR and UV behavior. As we will see, the IR behavior of the chiral field governs the behavior of the axial meson spectrum, another limitation of the solution (3.40). More generally, we can see that this issue is caused because the equation (3.36) is linear in  $\chi$ . With only one normalizable solution, only one constant survives the application of boundary conditions. As a result,  $m_q$  and  $\sigma$  cannot be independent. To remedy this, it was suggested [21] to examine higher-order terms in the scalar potential. A particular example of this will be examined in Section 3.2, and a more general approach will be discussed in Chapter 4.

## Scalar Sector

We now examine the fluctuations of the scalar field  $X$ , rather than its VEV, to determine the spectrum of the  $f_0$  scalar mesons. We use the expression in (3.20), though it does not matter which representation for the pseudoscalar component of the field is used,

$$X(x, z) = \left(S(x, z) + \frac{\chi(z)}{2}\right) e^{2i\pi(x, z)}. \quad (3.42)$$

To obtain the equations of motion, we vary the action with respect to the scalar field  $S(x, z)$ ,

$$\delta\mathcal{L}_S = \delta\left(e^{-\Phi}\sqrt{-g}\text{Tr}\left[g^{MN}\partial_M S(x, z)\partial_N S(x, z) + m_X^2 S(x, z)^2\right]\right)$$

$$\begin{aligned}
&= \delta \left( e^{-\Phi} \sqrt{-g} \text{Tr}(t^a t^b) (g^{\mu\nu} \partial_\mu S \partial_\nu S + g^{zz} \partial_z S \partial_z S + m_X^2 S^2) \right) \\
&= e^{-\Phi} a(z)^3 \eta^{\mu\nu} \partial_\mu S \delta \partial_\nu S + e^{-\Phi} a(z)^3 \partial_z S \delta \partial_z S + e^{-\Phi} a(z)^5 m_X^2 S \delta S \\
&= (-e^{-\Phi} a(z)^3 \partial_\mu \partial^\mu S - \partial_z (e^{-\Phi} a(z)^3 \partial_z S) + e^{-\Phi} a(z)^5 m_X^2 S) \delta S, \quad (3.43)
\end{aligned}$$

leaving the equation of motion,

$$e^\Phi a^{-3} \partial_z (e^{-\Phi} a^3 \partial_z S) + \partial_\mu \partial^\mu S - a^2 m_X^2 S = 0. \quad (3.44)$$

We separate the  $z$ -dependent part of the field by using Kaluza-Klein decomposition,

$$S(x, z) = \sum_{n=0}^{\infty} S_n(z) \mathcal{S}_n(x). \quad (3.45)$$

We use the AdS warp factor  $a(z) = 1/z$  and use Proca's equation

$$\partial_i \partial^i S_n = m_n^2 S_n, \quad (3.46)$$

to obtain the equation of motion

$$-\partial_z^2 S_n + \omega'_s \partial_z S_n = m_{S_n}^2 S_n, \quad (3.47)$$

where we have defined

$$\omega_s \equiv \Phi(z) + 3 \log z, \quad (3.48)$$

and  $(')$  represents differentiation with respect to  $z$ . We can eliminate the first derivative of the field  $S_n$  and put the equation of motion in Schrödinger-like form with the substitution

$$S_n = e^{\omega_s/2} s_n. \quad (3.49)$$

The final equation of motion is now

$$-s_n'' + \left( \frac{1}{4} \omega_s'^2 - \frac{1}{2} \omega_s'' + \frac{m_X^2}{z^2} \right) s_n = m_{S_n}^2 s_n. \quad (3.50)$$

## Pseudoscalar Sector

The pseudoscalar eigenstates correspond to the pions, the pseudo-Goldstone bosons of chiral symmetry. This sector is the most difficult to analyze because the pseudoscalar field couples to the longitudinal component of the axial-vector field,

$$A_\mu = A_{\mu\perp} + \partial_\mu \varphi. \quad (3.51)$$

This results in two coupled differential equations, one that comes from varying the action with respect to the pseudoscalar field  $\pi$ , and one that comes from varying with respect to  $\varphi$ . There are also subtleties in the choice of representation, as illustrated above in (3.20-3.21). The various issues involved in analyzing the pseudoscalar sector are discussed in Section 3.2.3.

### Vector Sector

We can derive the mass spectrum of the vector  $\rho$  mesons by varying the vector field and using the axial gauge condition  $V_z = 0$ . Varying the action, we find that

$$\begin{aligned}
\delta S_V &= -\delta \left( e^{-\Phi} \sqrt{-g} g^{\mu\rho} g^{\nu\sigma} (\partial_\mu V_\nu \partial_\rho V_\sigma - \partial_\mu V_\nu \partial_\sigma V_\rho) + e^{-\Phi} \sqrt{-g} g^{zz} g^{\mu\nu} \partial_z V_\mu \partial_z V_\nu \right) \\
&= -e^{-\Phi} \sqrt{-g} g^{\mu\rho} g^{\nu\sigma} (\partial_\mu V_\nu \delta \partial_\rho V_\sigma - \partial_\mu V_\nu \delta \partial_\sigma V_\rho) - e^{-\Phi} \sqrt{-g} g^{zz} g^{\mu\nu} \partial_z V_\mu \delta \partial_z V_\nu \\
&= e^{-\Phi} a(z) (\partial^2 V_\mu \delta V^\mu - \partial_\mu \partial^\nu V_\nu \delta V^\mu) + \partial_z (e^{-\Phi} a(z) \partial_z V_\mu) \delta V^\mu \\
&= (e^{-\Phi} a(z) \partial_\nu \partial^\nu V_\mu + \partial_z (e^{-\Phi} a(z) \partial_z V_\mu)) \delta V^\mu,
\end{aligned} \tag{3.52}$$

We can separate out the  $z$ -dependence of the field using Kaluza-Klein (KK) decomposition

$$V_\mu^n = \sum_{n=0}^{\infty} \mathcal{V}_\mu^n(x) V_n(z), \tag{3.53}$$

where  $V_n(z)$  are the Kaluza-Klein modes. The equation of motion is now one dimensional

$$-\partial_z^2 V_n + \omega' \partial_z V_n = m_{V_n}^2 V_n, \tag{3.54}$$

where we have defined

$$\omega \equiv \Phi(z) + \log z. \tag{3.55}$$

We can eliminate the first derivative of the field, bringing the equation of motion into Schrödinger-like form, using the substitution

$$V_n(z) = e^{\omega/2} v_n(z). \tag{3.56}$$

The equation of motion is now

$$-v_n'' + \left( \frac{1}{4} \omega'^2 - \frac{1}{2} \omega'' \right) v_n = m_{V_n}^2 v_n. \tag{3.57}$$



This is the general method for finding the equations of motion for the various fields. Using the asymptotic form of the dilaton  $\Phi = \lambda z^2$ , the mass eigenvalues can be found exactly for this model. The equation of motion is now

$$-v_n'' + \left( \lambda z^2 + \frac{3}{4z^2} \right) v_n = m_n^2 v_n. \quad (3.58)$$

The eigenvalues for this equation are  $m_n^2 = \lambda(4n+4)$  for  $n = 0, 1, 2, 3, \dots$ . The parameter  $\lambda$  is set by matching this trajectory to experimental data.

We can also determine the value of the 5D coupling constant  $g_5$  used in the action (3.19) by analyzing the vector sector. This is done by matching the vector two-point function  $\Pi_V(q^2)$  calculated from this model to the calculation from the operator product expansion of QCD [25]. As shown in [18, 42], we calculate the two-point function near the UV boundary. We begin by re-writing (3.52) in the hard-wall case  $\Phi' = 0$ ,

$$\partial_z \left( \frac{1}{z} \partial_z V_\mu(q, z) \right) + \frac{q^2}{z} V_\mu(q, z) = 0, \quad (3.59)$$

where  $V_\mu(q, z)$  is the 4D Fourier transform of  $V_\mu(x, z)$ , and we have used the Fourier-transformed version of the Proca equation,

$$\partial_i \partial^i V_\mu(q, z) = -q^2 V_\mu(q, z) \quad (3.60)$$

Evaluating the vector part of the action (3.19) leaves the boundary action

$$\mathcal{S}_b = -\frac{1}{2g_5^2} \int d^4x \left( \frac{1}{z} V_\mu \partial_z V^\mu \right)_{z=\epsilon}, \quad (3.61)$$

where  $\epsilon$  is a UV boundary close to  $z = 0$ . We define  $V_0^\mu$  to be the Fourier-transformed source of the vector current  $J^\mu = \bar{q} \gamma_\mu t^a q$  at the UV boundary,

$$V_0^\mu \equiv \int d^4x e^{iqx} J^\mu. \quad (3.62)$$

Re-writing the vector field in a separable form

$$V^\mu(q, z) = V(q, z) V_0^\mu(q), \quad (3.63)$$

we see that we should choose the UV boundary condition  $V^\mu(q, \epsilon) = 1$ . Using this separable form, (3.61) becomes

$$\mathcal{S}_b = -\frac{1}{2g_5^2} \int d^4x V_{0\mu} \left( \frac{\partial_z V(q, z)}{z} \right)_{z=\epsilon} V_0^\mu. \quad (3.64)$$

This expression shows why  $V(q, z)$  is often known as the *bulk-to-boundary* propagator. Twice differentiating the boundary action with respect to  $V_0$ , we obtain the vector current two-point function,

$$\int d^4x e^{iqx} \langle J_\mu^a(x) J_\nu^b(0) \rangle = \delta^{ab} (q_\mu q_\nu - q^2 g_{\mu\nu}) \Pi_V(q^2), \quad (3.65)$$

where

$$\Pi_V(Q^2) = -\frac{1}{g_5^2 Q^2} \left. \frac{\partial_z V(q, z)}{z} \right|_{z=\epsilon}, \quad (3.66)$$

where  $Q^2 = -q^2$ . In the limit of large  $Q^2$ , we can expand  $V(q, z)$  near the UV boundary,

$$V(Q, z) = 1 + \frac{Q^2 z^2}{4} \log Q^2 z^2 + \dots, \quad (3.67)$$

and to first order, the correlation function becomes

$$\Pi_V(Q^2) = -\frac{1}{2g_5^2} \log Q^2. \quad (3.68)$$

Matching to the large- $N_c$  QCD perturbative result,

$$\Pi_V(k^2) = -\frac{N_c}{24\pi^2} \log k^2, \quad (3.69)$$

where  $N_c$  is the number of colors, we find that

$$g_5^2 = \frac{12\pi^2}{N_c}. \quad (3.70)$$

In this work, we take  $N_c = 3$ , and assume that this value is large enough for the large  $N_c$  results to hold.

### Axial-Vector Sector

The equation of motion for the axial sector is derived using the same method. Varying the action with respect to  $A_\mu$  and using the axial gauge  $A_z = 0$ , we get an equation of similar form to (3.52), but with an additional chiral symmetry-breaking term  $\chi^2 A_\mu$ ,

$$\delta \mathcal{S}_A = (e^{-\Phi} a(z) \partial^2 A_\mu + \partial_z (e^{-\Phi} a(z) \partial_z A_\mu) + e^{-\Phi} g_5^2 a(z)^3 v^2 A_\mu) \delta A^\mu. \quad (3.71)$$

After KK decomposition,

$$A_\mu^n = \sum_{n=0}^{\infty} \mathcal{A}_\mu^n(x) A_n(z), \quad (3.72)$$

the equation of motion becomes

$$-\partial_z^2 A_n + \omega' \partial_z A_n + \frac{g_5^2 \chi(z)^2}{z^2} = m_{A_n}^2 A_n, \quad (3.73)$$

with  $\omega$  defined as in (3.55). To put the equation of motion in Schrödinger form, we make the substitution

$$A_n = e^{\omega/2} a_n, \quad (3.74)$$

yielding

$$-a_n'' + \left( \frac{1}{4} \omega'^2 - \frac{1}{2} \omega'' + g_5^2 \frac{L^2}{z^2} \chi^2(z) \right) a_n = m_{V_n}^2 a_n. \quad (3.75)$$

The only difference from (3.57) is the presence of the  $z$ -dependent mass term involving the chiral condensate. The IR asymptotic behavior of the chiral condensate  $\chi(z)$  controls the splitting between the vector and axial-vector mesons at large values of  $n$ . Experimentally, we see a constant splitting between the squared masses of the  $a_1$  and  $\rho$  mesons, which suggests that chiral symmetry is not restored for the higher excitations. In this model, we can see that the difference between the equations of motion (3.57) and (3.75) is given by

$$\Delta m^2 \equiv (m_{A_n}^2 - m_{V_n}^2)_{n \rightarrow \infty} = g_5^2 \frac{L^2 \chi^2}{z^2} (z \rightarrow \infty). \quad (3.76)$$

To obtain a constant mass splitting, this quantity must become a constant as  $z$  approaches infinity. This tells us that  $\chi \sim z$  in the IR limit.

The significant drawbacks for this simple soft-wall model are the relatively poor modeling of the ground state and lower resonances and the lack of independent spontaneous and explicit chiral symmetry breaking terms.

## 3.2 Modified Soft-Wall Model

An improvement on the soft-wall model, suggested in [21], is adding higher-order terms of  $X$  to the scalar potential, separating the spontaneous and explicit chiral symmetry breaking. The model established in [28] adds a quartic scalar term to the action:

$$\mathcal{S} = \int d^5x \sqrt{-g} e^{-\Phi(z)} \text{Tr} \left[ |DX|^2 + m_X^2 |X|^2 - \kappa |X|^4 + \frac{1}{2g_5^2} (F_A^2 + F_V^2) \right], \quad (3.77)$$

where  $\kappa$  is a dimensionless parameter to be fit to the data. To obtain the required linear Regge trajectories for the meson spectra, the dilaton field must be quadratic in  $z$  in the IR region,

$$\Phi(z \rightarrow \infty) = \lambda z^2, \quad (3.78)$$

where  $\lambda$  sets an energy scale for the model that is related to the slope of the Regge trajectories.

### 3.2.1 Chiral Symmetry Breaking

The chiral symmetry breaking of the model is examined by deriving the equation of motion for the vacuum expectation value of the scalar field  $X$ . Varying (3.77) with respect to  $X$ , we find

$$\begin{aligned} \delta \mathcal{S}_X = & -2e^{-\Phi} \sqrt{-g} \text{Tr} \left( g^{MN} \partial_M X \partial_N \delta X + \{A, X\} \{A, \delta X\} \right. \\ & \left. + [V, X][V, \delta X] + m_X^2 X \delta X - 2\kappa X^\dagger X |X| \delta X \right). \end{aligned} \quad (3.79)$$

Taking the trace, integrating by parts, and using  $|X| = \chi(z)/2 + S(x, z)$ , we find the variation of the action with respect to the chiral condensate,

$$\delta \mathcal{S}_\chi = \frac{1}{2} \left( \partial_z (e^{-\Phi} \sqrt{-g} g^{zz} \partial_z \chi) + e^{-\Phi} \sqrt{-g} m_X^2 \chi + e^{-\Phi} \sqrt{-g} \frac{\kappa}{2} \chi^3 \right) \delta \chi. \quad (3.80)$$

Using the AdS metric, we find that the chiral condensate  $\chi(z)$  now has a nonlinear equation of motion

$$\partial_z (a^3 e^{-\Phi} \partial_z \chi(z)) - a^5 e^{-\Phi} \left( m_X^2 \chi(z) - \frac{\kappa}{2} \chi^3(z) \right) = 0, \quad (3.81)$$

which simplifies to

$$\chi'' - \left( \Phi' + \frac{3}{z} \right) \chi' - m_X^2 \chi + \frac{\kappa}{2} \chi^3 = 0, \quad (3.82)$$

where  $(')$  denotes a derivative with respect to  $z$ .

The higher radially excited states of mesons have parallel Regge trajectories. However, the eigenstates of vector  $\rho$  mesons and the axial-vector  $a_1$  mesons do not become degenerate at large  $n$ , despite having the same spin. This indicates that chiral symmetry is not restored for the higher excitations. As noted in Section 3.1.2, the mass-splitting

between the highly-excited states of the  $a_1$  and  $\rho$  mesons is governed by the IR behavior of the chiral condensate field  $\chi$ ,

$$\Delta m^2 \equiv (m_{A_n}^2 - m_{V_n}^2)_{n \rightarrow \infty} = g_5^2 \frac{L^2 \chi^2}{z^2} (z \rightarrow \infty). \quad (3.83)$$

Because their trajectories are parallel but not equal, we know that this  $\Delta m^2$  must be a constant. Examining the right-hand side of (3.83), we see that this requirement implies that  $\chi(z) \sim z$  for large  $z$ . To match the AdS/CFT dictionary discussed in Chapter 1, the chiral condensate must retain the same UV asymptotic form (3.37). A suitable parameterization that matches the expected UV and IR asymptotic behavior was found and justified in [28]

$$\chi(z) = \alpha z + \beta z \tanh(\gamma z^2), \quad (3.84)$$

with the parameters defined as follows

$$\alpha = \frac{\sqrt{3} m_q}{g_5 L}, \quad \beta = \sqrt{\frac{4\lambda}{\kappa L^2}} - \alpha, \quad \gamma = \frac{g_5 \sigma}{\sqrt{3} \beta}, \quad (3.85)$$

where  $m_q$  is the quark mass,  $\sigma$  is the chiral condensate,  $\lambda$  is set by the experimental Regge trajectories, and  $g_5$  is determined by (3.70) as derived Section 3.1.2. For convenience, we will work in units where the AdS curvature radius  $L$  is unity. In the small- $z$  limit, the chiral field becomes

$$\begin{aligned} \chi(z \rightarrow 0) &= \alpha z + \beta \gamma z^3 \\ &= \frac{\sqrt{3}}{g_5} m_q + \frac{g_5}{\sqrt{3}} \sigma, \end{aligned} \quad (3.86)$$

where  $\sqrt{3}/g_5$  is a normalization factor discussed in [25]. It is clear that, up to normalization, (3.86) matches the UV form required by the AdS/CFT dictionary. In the large- $z$  limit, the chiral field becomes

$$\begin{aligned} \chi(z \rightarrow \infty) &= (\alpha + \beta) z \\ &= \sqrt{\frac{4\lambda}{\kappa}} z. \end{aligned} \quad (3.87)$$

The chiral field is linear in the IR, as required, and the dimensionless parameter  $\kappa$  introduced in (3.77) becomes the parameter that controls the axial-vector mass splitting.

The quark mass and chiral condensate can each be taken to zero independently, and the non-restoration of chiral symmetry does not depend on either of these parameters. Thus, the spontaneous and chiral symmetry breaking parameters are independent, as desired. Using (3.84) in (3.81) we can solve for the derivative of the dilaton field

$$\Phi' = \frac{1}{a(z)^3 \chi'} \left( \partial_z (a(z)^3 \chi') - a^5 \left( m_X^2 \chi - \frac{\kappa}{2} \chi^3 \right) \right). \quad (3.88)$$

Using (3.84) in (3.88), the asymptotic behavior of the dilaton is found to be

$$\Phi(z \rightarrow 0) = \frac{\kappa}{4} \alpha^2 z^2 + \mathcal{O}(z^6), \quad (3.89)$$

$$\Phi(z \rightarrow \infty) = \frac{\kappa}{4} (\alpha + \beta)^2 z^2 = \lambda z^2, \quad (3.90)$$

where the boundary condition  $\Phi(0) = 0$  is chosen to ensure a pure AdS metric in the UV limit. We can see that the desired IR dilaton behavior is recovered by this parameterization.

### 3.2.2 Meson Spectra

Using these parameterizations for the dilaton and chiral condensate fields, we can now calculate the mass eigenvalues of the scalar, vector, and axial-vector mesons. Equations of motion are then derived using the method of Section 3. Due to the more complicated forms for  $\chi$  and  $\Phi$ , the eigenvalues are not analytically solvable, so a numerical shooting method is used to calculate the mass spectra for the scalar, vector, and axial-vector sectors. For details on the shooting method, see Appendix A. The mass spectra resulting from this model for the  $f_0$ ,  $\rho$ , and  $a_1$  mesons can be found in [28].

#### Scalar Mesons

The mass spectrum of the scalar  $f_0$  mesons is determined by deriving the equations of motion for the scalar field  $S(x, z)$  and calculating its eigenvalues. The procedure is similar to that delineated in Section 3.1.2, but the quartic term in the scalar potential in (3.77) causes the fluctuations of the scalar field to couple to its own vacuum expectation value. Using a Kaluza-Klein decomposition

$$S(x, z) = \sum_{n=0}^{\infty} \mathcal{S}_n(x) S_n(z), \quad (3.91)$$

we vary the action (3.77) with respect to  $S$ , yielding

$$\partial_z(a^3(z)e^{-\Phi}\partial_z S_n(z)) - a^5(z)e^{-\Phi}\left(m_X^2 - \frac{3}{2}\kappa\chi^2(z)\right)S_n(z) = -a^3(z)e^{-\Phi}m_{S_n}^2 S_n(z), \quad (3.92)$$

The scalar equation of motion (3.92) can be brought into a Schrödinger-like form with the substitution

$$S_n(z) = e^{\omega_s/2} s_n(z), \quad (3.93)$$

with  $\omega_s$  as defined in (3.48). The eigenvalue equation becomes

$$-\partial_z^2 s_n(z) + \left(\frac{1}{4}\omega_s'^2 - \frac{1}{2}\omega_s'' - \frac{3}{2}\frac{\kappa\chi^2(z)}{z^2} - \frac{3}{z^2}\right)s_n(z) = m_{S_n}^2 s_n(z), \quad (3.94)$$

with the boundary conditions

$$\lim_{z_0 \rightarrow 0} s_n(z_0) = 0, \quad \partial_z s_n(z \rightarrow \infty) = 0. \quad (3.95)$$

## Vector Mesons

The mass spectrum of the vector  $\rho$  mesons is found by deriving the equation of motion for the vector field  $V(x, z)$  and solving for its eigenvalues. The vector field does not mix with the vacuum expectation value of the scalar field, so the form of equation of motion for the vector mesons is unchanged from (3.57). The only difference in the analysis of this sector is that the functional form for  $\Phi'$  is much more complicated, so the eigenvalue problem must be solved with the computational shooting method. Because the dilaton field's IR behavior is unchanged, the large- $n$  excitations follow the same linear Regge trajectory as found in Section 3.1.2, but the lower states differ.

## Axial-Vector Mesons

The mass spectrum of the axial-vector  $a_1$  mesons is calculated by deriving the equation of motion for the axial-vector field  $A(x, z)$  and determining its eigenvalues. The axial-vector field mixes with the chiral condensate field through its kinetic term. This mixing term is unaffected by the change to the scalar potential, so the equation of motion keeps the same form as in (3.75). Again, the behavior of the chiral and dilaton fields is too complicated for analytical solution, so the axial eigenvalues are found with a computational shooting method.

### 3.2.3 Pions in Modified Soft-Wall Model of AdS/QCD

The mass spectrum for the pseudoscalar mesons was not found in the original paper [28] because the equations of motion are coupled, second order differential equations, and because of some subtleties that arise when considering the representation of the pseudoscalar field. The paper [43] attempted to circumvent these problems by reducing the equations of motion to a single second-order equation, solvable by the shooting method, but their results seemed to miss certain essential features of the pion spectrum. The authors later address this apparent discrepancy in [44]. This modified soft-wall model was later completed in a paper to which the author contributed, [4], which clarified the discrepancies between two common representations of the pseudoscalar field, calculated the pion mass spectrum to good accuracy, and derived the Gell-Mann–Oakes–Renner relation from the model.

As mentioned above, the field  $X$  contains both the field representing the scalar mesons,  $S(x, z)$ , and the field representing the pseudoscalars,  $\pi(x, z)$ , as well as a non-trivial  $z$ -dependent vacuum expectation value,  $\chi(z)$ . There are two common ways to represent this field:

$$X_e = \left( \frac{\chi(z)}{2} + S(x, z) \right) I e^{2i\pi_e(x, z)^a t^a} \quad (3.96)$$

$$X_l = \left( \frac{\chi(z)}{2} + S(x, z) \right) I + i\pi_l(x, z)^a t^a \quad (3.97)$$

with  $I$  the  $N_f \times N_f$  identity matrix and  $t^a$  the  $SU(N_f)$  generators. We will refer to  $X_e$  as the exponential representation and  $X_l$  as the linear representation. Apparent differences between the representations arise as we note that  $\pi_e$  and  $\pi_l$  are of different dimension. In addition, the linear representation has a quartic interaction term in the Lagrangian, in contrast to the exponential representation. Despite these differences, we will show that the equations of motion derived from each representation are equivalent.

#### Exponential Representation

Let us take (3.97) and substitute it into (3.77), keeping terms that include the field  $\pi(x, z)$ , as well as terms that will mix with  $\pi$ ,

$$\mathcal{L}_e = -\sqrt{-g}e^{-\Phi(z)}\frac{1}{2}\delta^{ab}\left(g^{MN}(\chi^2\partial_M\pi\partial_N\pi + \chi^2A_MA_N - 2\chi^2\partial_MA_N)\right)$$



$$+\frac{g^{MP}g^{NR}}{g_5^2}(\partial_M A_N \partial_P A_R - \partial_M A_N \partial_R A_P)) + \dots \quad (3.98)$$

We work in the axial gauge,  $A_z = 0$ , and separate the action (3.98) into four-dimensional components and  $z$ -dependent terms,

$$\begin{aligned} \mathcal{L}_e = & -\frac{1}{2}e^{-\Phi(z)} \left[ \sqrt{-g} g^{\mu\nu} (\chi^2 \partial_\mu \pi \partial_\nu \pi + \chi^2 A_\mu A_\nu - 2\chi^2 \partial_\mu \pi A_\nu) \right. \\ & + \sqrt{-g} g^{zz} \chi^2 \partial_z \pi \partial_z \pi + \frac{\sqrt{-g} g^{\mu\nu} g^{\rho\sigma}}{g_5^2} (\partial_\mu A_\rho \partial_\nu A_\sigma - \partial_\mu A_\rho \partial_\sigma A_\nu) \\ & \left. + \frac{\sqrt{-g} g^{zz} g^{\mu\nu}}{g_5^2} (\partial_z A_\mu \partial_z A_\nu) \right]. \end{aligned} \quad (3.99)$$

We separate  $A_\mu$  into its transverse and longitudinal components:  $A_\mu = A_{\mu\perp} + \partial_\mu \varphi$ , where  $\partial_\mu A_\perp^\mu = 0$ . Expressing the action in terms of the longitudinal component,  $\varphi$  gives

$$\begin{aligned} \mathcal{L}_e = & -\frac{1}{2}e^{-\Phi(z)} \left[ \sqrt{-g} g^{\mu\nu} (\chi^2 \partial_\mu \pi \partial_\nu \pi + \chi^2 \partial_\mu \varphi \partial_\nu \varphi - 2\chi^2 \partial_\mu \pi \partial_\nu \varphi) \right. \\ & \left. + \sqrt{-g} g^{zz} \chi^2 \partial_z \pi \partial_z \pi + \frac{\sqrt{-g} g^{zz} g^{\mu\nu}}{g_5^2} (\partial_z \partial_\mu \varphi \partial_z \partial_\nu \varphi) \right]. \end{aligned} \quad (3.100)$$

Varying (3.100) with respect to  $\pi$  gives

$$\delta \mathcal{L}_e = \partial_z e^{-\Phi} \sqrt{-g} g^{zz} \chi^2 \partial_z \pi \delta \pi + e^{-\Phi} \sqrt{-g} \chi^2 g^{\mu\nu} \partial_\nu \partial_\mu (\pi - \varphi) \delta \pi. \quad (3.101)$$

Using a Kaluza-Klein decomposition,

$$\pi(x, z) = \sum_n \Pi_n(x) \pi_n(z), \quad (3.102)$$

$$\varphi(x, z) = \sum_n \Phi_n(x) \varphi_n(z), \quad (3.103)$$

and Proca's equation

$$\partial^2 \Pi_n(x) = m_n^2 \Pi_n(x), \quad \partial^2 \Phi_n(x) = m_n^2 \Phi_n(x), \quad (3.104)$$

we can express the system of equations in terms of its  $z$ -dependent parts

$$e^\Phi \partial_z \left( \frac{e^{-\Phi} \chi^2}{z^3} \partial_z \pi_n \right) + \frac{\chi^2 m_n^2}{z^3} (\pi_n - \varphi_n) = 0. \quad (3.105)$$

Varying (3.100) with respect to  $\varphi$  and breaking it down into KK modes gives the second equation of motion

$$e^\Phi \partial_z \left( \frac{e^{-\Phi}}{z} \partial_z \varphi_n \right) + \frac{g_5^2 L^2 \chi^2}{z^3} (\pi_n - \varphi_n) = 0. \quad (3.106)$$

As usual, we express (3.105) and (3.106) in a Schrödinger-like form,

$$\pi \rightarrow e^{f(z)} \pi \quad f(z) = \Phi(z) + \log \frac{z^3}{\chi(z)^2} \quad (3.107)$$

$$\varphi \rightarrow e^{\omega(z)} \varphi \quad \omega(z) = \Phi(z) + \log z. \quad (3.108)$$

After simplifying, the equations of motion become

$$\begin{aligned} -\pi_n'' + \left( \frac{\Phi'^2}{4} - \frac{\Phi''}{2} - \frac{\Phi' \chi'}{\chi} + \frac{3\Phi'}{2z} + \frac{15}{4z^2} - \frac{3\chi'}{\chi z} + \frac{\chi''}{\chi} - m_n^2 \right) \pi_n &= -m_n^2 \frac{\chi^2 L^2}{z^2} \pi_n \\ -\varphi_n'' + \left( \frac{\Phi'^2}{4} - \frac{\Phi''}{2} + \frac{\Phi'}{2z} + \frac{3}{4z^2} + \frac{g_5^2 \chi^2 L^2}{z^2} \right) \varphi_n &= g_5^2 \pi_n \end{aligned} \quad (3.110)$$

### Linear Representation

When considering the linear representation of the pseudoscalar field (3.97), there are terms quadratic and quartic in  $\pi$  that were not present in the exponential representation. After making the appropriate substitutions in the Lagrangian, it becomes

$$\begin{aligned} \mathcal{L}_l &= -\frac{1}{2} e^{-\Phi} \sqrt{-g} \left( g^{\mu\nu} \partial_\mu \pi \partial_\nu \pi + g^{zz} \partial_z \pi \partial_z \pi - 2\chi g^{\mu\nu} \partial_\mu \pi \partial_\nu \varphi + m_X^2 \pi^2 - \frac{\kappa}{2} \chi^2 \pi^2 \right. \\ &\quad \left. + g^{\mu\nu} \chi^2 \partial_\mu \varphi \partial_\nu \varphi + \frac{g^{\mu\nu} g^{zz}}{g_5^2} \partial_z \partial_\mu \varphi \partial_z \partial_\nu \varphi \right). \end{aligned} \quad (3.111)$$

Following the same procedure as above, we derive two coupled equations. Varying with respect to  $\varphi$  produces

$$e^\Phi \partial_z \left( \frac{e^{-\Phi}}{z} \partial_z \varphi_n \right) + \frac{g_5^2 L^2 \chi}{z^3} (\pi_n - \chi \varphi_n) = 0. \quad (3.112)$$

Varying with respect to  $\pi$  gives the second equation of the linear representation

$$z^3 e^\Phi \partial_z \left( \frac{e^{-\Phi}}{z^3} \partial_z \pi_n \right) - \left( \frac{m_X^2}{z^2} - \frac{\kappa L^2 \chi^2}{2z^2} \right) \pi_n + m_n^2 \pi_n = m_n^2 \chi \varphi_n. \quad (3.113)$$

We can express (3.112) and (3.113) in a Schrödinger-like form as above with the substitutions

$$\pi_n \rightarrow e^{\omega_s/2} \pi_n \quad (3.114)$$

$$\varphi_n \rightarrow e^{\omega/2} \varphi_n, \quad (3.115)$$

where  $\omega_s$  and  $\omega$  are defined as in (3.48) and (3.55), respectively. Simplifying the equations, we find

$$-\varphi_n'' + \left( \frac{\Phi'^2}{4} - \frac{\Phi''}{2} + \frac{3}{4z^2} + \frac{\Phi'}{2z} + \frac{g_5^2 L^2 \chi^2}{z^2} \right) \varphi_n = \frac{g_5^2 L \chi}{z} \pi_n \quad (3.116)$$

$$-\pi_n'' + \left( \frac{\Phi'^2}{4} - \frac{\Phi''}{2} + \frac{3}{4z^2} + \frac{3\Phi'}{2z} - \frac{\kappa L^2 \chi^2}{2z^2} - m_n^2 \right) \pi_n = -m_n^2 \frac{\chi L}{z} \varphi_n \quad (3.117)$$

### Representation Equivalence

The choice of representation for the pseudoscalar field should not affect any physical results obtained from the model. It is therefore desirable to show that the equations of motion derived from the two representations are equivalent.

We begin by expanding  $X_e$  to first order in the fields

$$\begin{aligned} X_e &= \left( \frac{\chi}{2} + S \right) (1 + 2i\pi_e + \dots) \\ &= \frac{\chi}{2} + S + i\pi_e \chi. \end{aligned} \quad (3.118)$$

Comparing (3.118) to (3.97), we infer that

$$\pi_e \chi(z) \rightarrow \pi_l \quad (3.119)$$

is the relationship between the two representations. Let us substitute  $\pi_e \rightarrow \pi_l/\chi(z)$  into the equations of motion of the exponential representation and attempt to obtain the equations of motion of the linear representation. The substitution into (3.106) immediately yields

$$e^\Phi \partial_z \left( \frac{e^{-\Phi}}{z} \partial_z \varphi \right) + \frac{g_5^2 \chi}{z^3} (\pi_l - \chi \varphi) = 0, \quad (3.120)$$

which is equivalent to (3.112) as expected.

Demonstrating the equivalence of the other two equations requires a bit more analysis. First we substitute for  $\pi_e$  in (3.105) and simplify the expression,

$$\frac{z^3 e^\Phi}{\chi} \partial_z \left( \frac{e^{-\Phi} \chi^2}{z^3} \left( \frac{\pi_l'}{\chi} - \frac{\pi_l \chi}{\chi^2} \right) \right) + m_n^2 (\pi_l - \chi \varphi) = 0, \quad (3.121)$$

which becomes

$$\pi_l'' - \left( \Phi' + \frac{3}{z} \right) \pi_l' - \frac{\pi_l}{\chi} \left( \chi'' - \Phi' \chi' - \frac{3}{z} \chi' \right) + m_n^2 (\pi_l - \chi \varphi) = 0. \quad (3.122)$$

Recalling the equation of motion for  $\chi(z)$  (3.81), which does not depend on the pseudoscalar representation:

$$\chi'' - \left( \Phi' + \frac{3}{z} \right) \chi' + \left( \frac{3}{z^2} + \frac{\kappa L^2 \chi^2}{2z^2} \right) \chi = 0. \quad (3.123)$$

Using (3.123) in (3.122), we find

$$\pi_l'' - \left( \frac{3}{z} + \Phi' \right) \pi_l' + \left( \frac{3}{z^2} + \frac{\kappa L^2 \chi^2}{2z^2} \right) \pi_l + m_n^2 (\pi_l - \chi \varphi) = 0, \quad (3.124)$$

which is equivalent to the other equation of motion of the linear representation (3.113). The equations of motion are equivalent, confirming that physical results do not depend on the representation.

### Pseudoscalar Mass Eigenvalues

The mass eigenvalues for the pions can be calculated in either the exponential or linear representation, using the numerical matrix method detailed in Appendix A. However, it turns out that the boundary conditions

$$\pi(z_0 \rightarrow 0) = 0 \quad \partial_z \pi(z \rightarrow \infty) = 0 \quad (3.125)$$

$$\varphi(z_0 \rightarrow 0) = 0 \quad \partial_z \varphi(z \rightarrow \infty) = 0 \quad (3.126)$$

are easier to enforce using the linear representation (3.97). This may be due to the relation (??) and the fact that the chiral field  $\chi$  also goes to zero in the UV, making it difficult to enforce the boundary condition on  $\pi_e$  simultaneously. The numerical results for the  $\pi_l$  eigenvalues are shown in Table 3.2.

For large- $n$  excitations the numerical technique develops problems with the boundary conditions. As the number of oscillations in the eigenfunctions increase for higher  $n$  modes, the routine finds eigenvalues that are skewed to larger values. To uncover the correct asymptotic behavior for large  $n$ , we take the large- $z$  limit of (3.116) and (3.117). As  $n$  increases, the eigenfunction is largely determined by the behavior of the effective potential at large  $z$ . At large  $z$ , the VEV and dilaton behave as

$$\chi(z) = (\alpha + \beta)z \equiv \Gamma \frac{z}{L} \quad (3.127)$$

$$\phi(z) = \lambda z^2. \quad (3.128)$$

n	$\pi$ Data (MeV)	$\pi_l$ (MeV)	Large- $n$ $\pi_l$
1	140	143	-
2	$1300 \pm 100$	1557	-
3	$1816 \pm 14$	1887	-
4	2070*	2095	-
5	2360*	2298	2245
6	-	-	2403
7	-	-	2551

Table 3.2: The observed masses [1] and calculated masses using the linear representations. The large- $n$  limit solutions are valid from  $n \approx 4$ . From that point onward, the numerical method used is increasingly inaccurate and fails to find the linear Regge trajectories expected. \*=Appears only in the further states of [1].

To take the large- $z$  limit of the linear representation, we introduce a new dimensionless parameter,  $\xi = \sqrt{\lambda}z$ , and expand in  $\xi$ . In the linear representation, we find that (3.116) and (3.117) at large  $\xi$  become

$$-\pi_k'' + \xi^2 \pi_k = \left( \frac{\kappa \Gamma^2}{2\lambda} - 2 + \frac{m_k^2}{\lambda} \right) \pi_k - \frac{m_k^2 \Gamma}{\lambda} \varphi_k \quad (3.129)$$

$$-\varphi_k'' + \xi^2 \varphi_k = \frac{g_5^2 \Gamma}{\lambda} (\pi_k - \Gamma \varphi_k) \quad (3.130)$$

where (') here indicates differentiation with respect to  $\xi$ . This set of equations has the form of coupled harmonic oscillators, the equations of motion of which are

$$-\varphi_k'' + \xi^2 \varphi_k = (2k+1)\varphi_k \quad (3.131)$$

$$-\pi_k'' + \xi^2 \pi_k = (2k+1)\pi_k \quad k = 0, 1, \dots \quad (3.132)$$

We make the reasonable assumption that  $\varphi_k = c_k \pi_k$ , which ensures that (3.129), and (3.130) have solutions. Using the form of (3.131) and (3.132) to solve for  $m_k^2$ , and making use of the fact that  $\Gamma^2 = \frac{4\lambda}{\kappa}$ , we find

$$m_k^2 = g_5^2 \Gamma^2 + (2k+1)\lambda. \quad (3.133)$$

Until now we have not made use of the fact that, in the AdS metric,  $z \geq 0$ . Because of this, the eigenfunctions  $\varphi_n$  and  $\pi_n$  describe *half* harmonic oscillators with half as

many modes; therefore, we must take  $k \rightarrow 2k$ . The mass eigenvalues for large  $n$ , where  $n = k + 1$ , in both representations then become

$$m_n^2 = (4n - 3)\lambda + g_5^2 \Gamma^2 \quad n = 4, 5, \dots \quad (3.134)$$

which are also listed in Table 3.2 and plotted in Figure 3.1. Combining (3.134) and the numerical technique, we obtain all the pseudoscalar eigenvalues. On inspection, we find that this method should be trusted over the numerical routine for  $n \geq 4$ .

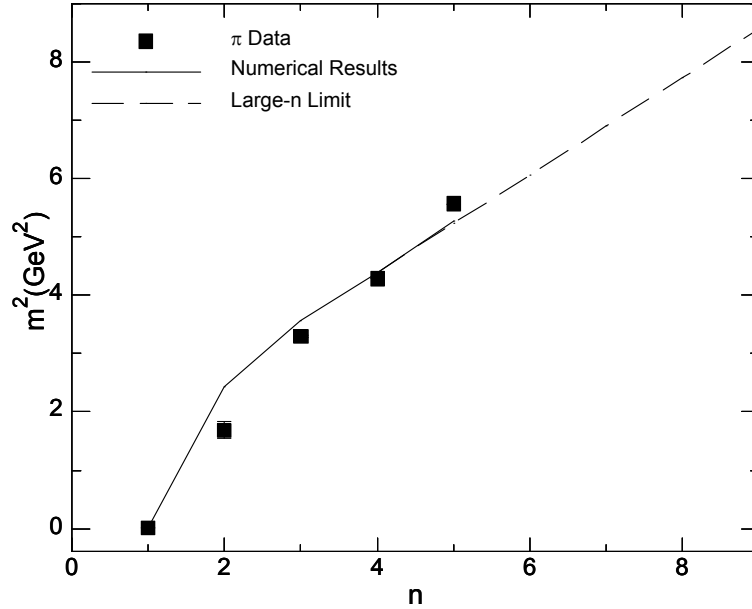


Figure 3.1: The pion mass spectrum calculated in the modified AdS/QCD model is plotted along with the experimental data [1]. The eigenvalues display two important characteristics of the experimental pion spectrum: (1) light ground state and (2) a large gap between the ground state and the first excited state. The large- $n$  mass trajectory clearly follows our calculated eigenvalues from  $n \approx 4$  when our numerical routine inadequately follows the oscillations of the higher eigenfunctions.

### 3.2.4 Gell-Mann–Oakes–Renner Relation

The mass of the ground-state pion is related to the spontaneous breaking of chiral symmetry. Whenever a continuous symmetry is spontaneously broken, a massless particle appears – this result is known as Goldstone’s Theorem. The resulting particles are known as Goldstone bosons, or, if the symmetry is also broken explicitly, they are called pseudo-Goldstone bosons because they are not truly massless. The ground-state pion is the pseudo-Goldstone boson of chiral symmetry, which is the reason for its small mass in comparison to the other meson ground states. The Gell-Mann–Oakes–Renner relation is a formula relating the mass of the pion to the quark mass and the chiral condensate [45].

A quark-antiquark pair may spontaneously appear from the vacuum, in keeping with Heisenberg’s Uncertainty Principle. This pair will have zero total momentum and angular momentum, resulting that a left-handed quark will be paired with a right-handed antiquark, and vice versa, resulting in a nonzero net chirality. The QCD vacuum contains a condensate of these chiral quark-antiquark states, resulting in a nonzero vacuum expectation value for the chiral operator

$$\langle \bar{q}q \rangle = \langle \bar{q}_L q_R + \bar{q}_R q_L \rangle \neq 0. \quad (3.135)$$

Thus, the vacuum mixes the two quark helicities, causing the light quarks to acquire an effective mass as they move through and interact with the vacuum.

We can explore the relationship of spontaneous chiral symmetry breaking to the pion by parameterizing the matrix element of the axial current

$$j^{\mu 5a}(x) = \bar{q}\gamma^\mu\gamma^5\tau^a q \quad (3.136)$$

between the vacuum and a pion [46]

$$\langle 0 | j^{\mu 5a}(x) | \pi^b(p) \rangle = -ip^\mu f_\pi \delta^{ab} e^{-ip \cdot x}, \quad (3.137)$$

where  $f_\pi$  is known as the *pion decay constant* and has dimensions of mass. Taking the derivative  $\partial_\mu$  of the left-hand side of (3.137) is equivalent to contracting the right-hand side with  $p_\mu$ , yielding

$$\langle 0 | \partial_\mu j^{\mu 5a}(x) | \pi^b(p) \rangle = -p_\mu (ip^\mu f_\pi \delta^{ab} e^{-ip \cdot x}) = -ip^2 f_\pi \delta^{ab} e^{-ip \cdot x}. \quad (3.138)$$

Taking  $x = 0$ , and making the substitution  $p^2 = m_\pi^2$  for an on-shell pion, we obtain the so-called partially conserved axial current (PCAC) relation

$$\partial_\mu j^{\mu 5a} = f_\pi m_\pi^2 \pi^a. \quad (3.139)$$

In the limit of zero quark mass, the axial current is exactly conserved, i.e.  $\partial_\mu j^{\mu 5}(x) = 0$ , implying that  $m_\pi^2 = 0$ , and the pion is massless, as required by Goldstone's theorem.

When the quark masses are not equal to zero, the chiral symmetry is said to be broken explicitly. This is because the QCD Lagrangian contains terms of the form  $m_q \bar{q}q = m_q(\bar{q}_L q_R + \bar{q}_R q_L)$ , which requires a mixing of the chiral components. The axial field is no longer exactly conserved, becoming

$$\partial_\mu j^{\mu 5a}(x) = i\bar{q}\{M, \tau^a\}\gamma^5 q, \quad (3.140)$$

where  $M$  is the mass matrix

$$M = \begin{pmatrix} m_u & 0 \\ 0 & m_d \end{pmatrix}. \quad (3.141)$$

Using this equation with 3.138, we find

$$\langle 0 | \partial_\mu j^{\mu 5a}(0) | \pi^v(p) \rangle = -p^2 f_\pi \delta^{ab} = \langle 0 | i\bar{q}\{M, \tau^a\}\gamma^5 q | \pi^b(p) \rangle. \quad (3.142)$$

We derive the Gell-Mann–Oakes–Renner relation using the argument presented in [47]. We calculate the quantity

$$I = \int d^4x e^{-ip \cdot x} \langle 0 | \text{Tr} \left( \partial^\mu j_\mu^{5a}(0) \partial^\nu j_\nu^{5b}(x) \right) | 0 \rangle. \quad (3.143)$$

Using the PCAC relation (3.139), we can substitute the pion operators and reduce the expression to the pion propagator,

$$I = f_\pi^2 m_p i^4 \int d^4x e^{-ip \cdot x} \langle 0 | \text{Tr} \left( \pi^a(0) \pi^b(x) \right) | 0 \rangle \quad (3.144)$$

$$= f_\pi^2 m_p i^4 \delta^{ab} i D_\pi(p). \quad (3.145)$$

Taking the limit  $p \rightarrow 0$ , the propagator becomes  $D_\pi = -1/m_\pi^2$ , and the expression for  $I$  reduces to

$$I = -i f_\pi^2 m_\pi^2. \quad (3.146)$$

Alternatively, we can calculate the quantity  $I$  by integrating by parts,

NEED TO FINISH GMOR.



### The Gell-Mann–Oakes–Renner Relation in Soft-Wall AdS/QCD

We now explore the Gell-Mann–Oakes–Renner relation in the soft-wall AdS/QCD model numerically. Inserting the established equivalence between the exponential and linear representations,  $\pi_e = \pi_l/\chi(z)$ , into the pion equation of motion (3.122), we obtain

$$\frac{g_5^2 L^2 \chi^2}{z^2} \partial_z \left( \frac{\pi_l}{\chi} \right) = m_\pi^2 \partial_z \varphi. \quad (3.147)$$

Following the method of [18], we construct a perturbative solution in  $m_\pi$  where  $\varphi(z) = A(0, z) - 1$  and use the established relation

$$f_\pi^2 = -L \frac{\partial_z A(0, z)}{g_5^2 z} \Big|_{z \rightarrow 0}. \quad (3.148)$$

Integrating (3.147) yields

$$\frac{\pi(z)}{\chi(z)} = m_\pi^2 \int_0^z du \frac{u^3}{\chi^2(u)} \frac{\partial_z A(0, u)}{g_5^2 u}. \quad (3.149)$$

The function  $u^3/\chi^2(u)$  has significant support only at small values of  $u \sim \sqrt{m_q/\sigma}$ , where we may use (3.148) to relate the derivative on  $A(0, u)$  to the pion decay constant, so that

$$\frac{\pi_l}{\chi} = -\frac{m_\pi^2 f_\pi^2}{2m_q \sigma}. \quad (3.150)$$

We find that letting  $\pi_l = -\chi(z)$  solves the axial-vector field's equation of motion

$$e^\Phi \partial_z \left( \frac{e^{-\Phi}}{z} \partial_z A_\mu(q, z) \right) - \frac{q^2}{z} A_\mu(q, z) - \frac{g_5^2 L^2 \chi^2}{z^3} A_\mu(q, z) = 0 \quad (3.151)$$

in the region of small  $z$  and as  $q \rightarrow 0$ . As a result, (3.150) becomes the expected Gell-Mann–Oakes–Renner (GOR) relation,

$$2m_q \sigma = m_\pi^2 f_\pi^2. \quad (3.152)$$

We solve for the ground-state pseudoscalar mass,  $m_\pi$ , for differing values of  $m_q$  to ensure that the numerical routine respects the GOR relation and gives a reasonable value for  $f_\pi$ . The results are plotted in Figure 3.2. We see linear behavior in the plot, indicating that as  $m_q \rightarrow 0$  we obtain a constant ratio of  $m_q/m_\pi^2$ . The slope of the line in Figure 3.2 suggests  $f_\pi = 90$  MeV, a result consistent with the input parameters as described in [28].

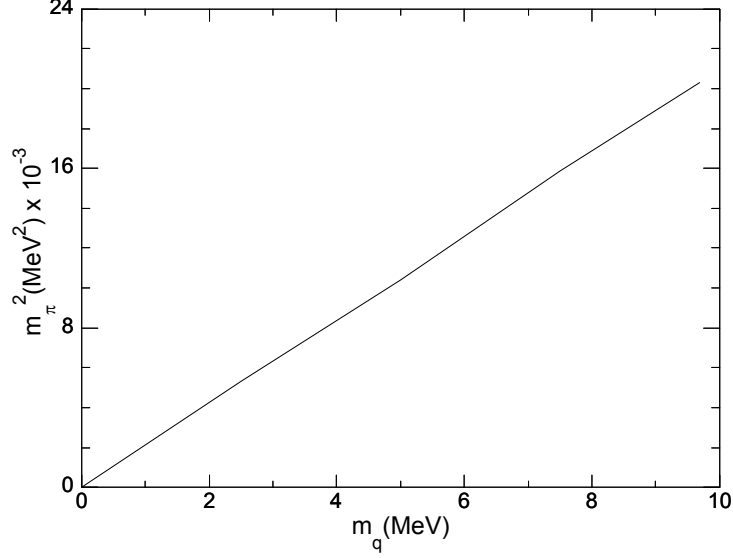


Figure 3.2: Plot of  $m_\pi^2$  vs  $m_q$  yields a straight line from which the pion decay constant  $f_\pi$  is calculated using (3.152).

### 3.3 Summary

In this chapter, we discussed the metric structure and field content of a soft-wall AdS/QCD model. We illustrated the field content of the simplest such model that describes light mesons and their spectra. We discussed the vacuum expectation value of the scalar field, which is related to the chiral symmetry breaking of the theory. The behavior of this chiral condensate was derived, and we discussed the shortcomings apparent in the simplest soft-wall models. We then derived the equations of motion for the scalar, vector, and axial-vector mesons.

We also discussed a modified soft-wall model that allows for the correct form of chiral symmetry breaking. In this model, we discussed the derivation of the pseudoscalar equations of motion, and the equivalence between the two common representations of the pseudoscalar field. Finally, we calculated the Gell-Mann–Oakes–Renner relation in the linear representation, showing that it is equivalent to that derived in the exponential representation. We confirmed the Gell-Mann–Oakes–Renner relation numerically in this

model, and calculated the value of  $f_\pi$ , in good agreement with the accepted value.

## Chapter 4

# Dynamical AdS/QCD

“When *I* use a word,” Humpty Dumpty said in rather a scornful tone,  
“it means just what I choose it to mean – neither more nor less.”

Lewis Carroll, *Through the Looking Glass*

In this chapter, we introduce the dynamical approach to soft-wall AdS/QCD, an attempt to be more rigorous than the version of the model discussed in Chapter 3. In the dynamical approach, the background fields including the dilaton and possibly other scalar fields are derived from a gravitational action, rather than parameterized and inserted to the model by hand. A typical setup for the dynamical AdS/QCD action is

$$\mathcal{S} = \int d^4x \sqrt{-g} e^{-2\Phi} \mathcal{L}_{grav} + \int d^4x \sqrt{-g} e^{-\Phi} \mathcal{L}_{meson} . \quad (4.1)$$

Note the difference in the overall exponential dilaton factor between the two sectors. This difference is due to the fact that  $\mathcal{L}_{grav}$  governs fields that exist in the bulk, where the strings are closed, and thus have two factors of the string coupling  $\lambda^2 \sim e^{-2\Phi}$ . The matter sector  $\mathcal{L}_{meson}$  is governed by open strings that attach to the  $N_c$  D-branes, so has only one factor of the string coupling [54]. This choice is intended to be evocative of a possible embedding in a non-critical string theory, but absent the details of the full string theory dual and the necessary compactification from ten dimensions to five, remains purely speculative. We will use a different choice of set-up for the action in Chapter 5.

We will discuss the basic setup of the model including the necessary and optional

terms in the gravitational action. There are a variety of approaches to describing the fields in the dynamical model. We will review the existing literature in this area and motivate the particular dynamical model that is described in detail in Chapter 5.

## 4.1 Gravity-Dilaton Action

The simplest dynamical AdS/QCD model includes the dilaton in the gravitational action [48, 33, 34]. We begin in the so-called string frame, where the geometry is purely  $AdS_5$ ,

$$ds^2 = \frac{L^2}{z^2}(-dt^2 + dx_i dx^i + dz^2), \quad (4.2)$$

where  $L$  is the AdS curvature radius, the index  $i$  runs over the three spatial dimensions, and  $z$  represents the extra dimension. The minimal gravitational action for a background dilaton is

$$\mathcal{S} = \frac{1}{16\pi G_5} \int d^5x \sqrt{-g} e^{-2\Phi} (R + \partial_M \Phi \partial^M \Phi - V(\Phi)), \quad (4.3)$$

where  $G_5$  is the five-dimensional Newton's constant,  $R$  is the Ricci curvature scalar,  $\Phi$  is the dilaton, and  $V(\Phi)$  is some unspecified potential involving the dilaton. The Ricci scalar is defined in Appendix B. For the  $AdS_5$  metric, the value of the Ricci scalar is  $R = -20/L^2$ . The overall constant factor in (4.3) is chosen to satisfy Einstein's equation, as discussed in Appendix B.

To derive the equations of motion that result from the gravitational action, it is convenient to perform a conformal transformation to the so-called Einstein frame, where the Ricci scalar appears without being multiplied by the dilaton pre-factor. The transformation to the Einstein frame is

$$g_{MN} = e^{4\Phi/3} \tilde{g}_{MN}, \quad (4.4)$$

where the tilde distinguishes the Einstein frame.

Let us examine how the conformal transformation affects each term of the action. In the string frame, there is an overall factor of

$$\sqrt{-g} = \sqrt{-\det(g^{MN})} = \left(\frac{1}{z}\right)^5 \quad (4.5)$$

In the Einstein frame, the overall factor becomes

$$\sqrt{-g_E} = \left( \frac{e^{-2\Phi/3}}{z} \right)^5 = \frac{1}{z^5} e^{-10\Phi/3}. \quad (4.6)$$

Comparing (4.6) to (4.5) it is evident that

$$\sqrt{-g_E} = e^{-10\Phi/3} \sqrt{-g}. \quad (4.7)$$

The potential term has the simplest transformation between the two frames,

$$\sqrt{-g} e^{-2\Phi} V(\Phi) = \sqrt{-g_E} e^{10\Phi/3} e^{-2\Phi} V(\Phi) \quad (4.8)$$

$$= e^{4\Phi/3} V(\Phi). \quad (4.9)$$

We define this as the Einstein frame potential, distinguished by a tilde,

$$\tilde{V} = e^{4\Phi/3} V. \quad (4.10)$$

The Ricci scalar is calculated using the same method as above, resulting in

$$\tilde{R} = -20/L^2 - \frac{4}{\sqrt{6}L^2} z \phi' - \frac{2}{L^2} z^2 \phi'^2 - \frac{8}{\sqrt{6}L^2} z^2 \phi'' \quad (4.11)$$

The transformation of the dilaton kinetic term is more involved.

The Einstein frame action becomes

$$\mathcal{S}_E = \frac{1}{16\pi G_5} \int d^5x \sqrt{-g_E} \left( \tilde{R} - \frac{1}{2} \partial_M \phi \partial_N \phi - \tilde{V}(\phi) \right), \quad (4.12)$$

where the dilaton is re-scaled  $\phi = \sqrt{8/3} \Phi$  for a canonical action.

The energy-momentum tensor derived from this action is

$$8\pi G_5 T_{MN} = \frac{1}{2} (\partial_M \phi \partial_N \phi - g_{MN} \mathcal{L}) \quad (4.13)$$

$$\mathcal{L} = \frac{1}{2} \partial_\lambda \phi \partial^\lambda \phi + \tilde{V}(\phi) \quad (4.14)$$

Two equations of motion are found by varying the Einstein frame action (4.26) with respect to the dilaton and the metric.

$$G_{MN} = 16\pi G_5 T_{MN} \quad (4.15)$$

$$\square \phi = \frac{\partial \tilde{V}}{\partial \phi}, \quad (4.16)$$

where  $\square \equiv \nabla_M \nabla^M$ , and  $\nabla_M$  is the covariant derivative with respect to the metric. It is useful to write (4.15) in the following combinations

$$\tilde{g}^{tt}G_{tt} - \tilde{g}^{zz}G_{zz} = 8\pi G_5(\tilde{g}^{tt}T_{tt} - \tilde{g}^{zz}T_{zz}) = \frac{1}{2}\tilde{g}^{zz}\phi'^2, \quad (4.17)$$

$$\tilde{g}^{tt}G_{tt} + \tilde{g}^{zz}G_{zz} = 8\pi G_5(\tilde{g}^{tt}T_{tt} + \tilde{g}^{zz}T_{zz}) = -\tilde{V}(\phi), \quad (4.18)$$

where we have made use of the fact that  $\tilde{g}^{tt} = -\tilde{g}^{zz}$ . Using the energy-momentum tensor defined in (4.13-4.14) and the Einstein metric defined in (4.2) and (4.4), the equations of motion become

$$\frac{z^2}{\sqrt{6}} \frac{d}{dz} \left( \frac{1}{z^2} \phi' \right) = 0. \quad (4.19)$$

$$e^{2\phi/\sqrt{6}} \frac{z^2}{L^2} \left[ \frac{\sqrt{6}}{2} \phi'' - \frac{3}{2} \phi'^2 - 3\sqrt{6} \phi' - \frac{12}{z^2} \right] = \tilde{V}(\phi) \quad (4.20)$$

$$e^{2\phi/\sqrt{6}} \frac{z^2}{L^2} \left[ \phi'' - 3\phi' \left( \frac{1}{z} + \frac{\phi'}{\sqrt{6}} \right) \right] = \frac{\partial \tilde{V}}{\partial \phi}. \quad (4.21)$$

Noting that we can re-write (4.10) in terms of the re-scaled dilaton  $\phi$  as  $\tilde{V} = e^{2\phi/\sqrt{6}}V$ , we see that (4.20-4.21) can be re-written in terms of the string frame potential

$$\frac{z^2}{L^2} \left[ \frac{\sqrt{6}}{2} \phi'' - \frac{3}{2} \phi'^2 - 3\sqrt{6} \phi' - \frac{12}{z^2} \right] = V(\phi) \quad (4.22)$$

$$\frac{z^2}{L^2} \left[ \phi'' - 3\phi' \left( \frac{1}{z} + \frac{\phi'}{\sqrt{6}} \right) \right] = \frac{\partial V}{\partial \phi}. \quad (4.23)$$

The gravity-dilaton action lacks a natural mechanism to describe chiral symmetry breaking, although the scalar vacuum expectation value can still be added by hand to the meson action [34]. Because of this obvious limitation in describing QCD phenomenology, we will not pursue this model further.

## 4.2 Gravity-Dilaton-Tachyon Action

A simple extension of the action in (4.3) is simply to include another scalar field in the action [29, 49, 50, 51]. It is hoped that with judicious choices for the behavior of this field, it may be possible to identify it as the chiral condensate field. We add a tachyonic field to the string frame action

$$\mathcal{S} = \frac{1}{16\pi G_5} \int d^5x \sqrt{-g} e^{-2\Phi} \left( R + \partial_M \Phi \partial^M \Phi - \partial_M \chi \partial^M \chi - V(\Phi, \chi) \right). \quad (4.24)$$

With the same conformal transformation (4.4), we can write the action (4.24) with the Einstein frame metric defined by (4.4). The Ricci scalar, dilaton kinetic term, and potential all transform in the same manner shown in Section 4.1. The transformation of the tachyon field is as follows

$$\begin{aligned}
\sqrt{-g}e^{-2\Phi}\partial_M\chi\partial^M\chi &= \sqrt{-g}e^{-2\Phi}g^{MN}\partial_M\chi\partial_N\chi \\
&= \sqrt{-g}e^{-2\Phi}\left(e^{-4\Phi/3}\tilde{g}^{MN}\right)\partial_M\chi\partial_N\chi \\
&= \left(e^{10\Phi/3}\right)\sqrt{-g_E}e^{-2\Phi}\left(e^{-4\Phi/3}\tilde{g}^{MN}\right)\partial_M\chi\partial_N\chi \\
&= \sqrt{-g_E}\partial_M\chi\partial^M\chi
\end{aligned} \tag{4.25}$$

The gravity-dilaton-tachyon action in the Einstein frame becomes

$$\mathcal{S}_E = \frac{1}{16\pi G_5} \int d^5x \sqrt{-g_E} \left( \tilde{R} - \frac{1}{2}\partial_M\phi\partial^M\phi - \frac{1}{2}\partial_M\chi\partial^M\chi - \tilde{V}(\phi, \chi) \right), \tag{4.26}$$

where again  $\tilde{V} = e^{4\Phi/3}V$ , and the dilaton is re-scaled  $\phi = \sqrt{8/3}\Phi$  for a canonical action.

The energy-momentum tensor derived from this action is similar to that found in (4.13-4.14), with the addition of the tachyon field

$$8\pi G_5 T_{MN} = \frac{1}{2}(\partial_M\phi\partial_N\phi + \partial_M\chi\partial_N\chi - g_{MN}\mathcal{L}) \tag{4.27}$$

$$\mathcal{L} = \frac{1}{2}\partial_\lambda\phi\partial^\lambda\phi + \frac{1}{2}\partial_\lambda\chi\partial^\lambda\chi + \tilde{V}(\phi, \chi). \tag{4.28}$$

Because of the presence of the additional tachyonic field, there is an additional equation of motion in comparison to the model in Section 4.1,

$$\tilde{g}^{tt}G_{tt} - \tilde{g}^{zz}G_{zz} = 8\pi G_5(\tilde{g}^{tt}T_{tt} - \tilde{g}^{zz}T_{zz}) = \frac{1}{2}\tilde{g}^{zz}(\phi'^2 + \chi'^2), \tag{4.29}$$

$$\tilde{g}^{tt}G_{tt} + \tilde{g}^{zz}G_{zz} = 8\pi G_5(\tilde{g}^{tt}T_{tt} + \tilde{g}^{zz}T_{zz}) = -\tilde{V}(\phi) \tag{4.30}$$

$$\square\phi = \frac{\partial\tilde{V}}{\partial\phi} \tag{4.31}$$

$$\square\chi = \frac{\partial\tilde{V}}{\partial\chi}. \tag{4.32}$$

Expanding these equations and writing in terms of the string frame potential  $V(\phi, \chi)$  yields

$$\frac{z^2}{\sqrt{6}}\frac{d}{dz}\left(\frac{1}{z^2}\phi'\right) = \chi'^2 \tag{4.33}$$



$$\frac{z^2}{L^2} \left[ \frac{\sqrt{6}}{2} \phi'' - \frac{3}{2} \phi'^2 - 3\sqrt{6} \phi' - \frac{12}{z^2} \right] = V(\phi, \chi) \quad (4.34)$$

$$\frac{z^2}{L^2} \left[ \phi'' - 3\phi' \left( \frac{1}{z} + \frac{\phi'}{\sqrt{6}} \right) \right] = \frac{\partial V}{\partial \phi} \quad (4.35)$$

$$\frac{z^2}{L^2} \left[ \chi'' - 3\chi' \left( \frac{1}{z} + \frac{\phi'}{\sqrt{6}} \right) \right] = \frac{\partial V}{\partial \chi}. \quad (4.36)$$

These equations are not all independent, however. Because the potential does not depend explicitly on the coordinate  $z$ , but only through the fields, the total derivative becomes

$$\frac{d}{dz} V(\phi, \chi) = \frac{\partial V}{\partial \phi} \phi'(z) + \frac{\partial V}{\partial \chi} \chi'(z). \quad (4.37)$$

This allows for the elimination of one of (4.35) or (4.36).

Let us examine the behavior of this model when the fields obey a power-law behavior. We make the ansatz

$$\chi(z) = \chi_0 z^n \quad (4.38)$$

for the behavior of the tachyonic field. Inserting this ansatz into (4.33) with the Dirichlet boundary condition  $\phi(0) = 0$  gives the solution for  $\phi$ ,

$$\phi(z) = \frac{n\sqrt{6}}{12(1+2n)} \chi_0^2 z^{2n}. \quad (4.39)$$

It was shown in [52, 29, 53] that such power-law behavior for the tachyonic field with  $n = 3$  or  $n = 1$  results in a mass term for  $\chi$  that implies  $m_\chi^2 L^2 = -3$ . This is the correct mass for the chiral condensate field that is dual to  $\langle \bar{q}q \rangle$ . In addition this power-law behavior is exactly the asymptotic behavior that it was argued the chiral field should assume. That is,  $\chi \sim z^3$  in the UV limit (in the limit of zero quark mass) and  $\chi(z) \sim z$  in the IR limit. This suggests that the tachyonic field can be identified as the chiral condensate.

However, this identification is of limited utility in the gravity-dilaton-tachyon model, as we can see by exploring the IR limit. Letting  $n = 1$ , we can see that the IR behavior of the dilaton is

$$\phi(z) = \frac{1}{6\sqrt{6}} \chi_0^2 z^2. \quad (4.40)$$

The string frame dilaton is given by  $\Phi = \lambda z^2$  in the IR limit, so the re-scaled dilaton becomes  $\phi = \sqrt{8/3} \lambda z^2$ . We see that the coefficient for the chiral field is determined

$$\chi_0 = 2\sqrt{6}\sqrt{\lambda} \quad (4.41)$$

and the axial-vector mass splitting in this model is set by the equation given by (3.76),

$$\Delta m^2 = \frac{g_5^2 \chi^2}{z^2} (z \rightarrow \infty) = g_5^2 \chi_0^2. \quad (4.42)$$

When the phenomenologically determined value for  $\lambda$  is inserted into this equation, the value that is calculated for  $\Delta m^2$  is too large by an order of magnitude.

Thus, we see that this gravity-dilaton-tachyon system fails because it does not allow separate parameters for the slope of the Regge trajectories and for the axial-vector mass splitting. Further, because (4.33) does not involve the scalar potential, there is no choice for the potential that will rectify this shortcoming of this model.

#### 4.2.1 Alternative Approach to Chiral Symmetry Breaking in Dynamical AdS/QCD

A different approach to including chiral symmetry breaking can be found in [31, 35]. Rather than placing a tachyon in the bulk (closed-string sector), this model keeps the gravity-dilaton action separate from the matter (open-string) sector of the action. It will be convenient to keep the string frame metric generic by writing it as

$$ds^2 = e^{2A_s(z)}(dx^2 + dz^2). \quad (4.43)$$

In a pure AdS metric,  $A_s(z) = -\ln(z/L)$ , and the AdS/CFT dictionary requires that the metric function take this form in the UV limit.

In the string frame, the gravity-dilaton action is written the same as (4.3),

$$\mathcal{S}_G = \frac{1}{16\pi G_5} \int d^5x \sqrt{-g} e^{-2\Phi} (R + 4\partial_M \Phi \partial^M \Phi - V_G(\Phi)), \quad (4.44)$$

while the matter action is written

$$\mathcal{S}_M = - \int d^5x \sqrt{-g} e^{-\Phi} \text{Tr} \left[ |DX|^2 + \frac{1}{2g_5^2} (F_A^2 + F_V^2) + V_M(|X|^2, \Phi) \right], \quad (4.45)$$

where  $V_M(|X|^2, \Phi)$  is some potential that could in principle involve both the scalar meson field and the dilaton. The scalar meson field  $X$  is a charged field, so it must appear in the potential only with an even exponent.

For the background dynamics, we must take the vacuum expectation value of both sectors and add them

$$\mathcal{S} = \langle \mathcal{S}_G \rangle + \frac{N_f}{N_c} \langle \mathcal{S}_M \rangle. \quad (4.46)$$

The factor of  $N_f/N_c$  included above represents the coupling of the open strings to the  $N_f$  D-branes that represent the flavored quarks and the  $N_c$  color D-branes [31]. The vacuum expectation value of  $\mathcal{S}_G$  is unchanged from (4.44), and

$$\langle \mathcal{S}_M \rangle = - \int d^5x \sqrt{-g} e^{-\Phi} \left( \frac{1}{2} \partial_M \chi \partial^M \chi + V_C(\chi, \Phi) \right), \quad (4.47)$$

where we have defined  $V_C = \text{Tr} V_M$ . In the Einstein frame, the total vacuum action becomes

$$S_{vac} = \frac{1}{16\pi G_5} \int d^5x \sqrt{g_E} \left[ \left( R_E - \frac{4}{3} \partial_M \Phi \partial^M \Phi - V_G^E(\Phi) \right) - \kappa e^{\Phi} \left( \frac{1}{2} \partial_M \chi \partial^M \chi + e^{\frac{4}{3}\Phi} V_C(\chi, \Phi) \right) \right]. \quad (4.48)$$

where  $\kappa = \frac{16\pi G_5 N_f}{L^3 N_c}$ . The equations of motion are derived as

$$-A_s'' + A_s'^2 + \frac{2}{3} \Phi'' - \frac{4}{3} A_s' \Phi' = \frac{\kappa}{6} e^{\Phi} \chi'^2, \quad (4.49)$$

$$\Phi'' + (3A_s' - 2\Phi') \Phi' - \frac{3\kappa}{16} e^{\Phi} \chi'^2 = \frac{3}{8} e^{2A_s - \frac{4}{3}\Phi} \frac{\partial}{\partial \Phi} \left( V_G + \kappa e^{\frac{7}{3}\Phi} V_C \right), \quad (4.50)$$

$$\chi'' + (3A_s' - \Phi') \chi' = e^{2A_s} \frac{\partial V_C}{\partial \chi}. \quad (4.51)$$

Examining (4.49) in the IR limit where  $\Phi = \lambda z^2$  with an AdS metric function  $A_s = -\ln z$ , we find that the chiral condensate takes the form

$$\chi(z) = \frac{12\sqrt{\pi\lambda}}{\kappa} \text{Erf} \left( \sqrt{\lambda} z \right), \quad (4.52)$$

meaning that in the IR limit  $\chi \rightarrow \text{const}$ , implying the restoration of chiral symmetry. To maintain the breaking of chiral symmetry, we must allow the metric function to deviate from pure AdS in the IR. In [31] it is suggested to take  $A_s' \rightarrow 0$  in the IR limit, reducing (4.49) to

$$\frac{2}{3} \Phi'' - \frac{\lambda}{6} e^{\Phi} \chi'^2 = 0, \quad (4.53)$$

which is solved by

$$\chi = \sqrt{8\lambda/\kappa} e^{-\Phi/2}. \quad (4.54)$$

The chiral field still becomes a constant in the IR, but it is shown in [31] that, with a constant metric function, this leads to the non-restoration of chiral symmetry in the

axial vector spectrum. The mass-splitting term in the Schrödinger-like potential for the axial-vector equation of motion becomes

$$m_A^2 - m_V^2 = g_5^2 e^{2A_s} \chi^2, \quad (4.55)$$

which becomes a constant in the large- $z$  limit, as required to match the constant axial-vector mass splitting for the large- $n$  states.

The authors of [31, 35] opt to solve (4.49-4.51) using a purely quadratic dilaton and parameterizing the chiral condensate to match the UV and IR limits. The metric function  $A_s(z)$  is then solved numerically to satisfy the background equations. For judicious choices of the parameters, this model gives good phenomenological results. However, the authors do not fully solve for the scalar potentials  $V_G$ ,  $V_C$ . It would be instructive to attempt to solve for these potentials, but this thesis will not pursue this model further.

### 4.3 Summary

In this chapter, we have introduced dynamical AdS/QCD, an approach intended to put AdS/QCD models on more consistent theoretical footing by deriving the background fields from a potential. We began by developing a simple gravity-dilaton action and showing how to transform between the string and Einstein frames. The equations of motion were derived in the Einstein frame. We also discussed the limitations of a gravity-dilaton model, namely the inability to model chiral symmetry breaking.

We then introduced two models that attempt to include chiral dynamics into a dynamical AdS/QCD model. The first model introduces a tachyon into the bulk, producing a gravity-dilaton-tachyon action. The asymptotic behavior and mass of this tachyonic field are appropriate for that of the chiral condensate field. However, we showed that under this assumption, it is not possible to include a separate parameter for the axial-vector mass splitting, so this model fails to produce the correct axial-vector meson spectrum, irrespective of the choice of scalar potential.

Finally, we introduced a model that introduces the chiral condensate in the open-string sector of the theory. We derived the equations of motion and showed that it is possible to get the correct axial-vector mass splitting if one allows the metric to

deviate from anti-de Sitter space in the IR. However, previous work on this model has used a parameterization for the dilaton and chiral condensate fields, and the full scalar potential for this model has not been determined.

In the next chapter, we will introduce a dynamical model of AdS/QCD that includes three background fields in the bulk. This will allow for the correct form of chiral symmetry breaking, and the calculation of all meson spectra. A full expression for the scalar potential will also be derived.

## Chapter 5

# Dynamical Three-Field Model

Think you're escaping and run into yourself.  
Longest way round is the shortest way home.

James Joyce, *Ulysses*

In this chapter, we expand upon the dynamical models of AdS/QCD introduced in Chapter 4. We pay particular attention to developing a model with the correct form of chiral symmetry breaking, as exemplified by the mass splitting between the axial-vector and vector meson sectors. To this end, we introduce a field that has not been included in the models presented so far – the glueball field. This field has fluctuations whose mass eigenvalues can be calculated, as well as a condensate that must be included in the analysis of the background fields. We will show that this additional background field allows the freedom to separate the parameter setting the overall mass scale of the meson spectra from the parameter controlling the axial-vector mass spectrum.

In contrast to the dynamical models in Chapter 4, we will not separate the action into gravitational and matter sectors. Rather, we will place all of the fields of the model in the bulk,

$$\mathcal{S} = \int d^4x e^{-2\Phi} (\mathcal{L}_{grav} + \mathcal{L}_{meson}). \quad (5.1)$$

This is in keeping with the original AdS/QCD models [18, 21], which placed the meson fields in the bulk. It is possible that one setup or the other may be easier to embed in string theory, but without such an argument, the choice is motivated by phenomenology. This model allows for good phenomenological results while also allowing the metric to

remain purely anti-de Sitter.

In this chapter, we derive the equations of motion for this three-field model. We construct a potential for the background fields that accounts for their asymptotic behavior. Using this potential, we parameterize solutions to the background fields that numerically solve the background equations. There is an additional term in the potential that is determined numerically and fit as a function of the dilaton. In Chapter 6, we will calculate the meson spectra that result from this model.

## 5.1 Review and Motivation

We assume that four-dimensional QCD can be modeled by the following five-dimensional action, written in the string frame:

$$\begin{aligned} \mathcal{S} = & \frac{1}{16\pi G_5} \int d^5x \sqrt{-g} e^{-2\Phi} \left( R + 4\partial_M \Phi \partial^M \Phi \right. \\ & \left. - \text{Tr} \left[ |DX|^2 + \partial_M \mathcal{G} \partial^M \mathcal{G} + \frac{1}{2g_5^2} (F_A^2 + F_V^2) + V_m(\Phi, X^2, \mathcal{G}) \right] \right). \end{aligned} \quad (5.2)$$

Here  $\Phi$  is the dilaton and the metric is pure AdS,  $g_{MN} = z^{-2} \eta_{MN}$ , with the AdS curvature defined to be unity. The constant  $g_5^2 = 12\pi^2/N_c$ , where  $N_c$  is the number of colors. The covariant derivative is defined as  $D_M = \partial_M + i[V_M, X] - i\{A_M, X\}$ . The scalar field  $X$ , which is dual to the  $\bar{q}q$  operator, obtains a  $z$ -dependent vacuum expectation value (VEV)

$$\langle X \rangle = \frac{\chi(z)}{2} I, \quad (5.3)$$

where  $I$  is the  $2 \times 2$  identity matrix. The glueball field  $\mathcal{G}$  similarly obtains a  $z$ -dependent VEV,  $G(z)$ . We examine the background dynamics of the fields

$$\mathcal{S} = \frac{1}{16\pi G_5} \int d^5x \sqrt{-g} e^{-2\Phi} \left( R + 4\partial_M \Phi \partial^M \Phi - \frac{1}{2} \partial_M \chi \partial^M \chi - \frac{1}{2} \partial_M G \partial^M G - V(\Phi, \chi, G) \right), \quad (5.4)$$

where  $V = \text{Tr}[V_m]$ . The scalar fields  $\Phi, \chi, G$  are dimensionless.

It is easier to search for the background fields in the Einstein frame, where the vacuum action takes the canonical form

$$\mathcal{S}_E = \frac{1}{16\pi G_5} \int d^5x \sqrt{-\tilde{g}} \left( \tilde{R} - \frac{1}{2} \partial_M \phi \partial^M \phi - \frac{1}{2} \partial_M \chi \partial^M \chi - \frac{1}{2} \partial_M G \partial^M G - \tilde{V}(\phi, \chi, G) \right). \quad (5.5)$$

The tilde distinguishes the two frames, with  $\tilde{V} = e^{4\Phi/3}V$ , and the dilaton is rescaled for a canonical action  $\phi = \sqrt{8/3}\Phi$ . The string and Einstein frame metrics are related by the conformal transformation

$$g_{MN} = e^{2\phi/\sqrt{6}} \tilde{g}_{MN}. \quad (5.6)$$

Previous work showed how to construct a potential for a gravity-dilaton-chiral system without the glueball condensate. We examine the behavior assuming that the fields have power-law behavior, which is accurate in both the UV and IR limits [49]. One of the equations of motion is independent of the choice of potential,

$$\dot{\chi}^2 = \frac{\sqrt{6}}{z^2} \frac{d}{dz} (z^2 \dot{\phi}). \quad (5.7)$$

To obtain linear confinement, the dilaton should have quadratic behavior in the IR limit,  $\phi(z) = \lambda z^2$ . The chiral field should have linear behavior in the IR,  $\chi(z) = Az$ , where  $A$  sets the mass splitting between the axial-vector and vector mesons for large radial quantum numbers  $n$ . This constant mass-splitting at large  $n$  occurs because of the non-restoration of chiral symmetry [55]. Inserting this into (5.7), we find that the chiral field behaves as

$$\chi(z) = 6^{3/4} \sqrt{\lambda} z, \quad (5.8)$$

which removes one of the independent parameters of the model in [28]. Using the phenomenological value of  $\lambda$ , which determines the slope of the radial Regge trajectories, we find a mass splitting that is much too large. Because this problem arises in the equation that is independent of the potential, this issue cannot be resolved by the choice of potential in models that do not consider the glueball condensate. Models that derive the field behavior using the superpotential method suffer from the same problem.

To resolve this problem, we consider the effects of the glueball condensate  $G$  on the background equations. This field must be linear in the IR for linear confinement, and behave as  $G \sim z^4$  in the UV to match the operator dimension in the AdS/CFT dictionary.

It is noted that the model proposed by Huang and Li [31, 35] accurately represents the non-restoration of chiral symmetry using a model with only two background fields, but their model differs from the work presented here in several respects. They place the meson fields and chiral dynamics in the open-string sector of the model. For linear



confinement, this requires that the chiral field approach a constant in the IR, which necessitates a modified metric to obtain the correct chiral dynamics. Our model allows the metric to remain purely AdS in the string frame. Finally, they do not determine an explicit form of the potential, which is the central goal of this work.

## 5.2 Construction of Potential

Consider the action in the Einstein frame (5.5). To simplify the equations of motion, we use a transformed potential,

$$V = e^{-2\phi/\sqrt{6}} \tilde{V}. \quad (5.9)$$

This is simply the potential in the string frame. We re-write it as

$$V = -12 + 4\sqrt{6}\phi + a_0\phi^2 + \frac{m_X^2}{2}\chi^2 + U. \quad (5.10)$$

Here  $U$  is more than quadratic in the fields. The AdS/CFT dictionary sets the mass for the fields according to the dimension of the dual operator,

$$m^2 L^2 = \Delta(\Delta - 4), \quad (5.11)$$

where  $L$  is the AdS curvature which we set to unity. The dimension of the  $q\bar{q}$  operator is 3, so  $m_X^2 = -3/L^2$ . The dilaton mass is undetermined and is not connected to the dimension of the corresponding operator, as discussed in [49]. It is related to the parameter  $a_0$  by  $a_0 = \frac{1}{2} [(m_\phi L)^2 - 8]$ . The potential should be an even function of  $\chi$ .

The equations of motion can be written as

$$\dot{\chi}^2 + \dot{G}^2 = \frac{\sqrt{6}}{z^2} \frac{d}{dz} (z^2 \dot{\phi}), \quad (5.12)$$

$$U = \frac{1}{2} \sqrt{6} z^2 \ddot{\phi} - \frac{3}{2} (z \dot{\phi})^2 - 3 \sqrt{6} z \dot{\phi} - 4 \sqrt{6} \phi - a_0 \phi^2 + \frac{3}{2} \chi^2, \quad (5.13)$$

$$\frac{\partial U}{\partial \phi} = 3 z \dot{\phi} - 2 a_0 \phi, \quad (5.14)$$

$$\frac{\partial U}{\partial \chi} = z^2 \ddot{\chi} - 3 z \dot{\chi} \left( 1 + \frac{z \dot{\phi}}{\sqrt{6}} \right) + 3 \chi, \quad (5.15)$$

$$\frac{\partial U}{\partial G} = z^2 \ddot{G} - 3 z \dot{G} \left( 1 + \frac{z \dot{\phi}}{\sqrt{6}} \right). \quad (5.16)$$

We assume that the potential has no explicit dependence on the coordinate  $z$ , so the equations 5.14-5.16 are not independent, and we can eliminate one.

### 5.2.1 Infrared Limit

The requirement of linear confinement requires a solution in the large  $z$  limit of the form

$$\phi = \lambda z^2, \quad (5.17)$$

$$\chi = Az, \quad (5.18)$$

$$G = Bz. \quad (5.19)$$

Substitution into (5.12) gives

$$A^2 + B^2 = 6\sqrt{6}\lambda. \quad (5.20)$$

The parameter  $\lambda$  is fixed by the slope of the linear trajectory and  $A$  is fixed by the axial-vector – vector mass difference. It is useful to write these as

$$\begin{aligned} A &= 6^{3/4}\sqrt{\lambda}\cos\theta, \\ B &= 6^{3/4}\sqrt{\lambda}\sin\theta, \end{aligned} \quad (5.21)$$

where  $\theta$  now becomes the parameter controlling the axial-vector – vector mass splitting. Inserting (5.19) into (5.13-5.16) suggests the following terms in our ansatz for the potential

$$U = a_1\phi\chi^2 + a_2\phi G^2 + a_3\chi^4 + a_4G^4 + a_5\chi^2G^2 + a_6G^2\tanh(g\phi). \quad (5.22)$$

We see that there must be a  $G^2$  term in the IR limit, but this is forbidden in the weak-field limit because the glueball condensate field is massless. To circumvent this, we propose the term  $G^2\tanh(g\phi)$  with  $g > 0$ . In the weak field limit this goes to  $g\phi G^2$ , which is acceptable. The tanh is suggested by 5.9, and it provides a rapid exponential transition from the weak field to the strong field limits that is supported by phenomenology. By substitution one finds the following constraints on the parameters:

$$\begin{aligned} U &\rightarrow 6 + a_0 + 6\sqrt{6}(\cos^2\theta a_1 + \sin^2\theta a_2) \\ &+ 6^3(\cos^4\theta a_3 + \sin^4\theta a_4 + \cos^2\theta \sin^2\theta a_5) = 0, \end{aligned} \quad (5.23)$$

$$\frac{\partial U}{\partial \chi} \rightarrow 2a_1 + 24\sqrt{6}\cos^2\theta a_3 + 12\sqrt{6}\sin^2\theta a_5 + \sqrt{6} = 0, \quad (5.24)$$

$$\frac{\partial U}{\partial G} \rightarrow 2a_2 + 24\sqrt{6}\sin^2\theta a_4 + 12\sqrt{6}\cos^2\theta a_5 + \sqrt{6} = 0, \quad (5.25)$$

$$\frac{\partial U}{\partial G} \rightarrow a_6 = -\frac{3}{2}. \quad (5.26)$$

We have chosen to exclude (5.14) because it is not independent. The parameter  $a_6$  is determined, and the others will be determined by an examination of the UV limit.

### 5.2.2 Ultraviolet Limit

Next we look for a solution in the small  $z$  limit. The AdS/CFT dictionary dictates that the leading-order UV behavior of the chiral and glueball condensate fields is determined by their dimension. Note also that we are working in the chiral limit where the quark mass is zero. We start by examining only the leading-order terms

$$\chi = \Sigma_0 z^3, \quad (5.27)$$

$$G = G_0 z^4. \quad (5.28)$$

Substitution into (5.12) and imposing the boundary condition  $\phi(0) = 0$  gives

$$\phi = \frac{\sqrt{6}}{28}\Sigma_0^2 z^6 + \frac{\sqrt{6}}{27}G_0^2 z^8. \quad (5.29)$$

Substitution of the desired solution into eqs. (5.13)-(5.16) results in

$$\tilde{U} = -\frac{3}{2}(z\dot{\phi})^2 - a_0\phi^2 \quad (5.30)$$

$$\frac{\partial \tilde{U}}{\partial \phi} = \frac{\sqrt{6}}{14}(9 - a_0)\Sigma_0^2 z^6 + \frac{2\sqrt{6}}{27}(12 - a_0)G_0^2 z^8 \quad (5.31)$$

$$\frac{\partial \tilde{U}}{\partial \chi} = -9\Sigma_0 \left( \frac{3}{14}\Sigma_0^2 + \frac{8}{27}G_0^2 z^2 \right) z^9 \quad (5.32)$$

$$\frac{\partial \tilde{U}}{\partial G} = -12G_0 \left( \frac{3}{14}\Sigma_0^2 + \frac{8}{27}G_0^2 z^2 \right) z^{10} \quad (5.33)$$

By substitution one finds the following constraints on the parameters:

$$\frac{\partial \tilde{U}}{\partial \phi} \rightarrow 3a_0 + 7\sqrt{6}a_1 - 27 = 0 \quad (5.34)$$

$$\text{and } 4a_0 + 9\sqrt{6}(a_2 + ga_6) - 48 = 0 \quad (5.35)$$

$$\frac{\partial \tilde{U}}{\partial \chi} \rightarrow \sqrt{6}a_1 + 56a_3 + 27 = 0 \quad (5.36)$$

$$\text{and } \sqrt{6}a_1 + 27a_5 + 36 = 0 \quad (5.37)$$

$$\frac{\partial \tilde{U}}{\partial G} \rightarrow \sqrt{6}(a_2 + ga_6) + 28a_5 + 36 = 0 \quad (5.38)$$

$$\text{and } \sqrt{6}(a_2 + ga_6) + 54a_4 + 48 = 0 \quad (5.39)$$

Using only this leading-order behavior in (5.13-5.16), the system of equations is inconsistent, as there are more equations from matching powers of  $z$  than unknown parameters. There are three equations from the IR limit and 6 equations from the UV limit, for a total of nine equations to be solved by only 8 parameters,  $a_0 - a_5$ ,  $a_8$  and  $g$ . To solve this problem, consider adding a term  $\Sigma_n z^n$  to  $\chi$ . Substituting into (5.12) and keeping only the lowest-order cross-term we find the additional term in  $\phi$

$$\Delta\phi = \frac{\sqrt{6}n\Sigma_0\Sigma_n}{(n+4)(n+3)}z^{n+3}. \quad (5.40)$$

From (5.13) we find that

$$U = -\frac{3}{2}(z\dot{\phi})^2 - a_0\phi^2 + 3\frac{n^3 - 13n + 12}{(n+4)(n+3)}\Sigma_0\Sigma_n z^{n+3}. \quad (5.41)$$

Since the  $\phi^2$  terms start out as  $z^{12}$ ,  $z^{14}$ ,  $z^{16}$ , and so do the terms in the potential, the  $n$  can only take the values 9, 11, etc. This term contributes only to the equation for  $\partial U/\partial \chi$ .

$$\frac{\partial U}{\partial \chi} = -9\Sigma_0 \left( \frac{3}{14}\Sigma_0^2 + \frac{8}{27}G_0^2 z^2 \right) z^9 + (n-3)(n-1)\Sigma_n z^n. \quad (5.42)$$

By power counting both  $n = 9$  and  $n = 11$  can contribute.

There could also be higher order terms in  $G$  such as  $G_m z^m$ . This leads to the additional term in  $\phi$

$$\Delta\phi = \frac{8mG_0G_m}{\sqrt{6}(m+5)(m+4)}z^{m+4}. \quad (5.43)$$

It contributes to the equation for  $\partial U/\partial G$  as

$$\frac{\partial U}{\partial G} = -12G_0 \left( \frac{3}{14}\Sigma_0^2 + \frac{8}{27}G_0^2 z^2 \right) z^{10} + m(m-4)G_n z^m. \quad (5.44)$$

The choice  $m = 8$  is not possible as there is no term of the same order to balance it. Terms with  $m = 10$  and  $m = 12$  are possible. These new terms cannot affect the

equation for  $\partial U/\partial\phi$  nor can they contribute to the equation for  $\partial U/\partial\chi$ . Considering higher order terms in both  $\chi$  and  $G$  leads to

$$U = -\frac{3}{2}(z\dot{\phi})^2 - a_0\phi^2 + 3\frac{n^3 - 13n + 12}{(n+4)(n+3)}\Sigma_0\Sigma_n z^{n+3} + \frac{4m(m-4)}{m+4}G_0G_m z^{m+4}. \quad (5.45)$$

The appearance of these terms can be understood by writing the following schematic expansions.

$$\begin{aligned}\chi &\sim \Sigma_0 z^3 + \Sigma_0^3 z^9 + G_0^2 \Sigma_0 z^{11} + \dots \\ G &\sim G_0 z^4 + \Sigma_0^2 G_0 z^{10} + G_0^3 z^{12} + \dots\end{aligned}$$

That is,  $\chi$  is an odd function of  $\Sigma_0$  and  $G$  is an odd function of  $G_0$ . These are the symmetries in the equations of motion. They also follow the spirit of the AdS/CFT correspondence in terms of the dimensionality of the operators and the powers of  $z$ .

Including now  $m = 10$  and  $12$ , and  $n = 9$  and  $11$ , we have the following set of equations in the small  $z$  limit, where LHS and RHS refer to the left and right sides of the respective equations:

$$\begin{aligned}U_{\text{LHS}} &= 3\Sigma_0^4 z^{12} \left[ 4\frac{\Sigma_9}{\Sigma_0^3} - \frac{(54 + a_0)}{2^3 \cdot 7^2} \right] \\ &+ \frac{1}{7}\Sigma_0^2 G_0^2 z^{14} \left[ 120\frac{G_{10}}{\Sigma_0^2 G_0} + 120\frac{\Sigma_{11}}{\Sigma_0 G_0^2} - \frac{(72 + a_0)}{9} \right] \\ &+ 2G_0^4 z^{16} \left[ 12\frac{G_{12}}{G_0^3} - \frac{(96 + a_0)}{3^5} \right], \quad (5.46)\end{aligned}$$

$$\begin{aligned}U_{\text{RHS}} &= \Sigma_0^4 z^{12} \left[ \frac{\sqrt{6}}{28}a_1 + a_3 \right] \\ &+ \Sigma_0^2 G_0^2 z^{14} \left[ \frac{\sqrt{6}}{27}a_1 + \frac{\sqrt{6}}{28}(a_2 + ga_6) + a_5 \right] \\ &+ G_0^4 z^{16} \left[ \frac{\sqrt{6}}{27}(a_2 + ga_6) + a_4 \right]. \quad (5.47)\end{aligned}$$

$$\left(\frac{\partial U}{\partial\chi}\right)_{\text{LHS}} = 3\Sigma_0^3 z^9 \left[ -\frac{9}{14} + 16\frac{\Sigma_9}{\Sigma_0^3} \right] + 8\Sigma_0 G_0^2 z^{11} \left[ -\frac{1}{3} + 10\frac{\Sigma_{11}}{\Sigma_0 G_0^2} \right], \quad (5.48)$$

$$\left(\frac{\partial U}{\partial\chi}\right)_{\text{RHS}} = \Sigma_0^3 z^9 \left[ \frac{\sqrt{6}}{14}a_1 + 4a_3 \right] + \Sigma_0 G_0^2 z^{11} \left[ \frac{2\sqrt{6}}{27}a_1 + 2a_5 \right]. \quad (5.49)$$

$$\left(\frac{\partial U}{\partial G}\right)_{\text{LHS}} = 6\Sigma_0^2 G_0 z^{10} \left[ -\frac{3}{7} + 10 \frac{G_{10}}{\Sigma_0^2 G_0} \right] + 32 G_0^3 z^{12} \left[ -\frac{1}{9} + 3 \frac{G_{12}}{G_0^3} \right], \quad (5.50)$$

$$\left(\frac{\partial U}{\partial G}\right)_{\text{RHS}} = \Sigma_0^2 G_0 z^{10} \left[ \frac{\sqrt{6}}{14} (a_2 + g a_6) + 2a_5 \right] \quad (5.51)$$

$$+ G_0^3 z^{12} \left[ \frac{2\sqrt{6}}{27} (a_2 + g a_6) + 4a_4 \right]. \quad (5.52)$$

Altogether, from both the UV and IR limits, there are ten independent equations for the twelve parameters  $a_0 - a_6$ ,  $\Sigma_9$ ,  $\Sigma_{11}$ ,  $G_{10}$ ,  $G_{12}$ , and  $g$ . We take  $g$  as the free parameter to use as the rate of transition from small  $z$  to large  $z$ . The parameters in the potential are found to be

$$a_0 = \frac{3}{2} \frac{1}{6 + \sin^2 \theta} \left[ 120 + 62 \sin^2 \theta + 63\sqrt{6}g \sin^2 \theta \right], \quad (5.53)$$

$$a_1 = -\frac{3\sqrt{6}}{4} \frac{1}{6 + \sin^2 \theta} \left[ 12 + 8 \sin^2 \theta + 9\sqrt{6}g \sin^2 \theta \right], \quad (5.54)$$

$$a_2 = -\frac{\sqrt{6}}{4} \frac{1}{6 + \sin^2 \theta} \left[ 32 + 24 \sin^2 \theta + 3\sqrt{6}g(9 \sin^2 \theta - 2) \right], \quad (5.55)$$

$$2a_3 \cos^2 \theta + a_5 \sin^2 \theta = \frac{1}{24} \frac{1}{6 + \sin^2 \theta} \left[ 24 + 22 \sin^2 \theta + 27\sqrt{6}g \sin^2 \theta \right], \quad (5.56)$$

$$2a_4 \sin^2 \theta + a_5 \cos^2 \theta = \frac{1}{24} \frac{1}{6 + \sin^2 \theta} \left[ 20 + 22 \sin^2 \theta + 3\sqrt{6}g(9 \sin^2 \theta - 2) \right], \quad (5.57)$$

$$a_6 = -\frac{3}{2}. \quad (5.58)$$

The coefficients  $a_0$ ,  $a_1$ ,  $a_2$  and  $a_6$  are determined, while there are two equations for the three coefficients  $a_3$ ,  $a_4$  and  $a_5$ . That leaves  $a_5$  as a free parameter, to be fit numerically, along with  $g$ ,  $\theta$ ,  $G_0$ ,  $\Sigma$ , and  $\lambda$ .

### 5.3 Numerical Solution

Using the potential discussed, we seek a numerical solution that simultaneously satisfies the UV and IR limits. We use equations (5.12, 5.15, 5.16), which allows for an additional term in the potential,  $\Delta U$ , such that

$$\frac{\partial}{\partial \chi} \Delta U = \frac{\partial}{\partial G} \Delta U = 0, \quad (5.59)$$

which will be determined from the numerical solution.

The differential equations represent a stiff system, and treatment of the problem as an initial value problem leads to numerical instabilities. We treat it instead as a boundary value problem, using Dirichlet boundary conditions at both boundaries. A relaxation method is used in combination with input approximations for the background fields, which are then iterated to find a stable solution to the system with the given boundary conditions. Because the system is nonlinear, the solution found is not guaranteed to be unique.

The IR boundary is chosen to be sufficiently large to capture the infrared behavior and to give accurate Regge behavior for the large- $n$  radial excitations of the mesons. The UV boundary should approach zero, but it cannot reach zero because of the singularity in the equations of motion. This becomes a problem because equation (5.12) allows constant and divergent terms

$$\Delta\phi(z) = c_1 + c_2 z^{-1}. \quad (5.60)$$

Symbolically, these terms can be set to zero by enforcing the Dirichlet boundary condition  $\phi(0) = 0$ , but this is impossible to enforce numerically. Creative choice of UV boundary conditions can eliminate one, but not both, of these unwanted terms without affecting the chiral and glueball fields. The behavior of the numerical solutions suggests that the desired UV behavior is an unstable solution to the equations, and therefore difficult or impossible to find with this iterative method.

As an alternative to direct solution, we parameterize the fields as follows:

$$\Psi(z) = \psi(z)_{UV} f(z) + \psi(z)_{IR} (1 - f(z)). \quad (5.61)$$

Here  $f(z)$  is some function that transitions smoothly from 1 at small values of  $z$  to 0 at large  $z$ , while  $\psi(z)_{xy}$  represents the known UV and IR limits of the fields  $\phi$ ,  $\chi$ , and  $G$ . The switching functions need not be the same for each field. We choose

$$f_\phi(z) = e^{-(\beta_1 z)^{10}}, \quad (5.62)$$

$$f_\chi(z) = e^{-(\beta_2 z)^4}, \quad (5.63)$$

$$f_G(z) = e^{-(\beta_3 z)^5}. \quad (5.64)$$

The powers of the exponential are chosen to be greater than the known power-law behavior of the fields in the UV limit so as to not interfere with this behavior. The  $\beta_i$  will be determined by numerical fitting.

The chiral condensate  $\Sigma$  is set using the Gell-Mann–Oakes–Renner relation:

$$(m_u + m_d)\Sigma = f_\pi^2 m_\pi^2. \quad (5.65)$$

Using  $m_\pi = 139.6$  MeV,  $f_\pi = 92$  MeV, and  $m_u + m_d = 7.0$  MeV yields a value of  $\Sigma = (286 \text{ MeV})^3$ .

In all, we have eight parameters to be determined numerically. The first constraint is to obtain the best global visual fit to the vector and axial-vector meson spectra. We do not simply do a chi-squared fitting to the experimental data because the measurement error for the ground state  $\rho$  meson is so much smaller than for the others that this would effectively act as the only constraint. Second, we seek to minimize the error in the finite-difference approximations to equations 5.12, 5.15, and 5.16. This is done to an accuracy of one part in  $10^4$ .

Three of the parameters are most phenomenologically relevant:  $\lambda$ , which controls the slope of the meson spectra in the large- $n$  limit;  $\theta$ , which controls the mass splitting between the  $a_1$  and  $\rho$  mesons at large  $n$ , and  $\beta_2$ , which controls the location of the “bend” in the  $a_1$  spectrum. For each set of these parameters, the other parameters are determined by a routine that minimizes the error in the equations of motion. The parameters found are shown in Table 5.1.

$\lambda^{1/2}$	304 MeV	$\beta_1$	3.04 GeV
$G_0^{1/4}$	552 MeV	$\beta_2$	274 MeV
$\theta$	1.44	$\beta_3$	558 MeV
$g$	3.20	$a_5$	1.63

Table 5.1: Best fit parameters for the phenomenological model. The parameters  $\lambda, \theta$ , and  $\beta_2$  are chosen for the best visual fit to the  $\rho$  and  $a_1$  data, with the rest set by minimizing the error in the equations of motion (5.12), (5.15-5.16).

The background fields that are obtained from this analysis are shown in Figures 5.1-5.3. The asymptotic power-law behavior of the fields is evident in the linear portions of the log-log scale plots shown. The “transition” behavior is most evident in the



dilaton because of the large value of  $\beta_1$ , which controls the value of  $z$  at which the field transitions from the UV limit to the IR limit.

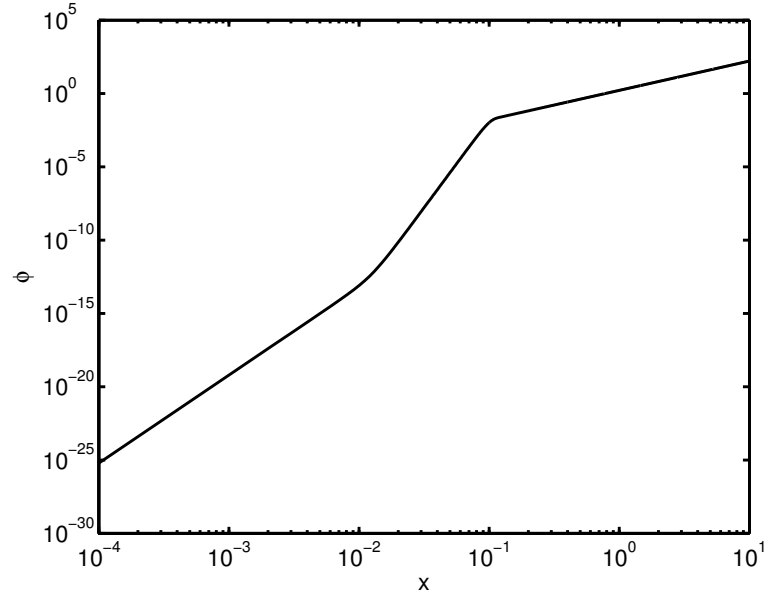


Figure 5.1: A plot of the dilaton field  $\Phi$  generated by the parameterization (5.63). The UV and IR asymptotic behavior is apparent. The coordinate  $x$  is a dimensionless re-scaling of the conformal coordinate,  $x = \sqrt{\lambda}z$ .

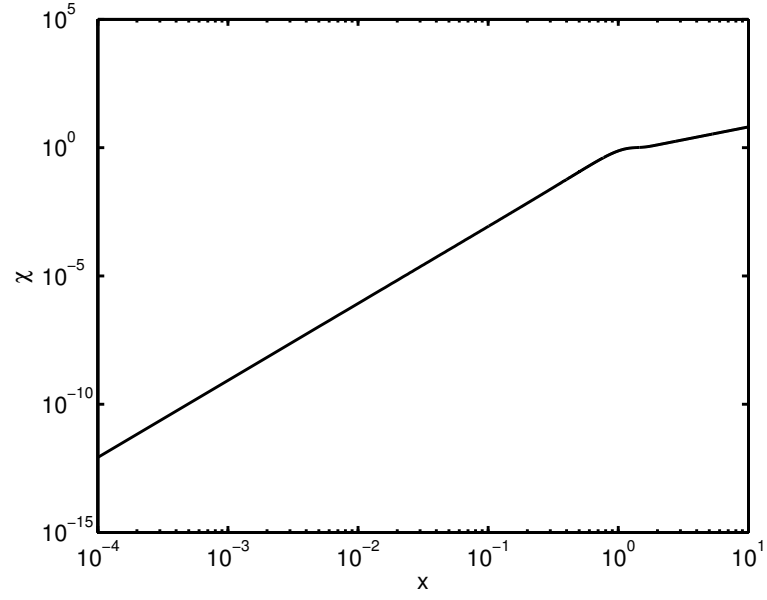


Figure 5.2: A plot of the chiral field  $\chi$  generated by the parameterization (5.64). The UV and IR asymptotic behavior is apparent, with a rapid transition between them. The coordinate  $x$  is a dimensionless re-scaling of the conformal coordinate,  $x = \sqrt{\lambda}z$ .

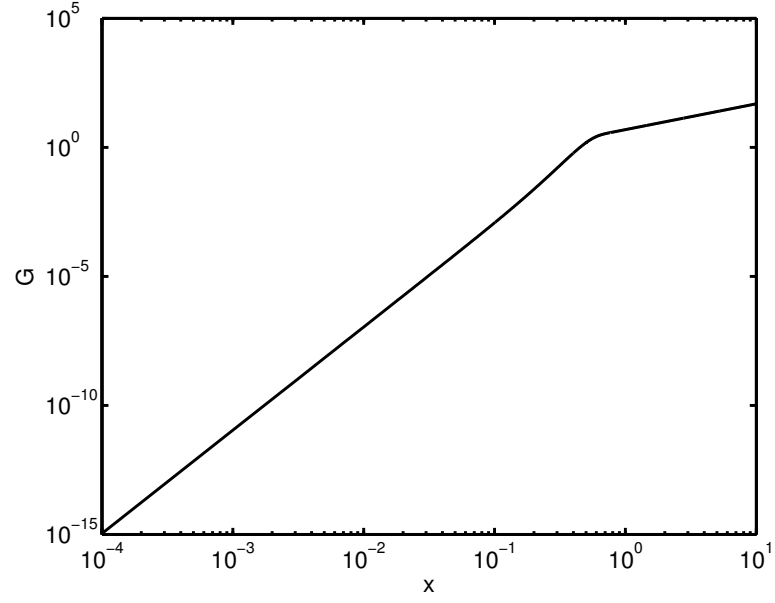


Figure 5.3: A plot of the glueball field  $G$  generated by the parameterization (5.64). The UV and IR asymptotic behavior is apparent, with a rapid transition between them. The coordinate  $x$  is a dimensionless re-scaling of the conformal coordinate,  $x = \sqrt{\lambda}z$ .

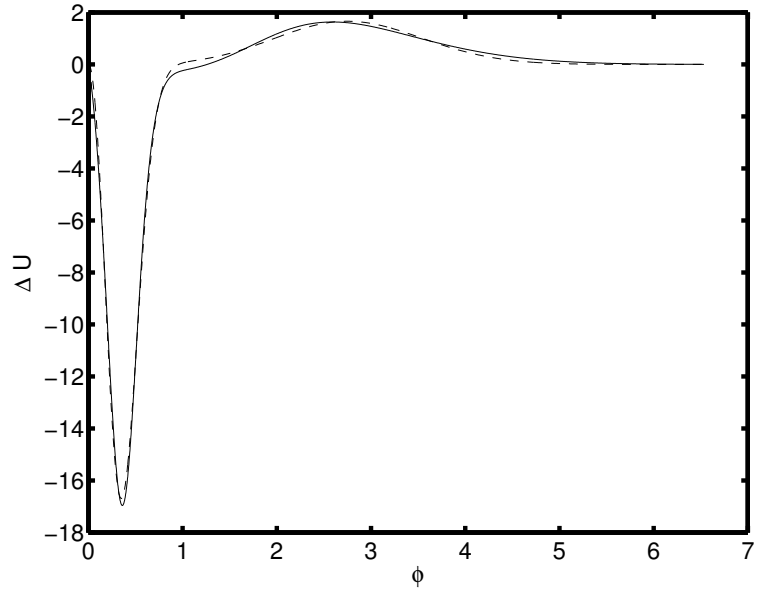


Figure 5.4: Plot of the “extra” term in the potential,  $\Delta U(\phi)$ . The solid line represents the numerical result, while the dashed line is the fitting of (5.66) using the parameters of Table 5.2.

We now analyze the “extra” term in the potential,  $\Delta U$ . We obtain this term numerically by subtracting the right-hand side of 5.13 from its left-hand side. This term can be approximated numerically as a function of the dilaton field,

$$\Delta U(\phi) = \alpha_1 \phi^2 e^{-(\phi-\gamma_1)^2/\delta_1} + \alpha_2 \phi^2 e^{-(\phi-\gamma_2)^2/\delta_2}. \quad (5.66)$$

The best-fit values for these parameters are shown in Table 5.2. The  $\Delta U$  as a function of  $\phi$  is shown in Figure 5.4.

$\alpha_1$	$-3.043 \times 10^1$	$\alpha_2$	$2.671 \times 10^{-4}$
$\gamma_1$	$7.086 \times 10^{-5}$	$\gamma_2$	$2.213 \times 10^{-2}$
$\delta_1$	$9.699 \times 10^{-5}$	$\delta_2$	$1.471 \times 10^{-2}$

Table 5.2: The dimensionless parameters for the fitting to  $\Delta U$ .

## 5.4 Summary

In this chapter we discussed the construction of a potential for the background fields of a soft-wall AdS/QCD model. The shortcomings of a dynamical AdS/QCD model containing only the dilaton and chiral condensate fields, are alleviated by adding a glueball condensate to the model. We analytically constructed a general potential  $U(\phi, \chi, G)$  that recovers the necessary asymptotic behavior of the background fields. Using this as a basis, we numerically constructed a potential that solves the selected background equations to within an accuracy of  $10^{-4}$ . There is an additional allowed term in the potential,  $\Delta U(\phi)$ , that does not affect the equations that were used in the numerical procedure. This term was found numerically, and fit as a function of the dilaton field.

The potential as constructed here is not guaranteed to be unique. If a different set of the background equations were chosen, the extra term would be expressed as a function of fields other than the dilaton. The parameterization in (5.63-5.64) could also be chosen differently, resulting in a different potential but making little difference to the resulting meson spectra. Finally, terms can be added that do not affect the equations of motion at all, namely, terms which satisfy

$$\Delta U = \Delta \frac{\partial U}{\partial \phi} = \Delta \frac{\partial U}{\partial \chi} = \Delta \frac{\partial U}{\partial G} = 0. \quad (5.67)$$

The background fields from this potential can be used to calculate mass spectra for the various light mesons. This work will be presented in the next chapter.

## Chapter 6

# Meson Spectra

If it disagrees with experiment it is wrong. In that simple statement is the key to science. It does not make any difference how beautiful your guess is. It does not make any difference how smart you are, who made the guess, or what his name is if it disagrees with experiment it is wrong. That is all there is to it. – Richard Feynman

In this chapter, we calculate the meson spectra for the vector, axial-vector, and pseudoscalar mesons from the dynamical three-field model of AdS/QCD introduced in the preceding chapter. The analysis is much the same as that presented in Chapter 3.

To calculate the spectra of the radial excitations of the mesons, we examine the relevant terms from the string frame action (5.2),

$$\mathcal{S}_{\text{meson}} = -\frac{1}{16\pi G_5} \int d^5x \sqrt{-g} e^{-2\Phi} \text{Tr} \left[ |DX|^2 + V_m(\Phi, X^2, \mathcal{G}) + \frac{1}{2g_5^2} (F_A^2 + F_V^2) \right]. \quad (6.1)$$

The  $2 \times 2$  field  $X$  contains the scalar and pseudoscalar fields  $(S, \pi)$ , as well as the VEV. We will use the exponential representation for the scalar field discussed in [4],

$$X_e = \left( S(x, z) + \frac{\chi(z)}{2} \right) I e^{2i\pi_e^a(x, z)t^a}, \quad (6.2)$$

where  $I$  is the  $2 \times 2$  identity matrix. The scalar potential  $V_m$  does not contribute to the equations of motion for the vector, axial-vector, or pseudoscalar mesons, although terms from the background potential  $U(\phi, \chi, G)$  will be useful in the pseudoscalar analysis.



## 6.1 Vector Sector

We find the equations of motion for the various meson fields by varying the meson action and performing a Kaluza-Klein decomposition. For the vector sector, the equation of motion takes the following form,

$$-\partial_z^2 V_n + \omega' \partial_z V_n = m_{V_n}^2 V_n, \quad (6.3)$$

where we have again defined  $\omega \equiv \Phi(z) + \log z$ . We can eliminate the first derivative of the field, bringing the equation of motion into Schrödinger-like form, using the substitution

$$V_n(z) = e^{\omega/2} v_n(z). \quad (6.4)$$

The equation of motion is now

$$-v_n'' + \left( \frac{1}{4} \omega'^2 - \frac{1}{2} \omega'' \right) v_n = m_{V_n}^2 v_n \quad (6.5)$$

These equations are analytically solvable in the IR limit, giving the same result found in Section 3, but full analysis requires the use of a numerical shooting method to find the mass eigenvalues. This model finds a better phenomenological fit than the results presented in [28], particularly for the ground state  $\rho$  meson, as shown in Figure 6.1.

n	$\rho$ experimental (MeV)	$\rho$ model
1	$775.5 \pm 1$	860
2	$1282 \pm 37$	1216
3	$1465 \pm 25$	1489
4	$1720 \pm 20$	1720
5	$1909 \pm 30$	1923
6	$2149 \pm 17$	2107
7	$2265 \pm 40$	2276

Table 6.1: The experimental [1] and predicted values for the masses of the vector mesons.

## 6.2 Axial-Vector Sector

Varying the action with respect to the axial vector field and performing a KK decomposition, the equation of motion becomes

$$-\partial_z^2 A_n + \omega' \partial_z A_n + \frac{g_5^2 \chi(z)^2}{z^2} = m_{A_n}^2 A_n. \quad (6.6)$$

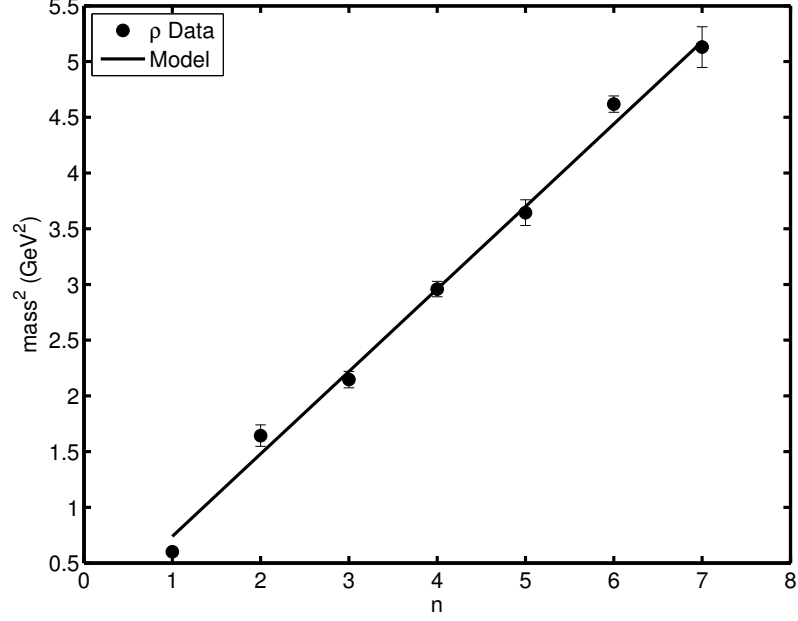


Figure 6.1: Comparison of the predicted mass eigenvalues for the vector sector with the experimental  $\rho$  meson spectrum [1].

To put the equation of motion in Schrödinger form, we make the substitution

$$A_n = e^{\omega/2} a_n, \quad (6.7)$$

yielding

$$-a_n'' + \left( \frac{1}{4} \omega'^2 - \frac{1}{2} \omega'' + g_5^2 \frac{L^2}{z^2} \chi^2(z) \right) a_n = m_{V_n}^2 a_n. \quad (6.8)$$

The results are plotted in Figure 6.2. The model fits the experimental data well, with the large- $n$  states following the linear trajectory, and the “bend” in the  $a_1$  spectrum at  $n = 2$ , which is controlled by the  $\beta_2$  parameter that was fit to this data in Section 5.3.

### 6.3 Pseudoscalar Sector

When using the exponential representation for the scalar field, the terms from the potential do not contribute to the equations of motion for the pion field. This can be

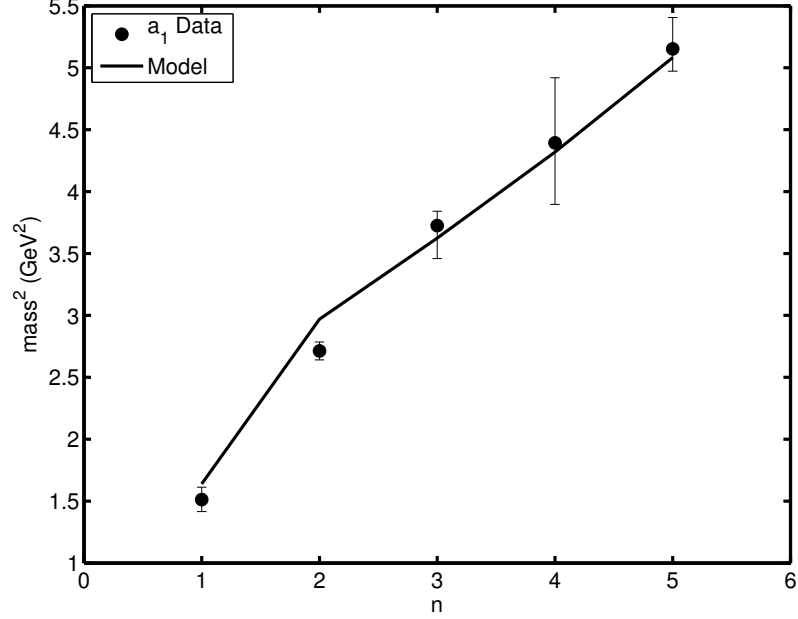


Figure 6.2: Comparison of the predicted mass eigenvalues for the axial-vector sector with the experimental  $a_1$  meson spectrum [1].

easily seen by noting that  $|X_e|^n$  does not contain any terms involving the pion field  $\pi_e$  field when  $n$  is even. We have required the potential to be an even function of  $X$ , so there are no such terms. This would seem to suggest that we use the exponential representation to calculate the pion mass spectrum. However, as noted in [4],  $\pi_e$  is extremely sensitive to boundary conditions, and the numerical results are not reliable. For this reason, we seek to work with an equation of motion written in the linear representation.

For convenience, we begin by deriving the equations of motion in the exponential representation. Working in the axial gauge  $A_z = 0$ , we rewrite the axial meson field in terms of its perpendicular and longitudinal components:  $A_\mu = A_{\mu\perp} + \partial_\mu\varphi$ . Only the longitudinal component of the axial field,  $\varphi$ , contributes to the pion equations of motion. We use (6.1), keeping only the relevant terms

$$\mathcal{L} = e^{-2\Phi} \sqrt{-g} \left[ \chi^2 (\partial_\mu \pi_e \partial^\mu \pi_e + \partial_\mu \varphi \partial^\mu \varphi - 2 \partial_\mu \pi_e \partial^\mu \varphi + \partial_z \pi_e \partial^z \pi_e) + \frac{1}{g_5^2} \partial_z \partial_\mu \varphi \partial^z \partial^\mu \varphi \right]. \quad (6.9)$$

n	$a_1$ experimental (MeV)	$a_1$ model
1	$1230 \pm 40$	1280
2	$1647 \pm 22$	1723
3	$1930^{+30}_{-70}$	1904
4	$2096 \pm 122$	2078
5	$2270^{+55}_{-40}$	2254

Table 6.2: The experimental [1] and predicted values for the masses of the axial-vector mesons.

Varying with respect to  $\varphi$  yields

$$e^{2\Phi} \partial_z \left( \frac{e^{-2\Phi}}{z} \partial_z \varphi \right) + \frac{g_5^2 \chi^2}{z^3} (\pi_e - \varphi) = 0, \quad (6.10)$$

while varying  $\pi_e$  gives

$$\frac{e^{2\Phi} z^3}{\chi^2} \partial_z \left( \frac{e^{-2\Phi} \chi^2}{z^3} \partial_z \pi_e \right) + m_n^2 (\pi_e - \varphi) = 0. \quad (6.11)$$

It was shown in [4] that the equations of motion are equivalent under the substitution  $\pi_e \rightarrow \pi_l / \chi(z)$ , so we make the appropriate substitution and expand the equations:

$$-\varphi'' + \left( 2\Phi' + \frac{1}{z} \right) \varphi' = \frac{g_5^2 \chi}{z^2} (\chi \varphi - \pi_l), \quad (6.12)$$

$$-\pi_l'' + \left( 2\Phi' + \frac{3}{z} \right) \pi_l' + \left( \chi'' - 2\chi' \Phi' - \frac{3\chi'}{z} \right) \frac{\pi_l}{\chi} = m_n^2 (\pi_l - \chi \varphi). \quad (6.13)$$

We can put these equations into Schödinger-like form with the following substitutions:

$$\varphi = e^{\omega/2} \varphi_n, \quad (6.14)$$

$$\pi_l = e^{\omega_s/2} \pi_n, \quad (6.15)$$

with  $\omega = 2\Phi + \ln z$  and  $\omega_s = 2\Phi + 3 \ln(z)$ . This yields

$$-\varphi_n'' + \left( \frac{1}{4} \omega'^2 - \frac{1}{2} \omega'' + \frac{g_5^2 \chi^2}{z^2} \right) \varphi_n = \frac{g_5^2 \chi}{z} \pi_n, \quad (6.16)$$

$$-\pi_n'' + \left( \frac{1}{4} \omega_s'^2 - \frac{1}{2} \omega_s'' + \frac{\chi''}{\chi} - \frac{2\chi' \Phi'}{\chi} - \frac{3\chi'}{z\chi} - m_n^2 \right) \pi_n = -m_n^2 \frac{\chi}{z} \varphi_n. \quad (6.17)$$

The dependence of these equations of motion on the scalar potential can be made explicit by using the background equation for the chiral field, written here in the string frame

$$z^2 \chi'' - 3z \chi' \left( 1 + \frac{z \Phi'}{\sqrt{6}} \right) = m_X^2 \chi + \frac{\partial U}{\partial \chi}. \quad (6.18)$$

Substituting, we can re-write (6.17) as

$$-\pi_n'' + \left( \frac{1}{4} \omega_s'^2 - \frac{1}{2} \omega_s'' + \frac{m_X^2}{z^2} + \frac{1}{z^2} \frac{\partial U}{\partial \chi} - m_n^2 \right) \pi_n = -m_n^2 \frac{\chi}{z} \varphi_n. \quad (6.19)$$

The results are shown in Figure 6.3 and in Table 6.3. It should be emphasized that all parameters were previously determined, so these are truly predictions of the model. The states with mass 2070 and 2360 MeV are listed in the PDG as further states, with less certainty assigned to them. We assume that these should be identified as the  $n = 4$  and  $n = 6$  states, leaving a vacancy at  $n = 5$  for a state still to be observed in future experiments. On the other hand, the PDG has two further states listed as X(2210) with unknown quantum numbers, either of which could be the  $n = 5$  state. We include this state in the figure and in the table, but it should be recognized that nothing in our work depends on this very speculative identification.

n	$\pi$ experimental (MeV)	$\pi$ model
1	140	0
2	$1300 \pm 100$	1580
3	$1816 \pm 14$	1868
4	$2070 \pm 35^*$	2078
5	$2210^{+79}_{-21} \dagger$	2230
6	$2360 \pm 25^*$	2389
7	—	2544
8	—	2686

Table 6.3: The experimental [1] and predicted values for the masses of the pseudoscalar mesons. The states marked with an \* appear only in the further states of the PDG. The state marked with a  $\dagger$  is an unconfirmed resonance X(2210) with unknown quantum numbers. Whether it really represents the  $n = 5$  state is pure speculation.

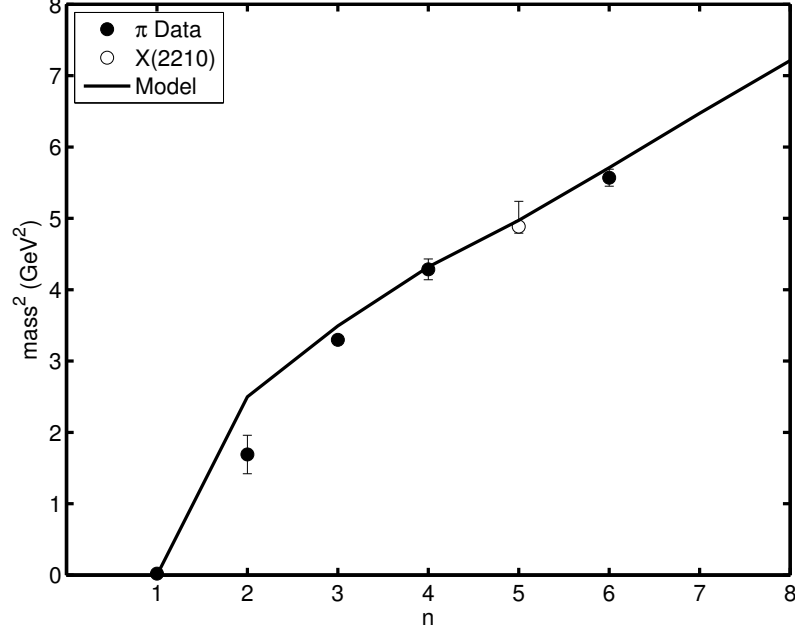


Figure 6.3: Comparison of the predicted mass eigenvalues for the pseudoscalar sector with the experimental  $\pi$  meson spectrum [1]. The states plotted here with  $n = 4$  and  $n = 6$  are identified as radial excitations of the pion only in the further states of the PDG. The unconfirmed state X(2210), with unknown quantum numbers, is plotted here as the  $n = 5$  state of the pion.

## 6.4 Summary

In this chapter, we calculated the meson spectra for the vector, axial-vector, and pseudoscalar mesons from the dynamical three-field AdS/QCD model discussed in Chapter 5. Portions of the vector and axial-vector spectra were used as inputs for the parameters used in the determination of the potential. While acknowledging these inputs, the overall goodness of fit is notable.

The pseudoscalar spectrum was not used to set any of the parameters in the model, so it can be regarded as a true prediction. The overall fit to the pion spectrum is quite good. The ground state pion is massless because the quark mass in this model is zero. We have speculatively identified the unconfirmed X(2210) state with unknown quantum numbers as the  $n = 5$  pion state. With this identification, and identifying the

pion states from the “further states” section of the PDG as the  $n = 4$  and  $n = 6$  states, the fit to the higher pion states is excellent. However, nothing in the analysis depends on this extremely tenuous identification.

The  $f_0$  meson spectrum is found by analyzing the fluctuations of the scalar field. However, the scalar field mixes with the glueball field, leading to a more complicated analysis. This analysis will be completed in the following chapter.

## Chapter 7

# Scalar and Glueball Sectors

The terms of the action relevant for the scalar meson and glueball fields have the form

$$\mathcal{S} = -\frac{1}{16\pi G_5} \int d^5x \sqrt{-g} e^{-2\Phi} \text{Tr} [ |DX|^2 + \partial_M \mathcal{G} \partial^M \mathcal{G} + V_m(\Phi, X^2, \mathcal{G}) ]. \quad (7.1)$$

Here, we are using the exponential representation for the scalar field,

$$X = \left( S(x, z) + \frac{\chi(z)}{2} \right) e^{2i\pi(x, z)}, \quad (7.2)$$

where  $S(x, z)$  is the scalar field fluctuations and  $\chi(z)$  is the chiral condensate. The glueball field  $\mathcal{G}$  also has a condensate, written as

$$\mathcal{G} = \left( H(x, z) + \frac{G(z)}{2} \right), \quad (7.3)$$

where  $H(x, z)$  are the fluctuations of the glueball field and  $G(z)$  is the glueball condensate.

The potential  $V_m$  is defined in such a way that  $\langle \text{Tr} V_m \rangle = V$ , where  $V$  is the potential for the background fields in the string frame,

$$V = -12 + 4\sqrt{6}\phi + a_0\phi^2 + \frac{m_X^2}{2}\chi^2 + U + \Delta U, \quad (7.4)$$

where  $\phi$  is the re-scaled version of the dilaton,  $\phi = \sqrt{8/3}\Phi$ . Here,  $U$  is more than quadratic in the fields,

$$U = a_1\phi\chi^2 + a_2\phi G^2 + a_3\chi^4 + a_4G^4 + a_5\chi^2 G^2 + a_6G^2 \tanh(\phi), \quad (7.5)$$



and  $\Delta U$  is assumed to be a function of  $\phi$  only.

The terms of  $\text{Tr}V_m$  that are relevant for the analysis of the scalar sector are those terms involving  $X, \mathcal{G}$ ,

$$\text{Tr}V_m \sim m_X^2 X^2 + 2a_1 \phi X^2 + 2a_2 \phi \mathcal{G}^2 + 8a_3 X^4 + 8a_4 \mathcal{G}^4 + 8a_5 X^2 \mathcal{G}^2 + 2a_6 \mathcal{G}^2 \tanh g\phi. \quad (7.6)$$

Expanding and keeping only terms that are quadratic in the fields  $S, H$ , we obtain

$$\text{Tr}V_m \sim (m_X^2 + 2a_1 \phi + 12a_3 \chi^2 + 2a_5 \mathcal{G}^2) S^2 + (2a_2 \phi + 12a_4 \mathcal{G}^2 + 2a_5 \chi^2 + 2 \tanh(g\phi)) H^2 + 4a_5 G \chi H S. \quad (7.7)$$

We can simplify the expression by writing

$$\text{Tr}V_m \sim \left( m_X^2 + \frac{\partial^2 U}{\partial \chi^2} \right) S^2 + \frac{\partial^2 U}{\partial G^2} H^2 + 4a_5 G \chi H S, \quad (7.8)$$

where

$$\frac{\partial^2 U}{\partial \chi^2} = 2a_1 \phi \chi + 4a_3 \chi^3 + 2a_5 \chi \mathcal{G}^2 \quad (7.9)$$

$$\frac{\partial^2 U}{\partial G^2} = 2a_2 \phi G + 4a_4 G^3 + 2a_5 \chi^2 G + 2a_6 G \tanh(g\phi) \quad (7.10)$$

The equations of motion are as follows. Varying with respect to  $S$  gives the equation of motion

$$\partial_z(z^{-3} e^{-2\Phi} S') - z^{-5} e^{-2\Phi} \left( m_X^2 + \frac{\partial^2 U}{\partial \chi^2} \right) S - 4a_5 z^5 e^{-2\Phi} G \chi H = -z^3 e^{-3} m_S^2 S. \quad (7.11)$$

Varying with respect to  $H$  yields the equation of motion

$$\partial_z(z^{-3} e^{-2\Phi} H') - z^{-5} e^{-2\Phi} \frac{\partial^2 U}{\partial G^2} H - 4a_5 z^5 e^{-2\Phi} G \chi S = -z^3 e^{-3} m_H^2 H. \quad (7.12)$$

To put the equations in Schrödinger form, we make the substitutions

$$S \rightarrow e^{\omega_s/2} S \quad (7.13)$$

$$H \rightarrow e^{\omega_s/2} H, \quad (7.14)$$

where  $\omega_s = 2\Phi + 3 \log z$ . This reduces the equations of motion to

$$-S'' + \left( \frac{1}{4} \omega_s'^2 - \frac{1}{2} \omega_s'' + m_X^2 - \frac{\partial^2 U}{\partial \chi^2} \right) S + 4a_5 G \chi H = m_S^2 S \quad (7.15)$$

$$-H'' + \left( \frac{1}{4} \omega_s'^2 - \frac{1}{2} \omega_s'' - \frac{\partial^2 U}{\partial G^2} \right) H + 4a_5 G \chi S = m_H^2 H \quad (7.16)$$

These equations need to be solved simultaneously for the eigenvalues  $m_S^2, m_H^2$ .

## Chapter 8

# Conclusion and Discussion

I'll go higher still!  
I'll build my throne higher! I can and I will!  
I'll call some more turtles. I'll stack 'em to heaven!  
I need 'bout five thousand, six hundred and seven!  
Dr. Seuss, "Yertle the Turtle"

This thesis began with an overview of gauge/gravity dualities and a motivational derivation of the anti-de Sitter space/conformal field theory correspondence. We sketched the string theoretical underpinnings for this duality and its potential usefulness for analyzing strongly-coupled regimes of gauge theories. With this in mind, we outlined the various applications to the study of quantum chromodynamics, specifically in the realm of hadronic physics, known as AdS/QCD.

In Chapter 3, we described the framework of a particular AdS/QCD model, known as the soft-wall model. This model uses a dilaton field to break the conformal symmetry of the five-dimensional AdS gravitational theory, in contrast to the simple cut-off of the conformal dimension used in the hard-wall model. Using the simplest form for the dilaton, we showed how to calculate the mass spectrum of the radially excited states of the light mesons. We showed the improvements that this simple soft-wall model exemplifies in comparison to the hard-wall model, as well as its shortcomings in modeling the ground states of the meson spectrum and in correctly describing the explicit and

spontaneous chiral symmetry breaking of QCD. We then introduced a modified soft-wall model with an improved description of chiral symmetry breaking. We showed the improved spectra for the scalar, vector, and axial-vector mesons, and explored the unique dynamics of the pseudoscalar sector. The phenomenological results of this model are quite good, but they still depend on an *ad hoc* parameterization of the dilaton and chiral condensate fields.

In Chapter 4, we introduced dynamical models of AdS/QCD, where all fields in the model are derived from a potential. The simplest models consist of a gravity-dilaton action, along with the matter fields that describe the meson content. We derived the equations of motion that result from examining the Einstein equation and varying the action with respect to the dilaton field in this model. We did not explore the phenomenology of this model, because it lacks a mechanism for chiral symmetry breaking. Next we described models with a gravity-dilaton-tachyon action, with the closed-string tachyon inserted to break chiral symmetry. We showed that the equations of motion for these models require a tachyon profile that cannot accurately model the chiral symmetry breaking, as evidenced by the inaccurate axial-vector mass splitting.

Finally, we summarized the results of a dynamical model that keeps the meson fields in the open-string sector, while introducing the gravity-dilaton action in the open-string sector. The background dynamics of the model are analyzed by examining the equations of motion for the background fields – the dilaton and the vacuum expectation value of the scalar meson field. To obtain the correct phenomenological results for the meson spectra, the chiral condensate field must have different behavior than the modified soft-wall model introduced in Chapter 3. Namely, the chiral condensate field becomes asymptotically constant in the infrared limit of the theory, which necessitates a warping of the metric in this regime. This model obtains good phenomenological results for the meson mass spectra, although it still makes use of a parameterization of the background fields, and the authors do not explicitly determine the scalar potential. We conclude this chapter by noting that it is impossible to obtain the correct mass spectra for all of the mesons within a model containing only the dilaton and chiral condensate background fields and maintaining a purely AdS metric.

In Chapter 5, we described in detail a dynamical AdS/QCD model including three background fields – the glueball condensate field is included along with the dilaton and

chiral condensate. In order to keep the string frame metric purely AdS, we chose to place all of the fields in the bulk, or closed-string sector, of the theory, in contrast to some models that place the matter fields in the open-string sector. From a practical standpoint, this modification keeps the overall dilaton factor the same in the string frame action, and simplifies the background equations of motion. This choice is in keeping with the phenomenological spirit of the original AdS/QCD models. Absent an action that is shown to be embeddable in string theory, there is no *a priori* reason to prefer one form of the action over the other. Instead, we make this choice based upon phenomenology and a desire to preserve the AdS metric.

After deriving the background equations of motion for this three-field model, we make an *ansatz* for the potential by examining the asymptotic behavior of the background fields. The infrared behavior of the background fields is determined by the confining behavior of the meson spectra, namely, the linear trajectories of the higher radial excitations and the constant mass-splitting between the higher radial excitations of the axial-vector and vector mesons. The ultraviolet asymptotics for the chiral and glueball condensates are set by the AdS/CFT dictionary (3.8) in relation to their corresponding field theory operator. We have set the UV behavior for the dilaton field by using the background equation that does not depend on the potential (5.12), rather than by identifying the dilaton with a particular field theory operator. By examining the behavior of the equations of motion in the UV and IR limits, we construct an *ansatz* for the potential that includes all allowed combinations of the background fields.

We then parameterize solutions for the background fields that result from the equations of motion including the full potential. Physical parameters are fit to the meson spectra, while the other free parameters are solved through a numerical minimization procedure that minimizes the error in the background equations. Our construction allows for an additional term that is a function of the dilaton only, which we find numerically and then fit as a function of the dilaton field. This work results in a potential that, while not guaranteed to be unique, does allow for solutions to the background field with the correct asymptotic behavior.

This model also yields good phenomenological results for the meson spectra, as shown in Chapter 6. The  $n \geq 3$  excitations of the  $\rho$  and  $a_1$  spectra were used to fit input parameters, as was the location of the “bend” of the  $a_1$  spectrum. The fit

to all of the experimental data is quite good, as shown in Figures 6.1 and 6.2. No additional parameters were used to fit the pion spectrum, which also showed good agreement, as seen in Figure 6.3. The ground state pion is massless, which is expected in a model where the quark mass is zero, as discussed in Section 3.2.4. Within this model, the equation of motion for the scalar  $f_0$  mesons mixes with the equation of motion for the scalar glueballs, as explored in Chapter 7. The mass spectra for the  $f_0$  mesons should be calculated and compared to experiment, while the scalar glueball spectrum can be compared to results from lattice QCD and other AdS/QCD models. An obvious improvement to this model would be to include a nonzero quark mass, which would allow for the calculation of the physical pion mass, and may alter other phenomenological results. A nonzero quark mass would change the UV asymptotics of the chiral condensate by adding a linear term, which would then affect the derivation of the potential.

This model can be extended to study QCD at finite temperature. It has been established experimentally that QCD matter changes phase at a critical temperature  $T_c$ , becoming a strongly-interacting plasma of freely associated quarks and gluons, rather than the bound states of hadrons [56, 57, 58]. Introducing a black hole into the gravitational side of the AdS/CFT correspondence allows for the calculation of thermodynamic quantities of the field theory using the established black hole thermodynamic relations [59, 60, 61, 62]. The temperature at which the black hole solution becomes energetically favored corresponds to  $T_c$ .

To analyze the thermodynamics of an AdS/CFT model, the string frame metric must be changed to an AdS-Schwarzschild metric,

$$ds^2 = \frac{L^2}{z^2} \left( -f(z)dt^2 + d\vec{x}^2 + \frac{dz^2}{f(z)} \right), \quad (8.1)$$

where  $f(z)$  is a function to be determined that sets the location of the horizon of the black hole. The presence of this metric function will modify the equations of motion (5.12-5.16), and must be solved for using these new background equations. The potential found in Section 5.2 can be used as a starting point for this analysis, and was part of the motivation for constructing such a potential.

With this finite-temperature AdS/CFT model in hand, it will be possible to study a variety of aspects of the deconfined phase of QCD matter, including the entropy, speed

of sound, and free energy. In addition, similar models have been used to study other phenomena relevant to heavy ion collisions, such as jet quenching. There have been other AdS/CFT models that analyze the finite temperature behavior, but these models suffer from inconsistencies with the zero-temperature meson spectra that the model in Chapter 5 was designed to address. A model that correctly describes the meson spectra and zero-temperature chiral symmetry breaking while also allowing for the investigation of finite-temperature effects would be an improvement upon existing work in the field.

In the research described in this thesis, we extended and improved upon the relatively simple AdS/QCD soft-wall model originally proposed in [21] and modified in [28]. We constructed a dynamical model with good phenomenological results for the mass spectra of mesons that is now ripe for extension into finite temperature. AdS/QCD is not yet a precision tool for the study of QCD, and a dual model that captures the full complexity of strongly-coupled QCD will require much further work and will likely necessitate the inclusion of stringy effects. However, we have found that a relatively simple model can give rich results for strongly coupled gauge theories.

# References

- [1] J. Beringer, J. F. Arguin, R. M. Barnett, K. Copic, O. Dahl, D. E. Groom, C. J. Lin, J. Lys, H. Murayama, C. G. Wohl, W. M. Yao, P. A. Zyla, C. Amsler, M. Antonelli, D. M. Asner, H. Baer, H. R. Band, T. Basaglia, C. W. Bauer, J. J. Beatty, V. I. Belousov, E. Bergren, G. Bernardi, W. Bertl, S. Bethke, H. Bichsel, O. Biebel, E. Blucher, S. Blusk, G. Brooijmans, O. Buchmueller, R. N. Cahn, M. Carena, A. Ceccucci, D. Chakraborty, M. C. Chen, R. S. Chivukula, G. Cowan, G. D'Ambrosio, T. Damour, D. de Florian, A. de Gouvêa, T. DeGrand, P. de Jong, G. Dissertori, B. Dobrescu, M. Doser, M. Drees, D. A. Edwards, S. Eidelman, J. Erler, V. V. Ezhela, W. Fetscher, B. D. Fields, B. Foster, T. K. Gaisser, L. Garren, H. J. Gerber, G. Gerbier, T. Gherghetta, S. Golwala, M. Goodman, C. Grab, A. V. Gritsan, J. F. Grivaz, M. Grünewald, A. Gurtu, T. Gutsche, H. E. Haber, K. Hagiwara, C. Hagmann, C. Hanhart, S. Hashimoto, K. G. Hayes, M. Heffner, B. Heltsley, J. J. Hernández-Rey, K. Hikasa, A. Höcker, J. Holder, A. Holtkamp, J. Huston, J. D. Jackson, K. F. Johnson, T. Junk, D. Karlen, D. Kirkby, S. R. Klein, E. Klempt, R. V. Kowalewski, F. Krauss, M. Kreps, B. Krusche, Yu. V. Kuyanov, Y. Kwon, O. Lahav, J. Laiho, P. Langacker, A. Liddle, Z. Ligeti, T. M. Liss, L. Littenberg, K. S. Lugovsky, S. B. Lugovsky, T. Mannel, A. V. Manohar, W. J. Marciano, A. D. Martin, A. Masoni, J. Matthews, D. Milstead, R. Miquel, K. Mönig, F. Moortgat, K. Nakamura, M. Narain, P. Nason, S. Navas, M. Neubert, P. Nevski, Y. Nir, K. A. Olive, L. Pape, J. Parsons, C. Patrignani, J. A. Peacock, S. T. Petcov, A. Piepke, A. Pomarol, G. Punzi, A. Quadt, S. Raby, G. Raffelt, B. N. Ratcliff, P. Richardson, S. Roesler, S. Rolli, A. Romanidou, L. J. Rosenberg, J. L. Rosner, C. T. Sachrajda, Y. Sakai, G. P. Salam, S. Sarkar, F. Sauli, O. Schneider, K. Scholberg, D. Scott, W. G. Seligman, M. H. Shaevitz, S. R. Sharpe, M. Silari, T. Sjöstrand, P. Skands,

- J. G. Smith, G. F. Smoot, S. Spanier, H. Spieler, A. Stahl, T. Stanev, S. L. Stone, T. Sumiyoshi, M. J. Syphers, F. Takahashi, M. Tanabashi, J. Terning, M. Titov, N. P. Tkachenko, N. A. Törnqvist, D. Tovey, G. Valencia, K. van Bibber, G. Venanzoni, M. G. Vinciter, P. Vogel, A. Vogt, W. Walkowiak, C. W. Walter, D. R. Ward, T. Watari, G. Weiglein, E. J. Weinberg, L. R. Wiencke, L. Wolfenstein, J. Womersley, C. L. Woody, R. L. Workman, A. Yamamoto, G. P. Zeller, O. V. Zenin, J. Zhang, R. Y. Zhu, G. Harper, V. S. Lugovsky, and P. Schaffner. Review of Particle Physics. *Physical Review D*, 86(1):010001, July 2012.
- [2] Yoshifumi Hyakutake. Quantum Near Horizon Geometry of Black 0-Brane. page 34, November 2013, 1311.7526.
- [3] Masanori Hanada, Yoshifumi Hyakutake, Goro Ishiki, and Jun Nishimura. Holographic description of quantum black hole on a computer. page 14, November 2013, 1311.5607.
- [4] Thomas M. Kelley, Sean P. Bartz, and Joseph I. Kapusta. Pseudoscalar mass spectrum in a soft-wall model of AdS/QCD. *Physical Review D*, 83(1):016002, January 2011, 1009.3009.
- [5] Sean P. Bartz and Joseph I. Kapusta. A Dynamical Three-Field AdS/QCD Model. page 17, June 2014, 1406.3859.
- [6] Alfonso V. Ramallo. Introduction to the AdS/CFT correspondence. page 64, October 2013, 1310.4319.
- [7] a Zaffaroni. Introduction to the AdS-CFT correspondence. *Classical and Quantum Gravity*, 17(17):3571–3597, September 2000.
- [8] Youngman Kim, Ik Jae Shin, and Takuya Tsukioka. Holographic QCD: Past, Present, and Future. *Progress in Particle and Nuclear Physics*, page 80, May 2012, 1205.4852.
- [9] J. Erdmenger, N. Evans, I. Kirsch, and E. J. Threlfall. Mesons in gauge/gravity duals. *The European Physical Journal A*, 35(1):81–133, February 2008, 0711.4467.



- [10] Jose D. Edelstein, Jonathan P. Shock, and Dimitrios Zoakos. The AdSCFT Correspondence and Non-perturbative QCD. In *PARTICLES AND FIELDS: Proceedings of the XIII Mexican School of Particles and Fields*, volume 1116, pages 265–284. ASCE, January 2009, 0901.2534.
- [11] Igor R. Klebanov. QCD and String Theory. *International Journal of Modern Physics A*, 21(08n09):12, September 2005, 0509087.
- [12] Steven S. Gubser and Andreas Karch. From Gauge-String Duality to Strong Interactions: A Pedestrian’s Guide. *Annual Review of Nuclear and Particle Science*, 59(1):145–168, November 2009, 0901.0935.
- [13] Edward Witten. Bound states of strings and p-branes. *Nuclear Physics B*, 460(2):335–350, February 1996, 9510135.
- [14] Gary T. Horowitz and Andrew Strominger. Black strings and p-branes. *Nuclear Physics B*, 360(1):197–209, August 1991.
- [15] Andreas Karch and Emanuel Katz. Adding flavor to AdS/CFT. *Journal of High Energy Physics*, 2002(06):043–043, June 2002, 0205236.
- [16] T. Sakai and S. Sugimoto. Low Energy Hadron Physics in Holographic QCD. *Progress of Theoretical Physics*, 113(4):843–882, April 2005, 0412141.
- [17] T. Sakai and S. Sugimoto. More on a Holographic Dual of QCD. *Progress of Theoretical Physics*, 114(5):1083–1118, November 2005, 0507073.
- [18] Joshua Erlich, Emanuel Katz, Dam Son, and Mikhail Stephanov. QCD and a Holographic Model of Hadrons. *Physical Review Letters*, 95(26):261602, December 2005, 0501128.
- [19] Leandro Da Rold and Alex Pomarol. Chiral symmetry breaking from five-dimensional spaces. *Nuclear Physics B*, 721(1-3):79–97, August 2005, 0501218.
- [20] Leandro Da Rold and Alex Pomarol. The scalar and pseudoscalar sector in a five-dimensional approach to chiral symmetry breaking. *Journal of High Energy Physics*, 2006(01):157–157, January 2006, 0510268.

- [21] Andreas Karch, Emanuel Katz, Dam Son, and Mikhail Stephanov. Linear confinement and AdS/QCD. *Physical Review D*, 74(1):015005, July 2006, 0602229.
- [22] Nick Evans and Andrew Tedder. Perfecting the ultra-violet of holographic descriptions of QCD. *Physics Letters B*, 642(5-6):546–550, November 2006, 0609112.
- [23] H. Grigoryan and A. Radyushkin. Structure of vector mesons in a holographic model with linear confinement. *Physical Review D*, 76(9):095007, November 2007, 0706.1543.
- [24] Herry Kwee and Richard Lebed. Pion form factor in improved holographic QCD backgrounds. *Physical Review D*, 77(11):115007, June 2008, 0712.1811.
- [25] Aleksey Cherman, Thomas Cohen, and Elizabeth Werbos. Chiral condensate in holographic models of QCD. *Physical Review C*, 79(4):045203, April 2009, 0804.1096.
- [26] P. Colangelo, F. De Fazio, F. Giannuzzi, F. Jugeau, and S. Nicotri. Light scalar mesons in the soft-wall model of AdS/QCD. *Physical Review D*, 78(5):17, July 2008, 0807.1054.
- [27] Song He, Mei Huang, Qi-Shu Yan, and Yi Yang. Confront Holographic QCD with Regge Trajectories of vectors and axial-vectors. page 9, October 2007, 0710.0988.
- [28] Tony Gherghetta, Joseph Kapusta, and Thomas Kelley. Chiral symmetry breaking in the soft-wall AdS/QCD model. *Physical Review D*, 79(7):076003, April 2009, 0902.1998.
- [29] Brian Batell and Tony Gherghetta. Dynamical soft-wall AdS/QCD. *Physical Review D*, 78(2):026002, July 2008, 0801.4383.
- [30] Danning Li and Mei Huang. Dynamical holographic QCD model: resembling renormalization group from ultraviolet to infrared. November 2013, 1311.0593.
- [31] Danning Li and Mei Huang. Dynamical holographic QCD model for glueball and light meson spectra. *Journal of High Energy Physics*, 2013(11):88, November 2013, 1303.6929.

- [32] Wayne de Paula, Tobias Frederico, Hilmar Forkel, and Michael Beyer. Dynamical holographic QCD with area-law confinement and linear Regge trajectories. *Physical Review D*, 79(7):075019, April 2009, 0806.3830.
- [33] W. de Paula and T. Frederico. Scalar mesons within a dynamical holographic QCD model. *Physics Letters B*, 693(3):287–291, October 2010, 0908.4282.
- [34] Qi Wang and An Min Wang. Chiral Symmetry Breaking in the Dynamical Soft-Wall Model. page 4, January 2012, 1201.3349.
- [35] Danning Li, Mei Huang, and Qi-Shu Yan. A dynamical soft-wall holographic QCD model for chiral symmetry breaking and linear confinement. *The European Physical Journal C*, 73(10):2615, October 2013, 1206.2824.
- [36] Andreas Karch, Emanuel Katz, Dam T Son, and Mikhail A Stephanov. On the sign of the dilaton in the soft wall models. *Journal of High Energy Physics*, 2011(4):66, April 2011, 1012.4813.
- [37] Juan M. Maldacena. The Large N Limit of Superconformal Field Theories and Supergravity. *Advances in Theoretical Mathematical Physics*, 2:20, November 1997, 9711200.
- [38] Igor R. Klebanov and Edward Witten. Ads/CFT correspondence and symmetry breaking. *Nuclear Physics B*, 556(1-2):89–114, September 1999, 9905104.
- [39] S.S. Gubser, I.R. Klebanov, and A.M. Polyakov. Gauge theory correlators from non-critical string theory. *Physics Letters B*, 428(1-2):105–114, May 1998, 9802109.
- [40] Edward Witten. Anti De Sitter Space And Holography. *Adv.Theor.Math.Phys.*, 2:253–291, February 1998, 9802150.
- [41] Peter Breitenlohner and Daniel Z. Freedman. Positive energy in anti-de Sitter backgrounds and gauged extended supergravity. *Physics Letters B*, 115(3):197–201, September 1982.
- [42] Hyun-Chul Kim and Youngman Kim. Quark-gluon mixed condensate of the QCD vacuum in holographic QCD. *Journal of High Energy Physics*, 2008(10):011–011, October 2008, 0808.3639.

- [43] Yan-Qin Sui, Yue-Liang Wu, Zhi-Feng Xie, and Yi-Bo Yang. Prediction for the mass spectra of resonance mesons in the soft-wall AdS/QCD model with a modified 5D metric. *Physical Review D*, 81(1):014024, January 2010, 0909.3887.
- [44] Yan-Qin Sui, Yue-Liang Wu, and Yi-Bo Yang. Predictive AdS/QCD Model for Mass Spectra of Mesons with Three Flavors. *Physical Review D*, 83(6):065030, March 2011, 1012.3518.
- [45] Murray Gell-Mann, R.J. Oakes, and B. Renner. Behavior of Current Divergences under  $SU_{\{3\}}SU_{\{3\}}$ . *Physical Review*, 175(5):2195–2199, November 1968.
- [46] D. Peskin, M. and Schroeder. An Introduction to Quantum Field Theory. 1995.
- [47] Walter Greiner, Stefan Schramm, and Eckart Stein. *Quantum Chromodynamics*. Springer, Berlin, 3rd edition, 2007.
- [48] Csaba Csáki and Matthew Reece. Toward a systematic holographic QCD: a braneless approach. *Journal of High Energy Physics*, 2007(05):062–062, May 2007, 0608266.
- [49] J. I. Kapusta and T. Springer. Potentials for soft-wall AdS/QCD. *Physical Review D*, 81(8):086009, April 2010, 1001.4799.
- [50] Umut Gürsoy, Elias Kiritsis, Liuba Mazzanti, and Francesco Nitti. Deconfinement and Gluon Plasma Dynamics in Improved Holographic QCD. *Physical Review Letters*, 101(18):181601, October 2008, 0804.0899.
- [51] U Gürsoy, E. Kiritsis, L. Mazzanti, and F. Nitti. Holography and thermodynamics of 5D dilaton-gravity. *Journal of High Energy Physics*, 2009(05):033–033, May 2009, 0812.0792.
- [52] Todd Springer. *Hydrodynamics of strongly coupled non-conformal fluids from gauge/gravity duality*. Ph.d. thesis, University of Minnesota, August 2009, 0908.1587.
- [53] S. S. Afonin. Holographic like models as a five-dimensional rewriting of large- $N_c$  QCD. *International Journal of Modern Physics A*, 25(31):33, January 2010, 1001.3105.

- [54] Elias Kiritsis. *String Theory in a Nutshell*. Princeton University Press, 2011.
- [55] M. Shifman and A. Vainshtein. Highly excited mesons, linear Regge trajectories, and the pattern of the chiral symmetry realization. *Physical Review D*, 77(3):034002, February 2008, 0710.0863.
- [56] Joseph I. Kapusta, Berndt Müller, and J. Rafelski. *Quark-Gluon Plasma: Theoretical Foundations*. 2003.
- [57] R.C. Hwa and X.-N. Wang. *Quark-Gluon Plasma 3*. 2004.
- [58] B. Kogut and Mikhail A Stephanov. *The Phases of Quantum Chromodynamics*. 2004.
- [59] P. Kovtun, D. Son, and A. Starinets. Viscosity in Strongly Interacting Quantum Field Theories from Black Hole Physics. *Physical Review Letters*, 94(11):111601, March 2005, 0405231.
- [60] Dam T. Son and Andrei O. Starinets. Viscosity, Black Holes, and Quantum Field Theory. *Annual Review of Nuclear and Particle Science*, 57(1):95–118, November 2007, 0704.0240.
- [61] Christopher Herzog. Holographic Prediction for the Deconfinement Temperature. *Physical Review Letters*, 98(9):091601, February 2007, 0608151.
- [62] C. Bayona, Henrique Boschi-Filho, Nelson Braga, and Leopoldo Zayas. On a holographic model for confinement/deconfinement. *Physical Review D*, 77(4):046002, February 2008, 0705.1529.

## Appendix A

# Numerical Methods for solving Ordinary Differential Equations

Ordinary differential equations can always be reduced to a system of coupled first-order differential equations, which is advantageous for numerical solutions. For example, the second-order equation

$$y''(x) + f(x)y'(z) = g(x) \tag{A.1}$$

can be rewritten as

$$y'(x) = z(x) \tag{A.2}$$

$$z'(x) = g(z) - f(x)z(x) \tag{A.3}$$

Written generically, an ordinary differential equations system is reduced to a set of  $N$  first-order differential equations

$$y'_i(x) = f_i(x, y_1, \dots, y_N) \quad i = 1, \dots, N \tag{A.4}$$

where the functions  $f_i$  are some known set of equations involving the coordinate  $x$  and the dependent variables  $y_i$ . For a unique solution, one must specify a set of  $N$  boundary conditions. If these conditions are all specified at a single point,  $x_0$ , this is known as an initial value problem, and one can simply choose an integration method and calculate the values for  $f_i$  over the desired domain. When some of the conditions are specified at point  $x_0$  and the rest are specified at the point  $x_f$ , this is known as a boundary value problem, and one must use one of the methods detailed below.

## A.1 Shooting Method

The shooting method turns boundary value problems into initial value problems. The classic example of a shooting method can be visualized as the firing of a cannon, with boundary conditions given by the location of the cannon and the location of the target. This is changed to an initial value problem by selecting an arbitrary value for the angle of the cannon and firing. The angle of the cannon is incremented until the cannonball hits the target, which matches the final boundary condition.

More concretely, the boundary value problem is written as in (A.4), with boundary conditions

$$B_{1j}(x_0, y_1, \dots, y_N) = 0 \quad j = 1, \dots, n_1 \quad (\text{A.5})$$

$$B_{2k}(x_f, y_1, \dots, y_N) = 0 \quad k = 1, \dots, n_2 \quad (\text{A.6})$$

with  $n_1$  boundary conditions at point  $x_0$  and  $n_2 = N - n_1$  at point  $x_f$ . These boundary conditions generically can be any algebraic combination of the variables.

For concreteness, consider a second-order eigenvalue problem of the type considered in this thesis,

$$\psi_n''(z) + V(z)\psi_n(z) = m_n^2\psi_n(z). \quad (\text{A.7})$$

This can be reduced to two first-order differential equations by making the substitutions  $y_1 = \psi$ ,  $y_2 = \psi'$ , resulting in the system

$$y_1' = y_2 \quad (\text{A.8})$$

$$y_2' = (m_n^2 - V(z)) y_1. \quad (\text{A.9})$$

The boundary conditions are  $y_1(z_0) = y_1(z_f) = 0$ .<sup>1</sup> In this instance, the eigenvalues are of greater importance than the behavior of the solutions  $y_1, y_2$ , so the overall normalization of the solutions is arbitrary.

This boundary value problem is changed to an initial value problem by setting

$$y_1(z_0) = 0 \quad (\text{A.10})$$

$$y_2(z_0) = c, \quad (\text{A.11})$$

---

<sup>1</sup> In the soft-wall model, we should take the limit  $z_f \rightarrow \infty$ . This is impossible to do numerically, but it is easy to make  $z_f$  sufficiently large that the eigenvalues are not effected.

where  $c$  is an arbitrary constant. A small test value for  $m_n$  is chosen, and the initial value problem is solved.

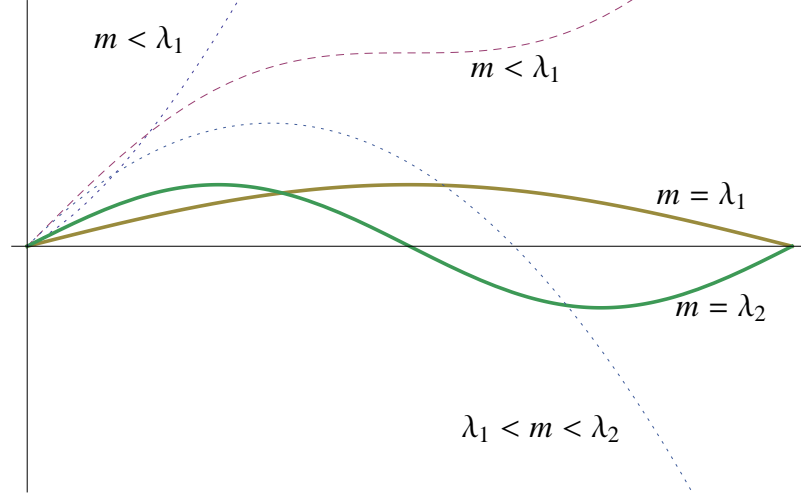


Figure A.1: An illustration of the shooting method.

As illustrated in Figure A.1, when the test value for  $m_n$  is less than the first eigenvalue  $\lambda_1$ , the value of  $y_1(x_f)$  is positive. As  $m_n$  is incremented, eventually  $y_1(x_f)$  becomes negative. A root-finding routine is used to approximate the values  $\lambda_n$  such that  $y_1(x_f) = 0$ . The number of antinodes in the wavefunction indicates to which excitation mode the eigenvalue corresponds.

## A.2 Matrix Method

The coupled second-order The equations of motion can be reduced to a set of second-order differential equations,

$$-\varphi'' + V_1(z)\varphi + f(z)\pi = 0, \quad (\text{A.12})$$

$$-\pi'' + V_2(z)\pi + g(z)\varphi = 0, \quad (\text{A.13})$$

where the eigenvalues are contained within the coefficient functions. These equations can be expressed as a system of first-order differential equations

$$\Phi' + W(z)\Phi = 0, \quad (\text{A.14})$$



where  $W$  is the matrix

$$W = \begin{pmatrix} 0 & 1 & 0 & 0 \\ V_1(z) & 0 & f(z) & 0 \\ 0 & 0 & 0 & 1 \\ g(z) & 0 & V_2(z) & 0 \end{pmatrix} \quad (\text{A.15})$$

and  $\Phi$  is the vector

$$\Phi_{\alpha i} = \begin{pmatrix} \varphi_i \\ -\varphi'_i \\ \pi_i \\ -\pi'_i \end{pmatrix} \quad (\text{A.16})$$

that forms an orthonormal basis of solutions. We can propagate the solution  $\Phi$  between two boundary points

$$\Phi(z_f) = U(z, z_f, z_0, m_n^2) \Phi(z_0), \quad (\text{A.17})$$

where we solve (A.14) with the appropriate boundary condition at  $z_0$ . The eigenvectors and eigenvalues of  $U$  are then calculated. Two of the solutions are divergent, but the solutions that correspond to the two smaller eigenvalues do not diverge. We label the non-divergent solutions as the eigenvectors  $u_3$  and  $u_4$ . The non-divergent solutions for  $\Phi_i$  can be written as a linear combination of  $u_3$  and  $u_4$

$$\Phi_i = \alpha u_3 + \beta u_4. \quad (\text{A.18})$$

Non-trivial values of  $\alpha$  and  $\beta$  satisfy

$$\begin{pmatrix} u_3^1 & u_4^1 \\ u_3^3 & u_4^3 \end{pmatrix} \begin{pmatrix} \alpha \\ \beta \end{pmatrix} = 0 \quad (\text{A.19})$$

for Dirichlet or

$$\begin{pmatrix} u_3^2 & u_4^2 \\ u_3^4 & u_4^4 \end{pmatrix} \begin{pmatrix} \alpha \\ \beta \end{pmatrix} = 0 \quad (\text{A.20})$$

for Neumann boundary conditions. The values of  $m_n^2$  that minimize the determinant of the matrix (A.19) or (A.20) are the eigenvalues of the system (A.12-A.13). An abrupt change in its behavior of the plot of the determinant vs. the value of  $m_n$  signals the location of an eigenvalue.

## Appendix B

# General Relativity Reference

This appendix contains the relevant general relativity calculations necessary for the dynamical AdS/QCD models in Chapters 4 and 5. The conventions used here are those from [?].

From a given metric  $g_{MN}$ , we must calculate the Riemann tensor, the Ricci scalar, and the Einstein tensor. This appendix will provide the relevant definitions and include the results for the  $AdS_5$  metric

$$g_{MN} = \frac{1}{z^2} \begin{pmatrix} -1 & 0 & 0 & 0 \\ 0 & 1 & 0 & 0 \\ 0 & 0 & 1 & 0 \\ 0 & 0 & 0 & 1 \end{pmatrix}. \quad (\text{B.1})$$

### B.1 Covariant Derivative and Christoffel Symbols

When working in curved spacetime, we must define the appropriate derivative operator for that coordinate system, known as the covariant derivative. The covariant derivative has differing expressions depending on what object it is acting on; for simplicity we will define it for a vector,

$$\nabla_M V^N = \partial_M V^N \Gamma_{ML}^N V^L, \quad (\text{B.2})$$

where capital Latin letters indicate any of the five spacetime coordinates. The symbol  $\Gamma_{ML}^N$  is a matrix known as the connection coefficients. There are a variety of choices for these connection coefficients, but we will use the Christoffel connection, which is

commonly used in the study of general relativity. The Christoffel connection is defined as

$$\Gamma_{MN}^P = \frac{1}{2}g^{PR}(\partial_M g_{NR} + \partial_N g_{RM} - \partial_R g_{MN}). \quad (\text{B.3})$$

In the  $AdS_5$  metric, the non-trivial Christoffel symbols are

$$\Gamma_{z\mu}^\mu = -\frac{1}{z} \quad (\text{B.4})$$

$$\Gamma_{\mu\mu}^z = \frac{1}{z} \quad (\text{B.5})$$

$$\Gamma_{zz}^z = -\frac{1}{z}, \quad (\text{B.6})$$

where Greek indices run over the 4D spacetime coordinates  $t, \vec{x}$ , and no sum is implied over repeated indices.

## B.2 Ricci Tensor and Ricci Scalar

The Ricci tensor is needed to calculate the Ricci scalar, and also appears in the Einstein equation, which is needed to calculate some of the equations of motion for the background fields from the dynamical action. The Ricci tensor can be calculated from the Riemann tensor, but because we have no need for the Riemann tensor, we calculate the Ricci tensor directly:

$$R_{MN} = \partial_N \Gamma_{MN}^L + \Gamma_{ML}^N \Gamma_{NR}^L - \Gamma_{MN}^R \Gamma_{LR}^L, \quad (\text{B.7})$$

where summation over the repeated indices is implied.

The non-trivial components of the Ricci tensor for the AdS metric are

$$R_{tt} = \frac{4}{z^2}, \quad (\text{B.8})$$

$$R_{ii} = -\frac{4}{z^2}, \quad (\text{B.9})$$

$$R_{zz} = -\frac{4}{z^2}, \quad (\text{B.10})$$

where the lower-case Latin index  $i$  represents the spatial coordinates  $\vec{x}$ , and no summation is implied over repeated indices.

The Ricci scalar is defined as

$$g^{MN} R_{MN}, \quad (\text{B.11})$$

and is calculated to be  $R = -20$  in the  $AdS_5$  geometry.

### B.3 Equations of Motion

The equations of motion for a gravitational field theory come from the Einstein equation, which relates the spacetime curvature to the energy content of the theory, as well as by varying the action with respect to the scalar fields in the theory. The Einstein tensor  $G_{MN}$  is defined in terms of the Ricci tensor and Ricci scalar as

$$G_{MN} = R_{MN} - \frac{1}{2}g_{MN}R. \quad (\text{B.12})$$

In the  $AdS_5$  geometry, the non-trivial components of the Einstein tensor are

$$G_{tt} = -\frac{6}{z^2}, \quad (\text{B.13})$$

$$G_{ii} = \frac{6}{z^2}, \quad (\text{B.14})$$

$$G_{zz} = \frac{6}{z^2}, \quad (\text{B.15})$$

where again the lower-case Latin index  $i$  represents the spatial coordinates  $\vec{x}$ , and no summation is implied over repeated indices. The Einstein equation relates the Einstein tensor to the energy-momentum tensor,

$$G_{MN} = 8\pi G_5 T_{MN}, \quad (\text{B.16})$$

where  $G_5$  is the five-dimensional gravitational constant.

Given a gravitational-scalar action of the standard form,

$$\mathcal{S} = \int d^d x \left( R - \frac{1}{2} \partial_\mu \phi \partial^\mu \phi - V(\phi) \right), \quad (\text{B.17})$$

we vary the action with respect to the scalar field  $\phi$ . The equation of motion that results is

$$\square \phi = -\frac{\partial V}{\partial \phi}, \quad (\text{B.18})$$

where the D'Alembertian operator  $\square$  is defined in terms of the covariant derivative,

$$\square = \nabla_\mu \nabla^\mu. \quad (\text{B.19})$$

The equations of motion for the dynamical AdS/QCD are all of the form B.16 or B.18.